WADC TECHNICAL REPORT 54-384, PART III
ASTIA DOCUMENT NUMBER AD - 130767

THE EFFECTS OF THERMAL RADIATION ON AIRCRAFT STRUCTURES

Part III - Structural Behavior of Box-Beams Under Combined Static and Thermal Loads

John C. Loria
Seymour J. Engel
James W. Mar

Massachusetts Institute of Technology

June 1957

Aircraft Laboratory
Contract No. AF 33(038)-8906
Project No. 1350

Wright Air Development Center
Air Research and Development Command
United States Air Force
Wright-Patterson Air Force Base, Ohio

FOREWORD

This report was prepared by the Aeroelastic and Structures Research Laboratory of the Massachusetts Institute of Technology, Cambridge, Massachusetts, under Air Force Contract No. AF 33(038)-8906, Project No. 1350, (UNCLASSIFIED TITLE) "Atomic Weapon Effects on Aircraft Systems". The authors, Mr. John C. Loria and Mr. Seymour J. Engel, are members of the D. S. R. Research Staff and Dr. James W. Mar is an Assistant Professor of Aeronautical Engineering at M. I. T. Dr. Emmett A. Witmer was the project leader in charge of the work covered under Contract No. AF 33(038)-8906. The work was administered under the direction of the Aircraft Laboratory, Wright Air Development Center, with Mr. Francis J. Janik, Jr. acting as project engineer. This report is one of a series of such reports which will appear as component parts of WADC TR 54-384.

The program was carried out under the general supervision of Professor Raymond L. Bisplinghoff. Work was started in September of 1954 and completed in February of 1957. The authors wish also to acknowledge the assistance of Mr. Louis Goldberg in the experimental program, Mr. Fred Merlis in the instrumentation phase of the program, and Mr. Lucien A. Schmit for developing the Whirlwind solutions. Credit is also due Mr. John McHugh for drawing the illustrations, Mr. George Falla for the photographs, and Miss Iris G. Ellis for typing the manuscript.

ABSTRACT

The present report is concerned with an examination of the structural behavior of a simple box-beam under the combination of an external static load and a thermal input, the definition of failure criteria, and the development of methods for predicting failure. The situation considered is one in which a box-beam under a uniform bending moment is heated on the tension cover plate until failure occurs. The external static loads on each model were uniform bending moments at different percentages of the static failing bending moment. The study gives evidence that the stresses due to external static and thermal loads can be superposed and predicted within the elastic region quite accurately. The plastic buckling failure of the type encountered in these combined loading tests serves as a failure criterion in itself since the initiation of plastic buckling is followed almost immediately by failure. In the case of a thermal input alone, failure results from material deterioration. The combined failure relationship can be adequately represented by interaction curves for the simple problem considered to predict failure.

PUBLICATION REVIEW

This report has been reviewed and is approved.

FOR THE COMMANDER:

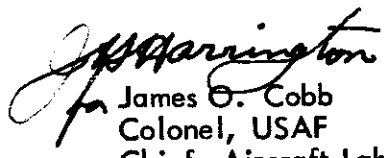

James O. Cobb
Colonel, USAF
Chief, Aircraft Laboratory
Directorate of Development

TABLE OF CONTENTS

LIST OF ILLUSTRATIONS

LIST OF ILLUSTRATIONS (CONTD.)

LIST OF ILLUSTRATIONS (CONTD.)

LIST OF TABLES

LIST OF TABLES (CONTD.)

LIST OF COMMON SYMBOLS

A	Cross-sectional area, sq. inches
b	Plate width, inches
E	Modulus of elasticity, psi
F	Fahrenheit temperature scale
GF	Strain-gage factor
I	Moment of inertia, $(\text{inches})^4$
K_s	Edge fixity factor
M	Applied static bending moment, in-lbs.
q	Thermal intensity, cal/sq. cm. sec.
R	Resistance, ohms; stress ratio
t	Plate thickness, inches
T	Temperature, $^{\circ}F$
[u]	Square matrix of coefficients
z	Neutral axis shift, inches
z_i	Distance from the original neutral axis to the gage location or centroid of element i, inches
z_{ie}	Distance from the neutral axis to the centroid of the i^{th} element, inches
α	Coefficient of thermal expansion, $\text{in/in}^{\circ}F$; diffusivity, $\text{in}^2/\text{sec.}$
δ	Galvanometer displacement, 1/50th of an inch
Δ	Increase above initial value
ϵ	Strain, inches/inch
η	Plasticity correction factor
ν	Poisson's ratio
σ	Stress, psi

LIST OF COMMON SYMBOLS (CONTD.)

Subscripts

i	Refers to i^{th} element
j	Refers to j^{th} time interval
s	Static bending moment
ST	Static
T	Total thermal energy; thermal load stress
t	Tangent

SECTION I

INTRODUCTION

The behavior of aircraft structures under a combination of external and thermal loads is of current interest because of the problems associated with aircraft under flight loads which may be exposed to the added effects of aerodynamic heating or thermal radiation from atomic explosions. The flight loads may be the normal level flight loads, maneuver loads, gust loads, or in the case of the atomic explosions, the loads may be due to the ensuing blast wave. The temperatures induced in the aircraft structure by these heating effects may be critical in themselves or they may act in combination with the flight loads to produce failure.

The present report is concerned with a study of the combined loading of a structure which is initially under a static external load and then heated until failure occurs. The purpose of the study is threefold:

1. To examine structural behavior under combined loading,
2. To define failure criteria, and
3. To establish methods for predicting failure.

The structural models employed were extruded rectangular aluminum alloy tubings. Each of the models was loaded in pure bending to a percentage of the room temperature failure load and then irradiated on one cover with a "step" thermal input. Each model was heated until it was certain from visual observation that failure had occurred. The failure conditions will be discussed in more detail in the body of this report.

From this description of the loading technique, it is obvious that the problem considered is actually a "static combined loading problem" in contrast to the case in which the model is initially heated and then loaded dynamically or else initially loaded dynamically and then heated. These latter loading sequences may be termed "dynamic combined loading problems". The "static combined loading

---

Manuscript released by authors March 15, 1957 for publication as a WADC Technical Report.

problem" is analogous to the case where the aircraft is undergoing steady level-flight loads or a steady maneuver load and is then thermally irradiated by an atomic explosion. The dynamic combined loading problems would represent extensions of this in that the aircraft might be considered to be exposed to the blast loading of the atomic explosion following exposure to thermal radiation or it might be undergoing transient maneuver loads when irradiated. These initial studies deal only with the static combined loading problem and, for the sake of simplicity, the term "combined loading" will be used in the remainder of the report to imply this type of loading.

The temperatures caused by aerodynamic heating or thermal radiation may range anywhere from insignificant levels up to the melting, burning, or even the vaporization point of the exposed materials. The same applies in the case of external loads in that these loads can range from low levels up to ultimate, depending on the situation. These conditions represent the two extremes of the combined loading problem in that failure may be caused by the thermal effects alone or it may be due solely to external loads. The present investigation of the combined loading problem is concerned with the region between these two extremes.

The transient temperature gradients themselves lead to the three following primary effects:

1. Transient stresses are induced by the time-varying differential expansion of different portions of the structure. These thermal stresses can cause failure, or they can combine with external or airload stresses to reach failure levels.
2. The properties of the materials are adversely affected. This may extend from small reductions in the strength of the material through thermoplastic yielding, melting, and even complete disintegration of the material. These effects are also transient, but they may result in permanent changes in the material properties.
3. The shape of the aircraft structure is distorted leading to interactions with flight loads. These distortions may be simple panel buckling or they may extend to gross distortions of the complete structure.

When transient temperature gradients are induced in a structure which is initially under a static external load, these three primary effects still act, but the structural behavior may vary depending on the initial static loading. A simple example of this is the case concerning the amount of thermal energy required to cause failure in a simple rod attached between two rigid insulated walls. If the rod is loaded in tension between these walls and then heated uniformly, the stresses in the rod will actually be relieved by the consequent expansion of the rod. Furthermore, it would probably take considerable thermal energy to increase the expansion of the material to the point where compressive stresses would be generated such as to buckle and fail the rod. The rod might even fail by melting before a buckling failure would occur. If, instead, the rod is initially placed between these two walls in compression, the uniform heating would immediately increase the compressive stress and buckling failure of the rod would be effected with considerably less thermal energy. It can be seen from this simple example that both the thermal energy required and the mode of failure of this rod are different even though the initial stresses might be equal in magnitude because the two initial static stresses are opposite in sense. Thus, the behavior pattern, failure criteria, and failing loads of a structure can be drastically altered by the mode of application of the initial load. The rate of application of the thermal energy may also prove important.

The simple example above serves to indicate the importance of specifying the exact conditions and conduct of the tests and the limitations which should be imposed in attempting to extrapolate or generalize test results. In the present series of tests, a single mode of load application was employed and only the magnitude of the load was varied.

The extruded aluminum rectangular tubes employed as models are referred to as "box-beams" and are described in detail in Section II. External static loadings were employed which were very nearly uniform bending moments and put the unexposed cover of the box-beams in compression and the exposed cover in tension. Approximate step-inputs of radiant flux were used as the thermal inputs and these were applied only to the tension covers of the box-beams. The manner of loading and heating will also be discussed in Section II.

The present study was conducted using two series of box-beam test specimens. The failing static loads of the beams of each series were first established at room temperature for the uniform bending moments acting alone. Once this static failing load was established, each model in a series was loaded to a specified percentage of its respective static failure load before being exposed to the thermal input. The structural behavior of all beams was visually observed and pertinent test data was simultaneously recorded oscillographically. Section IV describes the experimental procedure. The recorded data consisted of temperatures, strains, and displacements.

In order to determine the influence of the rate of thermal input on the combined loading failure, two values of radiant flux intensity were used. Tests were conducted on the first series (series-1) of box-beams using a radiant flux intensity of 4 cal/sq. cm. sec. On the second series of beams (series-2), the radiant flux intensity was increased to 8 cal/sq. cm. sec.

The radiant heater employed in these series of tests was the M. I. T. Mark I Globar heater (Ref. 1.1). Briefly, the heater consists of two halves each of which contains twenty equally spaced silicon-carbide heating elements (Globars) with seven inch heating lengths. The length of each heater half is twenty-four inches. Only the lower half of the heater was used. The electrical circuit consisted of ten parallel connections each of two elements in series powered by an 87 KW Ward-Leonard motor-generator system. The heating elements are capable of sustaining a temperature of 3000°F for a short period in free air. In series-1 they were operated at 2400°F five inches below the model and for series-2 at 2800°F four inches below the model. The measured radiant flux intensity versus distance from the heater is shown in Fig. 1.1 for various Globar temperatures. The Mark I heater is shown in Fig. 1.2; a more detailed description of the heater is contained in Reference 1.1.

SECTION II

EXPERIMENTAL PREPARATION

2.1 The Test Specimens

The test specimens used in both series were two-foot lengths of sharp cornered, rectangular, extruded 63 S-T5 aluminum tubing of cross-sectional area two inches by five inches with 1/8-inch thick walls. Figure 2.1 shows a cross-section of this specimen and lists some of its room temperature material properties obtained from reference 2.1. A photograph of a typical model is shown in Fig. 2.2.

Although the box-beams of series-1 and series-2 were made of the same material, they were extruded from different lots and it was found that the failing static bending moments differed radically between the two lots. For this reason the series-1 and series-2 designations were employed and these imply a difference in material strength as well as a difference in the rate of heat input of 4 cal/sq. cm. sec. and 8 cal/sq. cm. sec., respectively.

In the interest of eliminating many of the complicating factors involved in built-up sections such as joint contact resistances and rivet slippage, it was decided to employ simple models in these studies. The dimensions and shape of the 63S-T5 aluminum alloy extrusion fit this requirement well and its availability also made it attractive. However, the elevated temperature properties of this material were not available and it was subsequently found necessary to initiate an experimental program to determine these properties. The five-inch width was well suited for use with the Mark I heater and the two-inch depth gave the models cross-sectional dimensions somewhat representative of typical wing sections. The shallow depth of the model was also desirable in that a small moment of inertia about the horizontal axis meant correspondingly lower applied loads. On the other hand, the two-inch depth made the installation of strain-gages and thermocouples on the inside of the model quite difficult.

2.2 Static Loading System

A dimensional sketch of the loading system, positioning frame and heater are shown in Fig. 2.3. A uniform bending moment was applied across the length of each model by loads applied at the ends of lever arms fitted into each

end of the box-beams and supported at pivot points on the loading frame. The lever loading arms were made of cold-rolled steel bar material, thirty-inches in length and of the same cross sectional area as the box-beam models. A four-inch length of each lever arm was machined for a close fit into each end of the box-beams. The remaining twenty-six inches of each loading arm extended beyond the model at each end. The loading arms were secured to the model by four 1/4-inch bolts which passed through the model, loading arm, and a bracket which held the pivot points about which the loading arms rotated under the external loading system. Each pivot point consisted of a pair of self-aligning ball-bearings spaced sixteen inches apart, and the spanwise distance between pivot points was twenty inches. The ball-bearing pivots were mounted in a steel frame-work that held the model in position during the tests. An exploded view photograph of a load arm and pivot point assembly is shown in Fig. 2.4.

The model positioning frame-work was constructed of 2-1/2-inch steel angle-iron sections welded to two 3-inch iron channel sections which acted as a track for the ball-bearing pivot points. The whole positioning frame-work was bolted to the bedplate so that it straddled the tracks of the Mark I heater. Figure 2.5 is a photograph of this test arrangement.

The concentrated loads were applied at the free end of each loading arm by means of hydraulic cylinders which were actuated by hydraulic hand-pumps. The applied load was indicated on a hydraulic pressure gage attached to each hydraulic cylinder. Each of the two hydraulic load systems was initially calibrated in pounds of applied force versus indicated pressure reading. The calibration curves of both were identically linear and equal to 1.47 lbs/psi. A photograph of the hydraulic loading system is shown in Fig. 2.6.

A hydraulic loading system was employed rather than a weight and pulley loading system because of the amount of loading that had to be applied and the necessary increments of static loading that were desired. These conditions would be cumbersome and difficult to obtain with a weight and pulley system. However, the use of a hydraulic loading system required constant monitoring and adjusting during each test run to compensate for the thermal expansion of the model .

SECTION III

INSTRUMENTATION

3.1 Scope of Instrumentation

The quantities measured during the experimental program were temperatures, strains, deflections, and radiant flux intensities; all were recorded versus time. In order to eliminate any "end effects" which might have been present, the measurements were made at the center of the model.

The recording equipment consisted of Heiland recording oscillographs, Nosker and Heiland bridge balance units, radiometers, dial gages, a 16-mm motion picture camera, and a stop-watch.

3.2 Temperature Measurements

The temperatures at various points in the box-beam models were obtained using copper-constantan and iron-constantan thermocouples made from No. 28 gage insulated, double conductor, thermocouple wire. These thermocouples were spot-welded to the surface of the models around one-half the periphery at the center-span station. The exact locations of these thermocouples are shown in Fig. 3.1 designated by the symbol T and numbered consecutively.

Iron-constantan thermocouples were employed at locations T_1, T_2, and T_3 where the highest temperatures were anticipated; these were mounted on the inside surface so that they would not be exposed to the direct thermal radiation. Because of the inaccessibility of this location, "thermocouple plugs" were devised and used for these three positions. These plugs consisted of taper pins with a mean diameter of 1/8-inch and a length of 1/4-inch which were machined from the box-beam material. A pair of very fine holes were drilled 1/8-inch deep next to one another into the small diameter end of each tapered plug to accommodate the two thermocouple leads and these were spot-welded at the bottom of the holes. The pin was then crimped to hold the leads more firmly. The thermocouple lead wires were first fed into holes drilled at the location desired and then through the model to the recorder. The drilled holes are slightly undersize so that the plugs were then held by a press-fit. A typical thermocouple plug is illustrated in Fig. 3.2.

The other thermocouples were spot-welded on the outside surface of the model in the usual manner. Besides the usual braided asbestos and fiber-glass thermocouple covers, glyptol was applied to the thermocouples at the welds to provide further thermal and electrical insulation and the leads were also shielded from direct radiation with aluminum foil and glass tape. Some of these mounted thermocouples are shown in Fig. 3.3. In the later tests, Armstrong A-2 adhesive was used in place of glyptol as an insulating coating.

The temperatures of the twenty Globar heating elements of the 7" x 24" Mark I heater were monitored before each run with a Leeds and Northrup optical pyrometer to insure that the radiant flux intensity was the same for each run in each of the two series. The Globars were maintained at a mean operating temperature of 2400°F in series-1 and 2800°F in series-2, within $\pm$ 20°F, once the silicon carbide slab in the bed of the heater reached an equilibrium temperature. A heater stabilization time of approximately 1/2 hour was required for this.

3.3 Strain Measurements

Nine strain measurements were made on most of the models using Baldwin, types EBDF-7D and EBDF-13D, temperature-compensated, wire-wound, electric strain-gages. These gages were also located at the 12-inch station around half the periphery of the box-beam and were cemented and baked on the models according to the manufacturer's recommended procedures. The strain-gages are designated by the symbol, S, followed by consecutive numbers as shown in Fig. 3.1. Strain-gages S1, S2, and S3 were mounted on the inside of the exposed surfaces of the models since they, like the thermocouples, should not be exposed to direct radiation.

The method of mounting these three gages was that first used in reference 3.1. Briefly, two wooden wedges were cut to the exact width of the inside dimension of the models. On one of the wedges a piece of rubber was glued to act as a mat for the strain-gages. The three strain-gages were coated with strain-gage cement on one side and were attached temporarily with rubber cement on the other side to the rubber mat at the desired chordwise locations. This wedge was inserted in one end of the box-beam to the 12-inch station and the other wedge, exactly the same as the first without the raised portion, was inserted in

the other end of the model until both wedges met. By forcing the two wedges together, sufficient pressure was achieved to effect a good bond between the strain-gages and the inside of the exposed surface of the model. This is shown in Fig. 3.4.

3.4 Radiometer Measurements

The radiant flux intensity of the Mark I heater was obtained by use of circular foil radiometers and an instrumented thin flat plate. The radiometers were based on the design of R. Gardon (Ref. 3.2) and built by the Model Shop of the Aeroelastic and Structures Research Laboratory of the Massachusetts Institute of Technology. Calibration of these radiometers was performed by the Naval Material Laboratory at the Brooklyn Navy Yard (Ref. 3.3). The radiometers were employed to survey the radiation field of the Mark I source using a sliding cantilevered arm as shown in Fig. 3.5. This was carried out for various source temperatures at different distances above the Globar plane. The thin flat plate was instrumented with five thermocouples and was used to spot-check the radiometer measurements. The radiant flux is shown in Fig. 1.1.

3.5 Deflection Measurements

During the static loading tests, deflection measurements were made using dial-gages over the span of the box-beam to obtain the radius of curvature of the top surface of the model. The bending moment corresponding to this radius of curvature was calculated in addition to the bending moment corresponding to the applied loads and the bending moment corresponding to the strain-gage readings. These three separate determinations yielded an accurate assessment of the static failure bending moment in each of the succeeding combined loading tests.

During the combined loading tests, only one dial gage was used and it was located on the top surface of the model at the center-span station as shown in Fig. 2.5. A stop watch was mounted beside this dial gage and the deflections of both instruments were filmed by a 16 mm motion picture camera during the combined loading test. The deflection time history of the box-beam was then obtained from the readings on the film. An indication of the failure time was afforded by these readings by a sudden increase in the rate of deflection. Further indication of failure was provided by a drop-off of the pressure gage readings in the loading system while attempting to maintain the initial static load by means of the hydraulic hand pumps.

3.6 Recording Equipment

Up to seventeen oscillograph channels were used to record all the information from the strain-gages and thermocouples on all except the last box-beam model used in the test program. In this particular model, fifty-one channels were used for reasons to be explained. For the first series of models, a 12-channel and a 6-channel portable Heiland recording oscillograph were used. The 12-channel Heiland was powered by a 0-28 volt Mallory power supply and the 6-channel Heiland was operated on a 0-12 volt Mallory power supply. Heiland types A and G-150 galvanometers were used in conjunction with two Nosker bridge balance units, to record the strain-gage signals. Heiland type-B galvanometers were used to record the thermocouple signals. The 12-channel Heiland oscillograph, the Mallory power supply, and a Nosker bridge balance unit are shown in Fig. 3.6 in the upper part of the page.

The thermocouples were connected directly in series with the B-type galvanometers since their proper damping resistance was provided by the resistance of the thermocouple wire itself. This thermocouple-measuring circuit is shown in Fig. 3.7.

Each strain-gage was connected as the active arm of a Wheatstone bridge circuit with the three dummy arms consisting of wire-wound precision resistors. Each of these strain-gage bridge circuits was connected to one of the six channels of each of the two Nosker bridge balance units used. To obtain the proper sensitivity, the strain-gage Wheatstone-bridge circuits were excited with 7.5 volts obtained from a bank of dry-cell batteries. From the two 6-channel Nosker bridge balance units, the strain-gage signals were fed through 150-ohm series damping resistors to the A-type galvanometers and through 250-ohm series damping resistors to G-150 type galvanometers in the Heiland recording oscillographs to obtain proper circuit damping. This strain-gage measuring circuit is shown in Fig. 3.8. Methods used in the calibration of the recording circuits are presented in Sections 4.2 and 4.3.

Between the first and second series of tests, new recording equipment was obtained which aided considerably the conduct of the second series of tests. This equipment consisted to two new 60-channel Heiland oscillographs, fifty-seven associated galvanometers, and five 6-channel bridge-balance units. A typical rack-mounted oscillograph and bridge balance unit is shown in the photograph of Fig. 3.6, on the lower part of the page.

The thermocouple and strain-gage circuits were much the same as before; the only difference was that in the thermocouple circuits, damping resistors were used and in the strain-gage circuits, various excitation voltages were used, depending upon the type of galvanometer and sensitivity desired.

For all of the series-2 except the last box-beam tested, only one oscillograph was required to record the seventeen channels of information. The 0-12 volt Mallory power supply was used as the excitation source for the strain-gage circuits, with each gage having a separate control to obtain its specific excitation voltage.

In the series-2 tests, the last box-beam tested was instrumented at two additional spanwise stations to determine the extent of the end effects on the temperature and stress patterns. The stations instrumented, in addition to the 12-inch station, were the 9-1/2-inch and 7-inch stations. Nine strain-gages and eight thermocouples were employed at each station as indicated in Fig. 3.1.

SECTION IV

EXPERIMENTAL PROCEDURE

4.1 Calibration of Measuring Instruments

In order to convert the oscillograph records from displacements to temperatures, strains, and radiant intensities, it is necessary that each of the recording circuits be calibrated with the galvanometers used to record the data. Since many tests were planned, it proved expedient to employ the same calibrated circuits for all tests. The calibration circuits and procedures which were devised are described below.

4.2 Strain-Gage Calibration

A typical strain-gage Wheatstone-bridge circuit is shown in Fig. 3.8. Each of these strain-gage circuits was calibrated by the following procedure:

1. A precision decade variable resistance was substituted in place of the active arm of the bridge and the bridge was balanced so that there was zero current through the galvanometer and its series resistance, if any. The strain-gage bridge circuit excitation voltage was checked periodically to insure that it remained constant.
2. By changing the variable resistance of the precision decade box in increasing steps, incremental changes in the strain-gage signal were simulated causing unbalance of the Wheatstone bridge. The increasing current flows associated with the incremental unbalancing of the bridge circuit caused corresponding galvanometer deflections which were tabulated along with the initial resistance changes.
3. Knowing the initial bridge balancing resistance, R, the strains, ϵ, were calculated using:

$$\epsilon = \frac{\Delta R/R}{GF}$$

where GF is the manufacturer's strain-gage factor and ΔR is the incremental change in resistance set by the decade box.

4. A calibration curve of calculated strain versus galvanometer deflection was plotted for each strain-gage circuit. These were found to be linear except for large galvanometer deflections so that a single strain calibration factor, ϵ/δ, in units of microinches per inch per 1/50th of an inch deflection were employed for each strain-gage circuit.

Another calibration procedure for the strain-gage circuits was carried out on each model just before testing, which yielded a stress calibration in contrast to the strain calibration of the method above. This was accomplished in the following manner:

1. Actual static loads were applied to the model in steps by means of the hydraulic loading system. These step loads were tabulated along with the corresponding galvanometer deflections associated with each of the strain-gage circuits.
2. The stress, σ, at each gage location was calculated from the familiar expression,

$$\sigma = \frac{Mz_i}{I_x}$$

where z_i = the distance from the neutral axis of the model to the gage location (see Fig. 2.1),

I_x = the moment of inertia of the model about the x-axis, and

M = applied static bending moment equal to the load times the lever arm.

3. A stress sensitivity calibration factor of stress per unit deflection, σ/δ, in terms of psi per 1/50th of an inch galvanometer deflection was obtained for each circuit in the same manner as the strain sensitivity calibration factor.

Using the tabulated value of $E = 10^7$ psi (see Fig. 2.1), the correlation between the strain sensitivity and stress sensitivity was excellent. Besides providing a check on the strain sensitivity calibration factors, the stress calibration insured that the strain-gage circuits were working properly just prior to the tests in a simple manner.

The final method employed to calibrate the strain-gage circuits made use of a Dumont Strain Calibrator. In place of the decade resistance, this simple device employs a series of internal precision resistors which are connected to a switching arrangement to unbalance the bridge. Depending upon the nominal resistance of strain-gage and gage factor, a strain in microinches per inch is read from a calibration chart containing a family of curves of nominal resistances for a range of gage factors. Each precision resistor in the switching arrangement represents a percentage of the strain determined by the calibration chart. This method was checked against the first method of calibration and was found to be equally reliable. Use of the Strain Calibrator proved much simpler since the galvanometer deflections were related directly to strain.

4.3 Thermocouple Calibration

From previous experiments, it was found that the welded thermocouples used in these series of tests could be used with standard temperature versus millivoltage thermocouple calibration tables.

In the thermocouple measuring circuit, Fig. 3.7, the standard method of using one thermocouple junction as a reference or cold junction in an icewater bath in series with another thermocouple junction which is the measuring or hot junction was employed. The recording galvanometer and any necessary damping resistances are in series with the hot and cold junctions to complete the measuring circuit.

In the thermocouple calibration circuit, Fig. 4.1 , the hot and cold junctions of each thermocouple were electrically insulated from each other and placed together so that they would be at the same temperature. A 1.5-volt dry-cell battery was used as the excitation voltage of the circuit to simulate a temperature rise. The decade resistance in series with the 1.5-volt battery was used to control the excitation voltage. A Rubicon null-balancing bridge millivoltage potentiometer was used to measure the voltage across the resistance of the galvanometer and thermocouple. The 100,000 ohm resistor shown in Fig. 4.1 was placed in series with the 1.5 volt source only when small millivoltages corresponding to room temperature levels were desired. The thermocouple calibration procedure was as follows:

1. A signal of either 1.32 mv or 1.01 mv was applied to the galvanometer and thermocouple circuit, depending on whether the thermocouple was iron-constantan or copper—constantan, to simulate

a room temperature of 78°F with a cold junction of 32°F, which was the reference temperature used during the test program.

2. Temperatures (up to 700°F for copper-constantan thermocouples and up to 1200°F for iron-constantan thermocouples) were simulated by first unbalancing the Rubicon potentiometer to a millivoltage corresponding to a desired temperature. By rebalancing the potentiometer, the millivoltage corresponding to the desired temperature acted across the galvanometer and thermocouple circuit. With the Rubicon rebalanced the deflection of the galvanometer was recorded.
3. Step (2) was repeated for a series of prescribed millivoltages corresponding to changes of temperature of 40°F. A tabulation of these millivoltage steps and the corresponding deflections were recorded on the Heiland Oscillograph.
4. Steps (1) through (3) were repeated for each thermocouple circuit. As with the strain-gage calibration, an average thermocouple circuit calibration factor in terms of millivolts per 1/50th of an inch galvanometer deflection, mv/δ was obtained for each thermocouple and galvanometer circuit from plots of millivolts versus deflection.

It was only necessary to calibrate the thermocouple circuits once since the same combination of thermocouples and corresponding galvanometers were used on each model for both series of tests. The only variable factor was the resistance of the thermocouple weld, and it was found to be negligible from actual resistance measurements.

4.4 Test Procedure

The conduct of each series of tests was as follows:

1. The static failing bending moment of the box-beams of each of the two series was established at room temperature using two specimens from each series. As mentioned earlier, the strength properties of the beams in the two series differed even though they were of the same material because they were extruded

from different lots which probably experienced different heat treatments. The criterion for failure was selected as the observed buckling load. Both models in each series buckled at loads within 3 percent of one another. When buckling occurred, it was no longer possible to maintain a constant load with the hydraulic jacks, and this served to check the visual observations of buckling. A typical beam with a permanent buckle is shown in Fig. 4.2.

2. The total heat input required for a buckling failure without external loads was determined by subjecting a model from each series to a step-type input from the Mark I radiant heater. The failure in this case was actually due to the deterioration of material properties with temperature which caused the box-beam to buckle under its own weight.
3. A percentage of the observed static failing bending moment established in step (1) was applied to a box-beam which was then subjected to a radiant flux intensity as in step (2) until buckling failure occurred. The time to failure, strains, temperatures, and the deflection of the center of the model were recorded.
4. Step (3) was repeated for loads of 20, 40, 60, and 80 percent of the static failing bending moment for series-1 and for loads of 28, 56, 80, and 90 percent of the static failing bending moment for series-2.

Series-1 employed a radiant flux intensity of 4.0 cal/sq. cm. sec. and that of series-2 was 8.0 cal/sq. cm. sec.

The sequence of test operations for each model was as follows:

1. The heater was brought up to temperature and allowed to stabilize at a position remote from the model.
2. An 18" x 30" x 1/4" steel plate thermal shield shown in Fig. 4.3 was positioned just below the model surface before being exposed.
3. The heater was pulled into position below the model and shield.
4. The model was exposed to the radiant source by suddenly removing the thermal shield.

5. After observed failure, the thermal shield was again interposed between the model and heater and the heater was moved to a remote position.

The exposed surfaces of the box-beams were coated with camphor black to maximize the absorption of the radiant flux and to provide a common surface condition for all the models. Polished aluminum shielding plates 4" x 16" x 5/32" were attached to the pivot points assembly in the same plane as the exposed surface of the models 1/64" from each side to shield the sides of the model from direct radiation. These are shown in Fig. 4.4. In addition, the sides and top surfaces of the models and all leads and equipment which might be exposed directly to the heat source were shielded by wrapping them with aluminum foil.

4.5 Elevated Temperature Properties

Since there was no information available on the elevated-temperature properties of 63S-T5, it was found necessary to conduct a series of elevated-temperature tests on tensile test coupons cut from the two lots of box-beam extrusions. In particular, the variation of the modulus of elasticity with temperature was needed to obtain the correct stress data from the experimental strain measurements.

Standard tensile test coupons were machined from the box-beam material. Each coupon was heated to a predetermined temperature by a small circular oven which was designed specifically to envelop the coupon when mounted in the tensile test machine. An overall view of a typical tensile test coupon as it was held in the testing machine is shown in Fig. 4.5 and the tensile coupon inserted in the oven is shown in Fig. 4.6.

A Calrod heating element was employed in the small oven. This element was formed into a 2-1/2-inch diameter coil 3-inches long and mounted in a 5-inch length of transite pipe 6-inches in diameter. The ends of the pipe were covered with 1/8-inch thick transite plates with 3/16-inch slots at both ends to allow insertion of the tensile coupons. The Calrod heating coil was centered in the transite pipe by three transite spacers. The space between the outside diameter of the heating coil and the inside diameter of the transite pipe was packed with Fiber-Fax. A photograph of the Calrod oven with one of its covers and a portion of the insulation removed is shown in Fig. 4.7. The oven was powered from a 110-volt AC source and was controlled by a Variac to establish the desired temperatures.

Each test coupon was instrumented with three spot welded, No. 28 gage, iron-constantan thermocouples; one was located at the center of the gage length and the other two were spaced one inch on either side of the center, along the gage length. Two Baldwin type EBDF-7D+ strain-gages, one on each side of the center of the gage length of the tensile coupons, were used to measure the strains during the tensile tests. A tensile test coupon instrumented with thermocouples is shown in Fig. 4.8. A Heiland oscillograph was used to record the strain data and a Rubicon potentiometer was used to monitor the temperatures.

A family of experimental stress-strain curves ranging from room temperature to 800°F was obtained for the material of each of the two series. These are shown in Figs. 4.9 and 4.10. An average experimental curve of modulus of elasticity versus temperature was plotted from this stress-strain data and is shown in Fig. 4.11.

In order to facilitate the data reduction process involved in obtaining the stresses corresponding to the corrected strain-gage data, interpolation charts were drawn up based on the curves of Figs. 4.9 and 4.10. The data from these two curves was cross-plotted to obtain faired stresses versus temperature curves for various strain levels for each of the series. These curves were in turn cross-plotted to yield approximate stress-strain interpolation charts for various temperature rises for each of the series as shown in Figs. 4.12 and 4.13.

4.6 High Temperature Strain-Gage Study

The use of strain-gages to obtain the stress distribution in a structure in the presence of high temperatures has been a limiting factor in most experimental stress programs. A strain transducer which is unaffected by temperature and which will yield only the real strains present in a structure regardless of the thermal and static loading is unavailable. The temperature-compensated strain-gages used in this experimental program were guaranteed to be reliable as long as the operating temperatures were below 300°F. However, in this study temperatures as high as 1100°F were experienced. To correct for apparent strains, several experimental tests were performed to determine the amount of temperature compensation required for the type of strain-gage used. This was accomplished by mounting several strain-gages and thermocouples on 5" x 32" x 1/8" 63S-T5 plates which were heated with the Mark I heater at the same rate and in the same manner as the box-beams.

From the oscillograph records of strain and temperature versus time, curves of strain versus temperature were plotted. These curves were all within 10 percent of one another. Therefore, an average apparent strain curve was employed and is shown in Fig. 4.14. Strains of less than 100 microinches/inch were considered negligible and were not corrected.

SECTION V

DATA REDUCTION AND THEORETICAL ANALYSIS

5.1 Experimental Temperatures

The thermocouple data was reduced in the following manner to obtain the experimental temperatures:

1. Oscillograph deflection readings were multiplied by their respective circuit sensitivities to convert to millivoltage readings.
2. Standard thermocouple charts were employed to convert from millivolts to temperatures.
3. A room temperature value of 78°F was subtracted from the above values to yield the actual temperature rises.

Since the box-beams in each series of tests were heated in the same manner, the temperature responses of each series were averaged separately to yield the tabulated results which are included in Tables 5.1 and 5.2 and shown as faired curves in Figs. 5.1 and 5.2. The average temperature distributions around the periphery of the box-beams are shown in Figs. 5.3 and 5.4 for each series of tests at various time intervals. These curves were obtained by cross-plotting the data shown in Figs. 5.1 and 5.2. From physical reasoning it is known that the slopes of the temperature curves at $s = 7$ should be zero; this is not the case with the curves of Figs. 5.3 and 5.4 which casts some doubt on the validity of this representation.

5.2 Experimental Stresses

The reduction of the measured strain data to stresses involves a correction for apparent strain due to temperature beyond the compensated range of the strain-gages and a correction for the reduction in modulus of elasticity with temperature of the material. The following procedure was employed to obtain the experimental stresses:

1. The oscillograph strain deflections were multiplied by their respective circuit strain sensitivities to obtain the uncorrected strain values.
2. Using Fig. 4.14, the apparent strains corresponding to the temperatures associated with the uncorrected strain data are determined and these are added algebraically to obtain the corrected strain.

3. Using the values of corrected strain and the corresponding temperature rises at each gage location the stress-strain interpolation charts, Figs. 4.12 and 4.13, were used to obtain the stresses.

These stresses are tabulated in Tables 5.3 through 5.12 for each model tested. The stress time histories for model 10 of the series-2 tests are shown in Fig. 5.5. The time scale refers to exposure to the radiant heat step input of 8 cal/sq. cm. sec. At zero time the external static bending moment is evidenced by the initial stresses shown. When the tension cover is heated, the stresses at locations S_1, S_2, and S_3 are seen to be initially relieved. Because the tension cover is heated, the neutral axis shifts in the direction of the unheated cover and leaves gage S_5, which originally corresponded to the neutral axis position, in the tension regime. This behavior is evidenced by the time history of S_5 in Fig. 5.5.

5.3 Theoretical Analysis

In addition to the experimental program, the temperatures and stresses were predicted analytically employing the theoretical approach presented in reference 5.1. Briefly, the theoretical solutions are based on a finite-difference technique. The cross-section of the box-beam was divided into 54 elements and the following assumptions were employed:

1. The heat input to the exposed box-beam surface is a constant time-wise step input with a known chordwise variation.
2. The initial temperature distribution in the model is uniform.
3. No temperature gradients exist across the box-beam wall thickness. (The temperature in any element at any time is uniform.)
4. Spanwise heat flow is negligible.
5. Heat losses by convective cooling and reradiation are negligible.
6. The thermal properties of 63S-T5 are constant with respect to temperature.

The system of heat balance equations used can be summarized in matrix form as demonstrated in reference 5.2, namely;

$$\left\{ T_{i,j} \right\} = \left\{ \begin{matrix} \text{Heat} \\ \text{Input} \end{matrix} \right\} + [u] \left\{ T_{i,j} \right\} \qquad (5.1)$$

where

$\left\{ T_{i,j} \right\}$ is a column matrix of the temperature of the i^{th} element at the j^{th} time increment.

$[u]$ is a square matrix of coefficients comprised of the area of the element, the heat transfer coefficient, the specific heat of the material, and the density of the material; all of which are constant.

$\left\{ \begin{matrix} \text{Heat} \\ \text{Input} \end{matrix} \right\}$ is a column matrix of the thermal step input.

$\left\{ T_{i,j-1} \right\}$ is a column matrix of the temperatures of the i^{th} element during the previous time increment, $j-1$.

The above system of equations were solved using the M. I. T. Whirlwind I Computer. The temperatures calculated at specific locations, including the instrumented points, are given in Tables 5.13 and 5.14 for 5-second intervals for each series of models. The series-1 program was computed for 25 seconds of heating time and series-2 program for 15 seconds of heating time.

The stress analysis is based upon the above temperature distribution. The basic equations are presented in references 5.1 and 5.2. In the present solution, the modulus of elasiticity and the coefficient of thermal expansion are allowed to vary with temperature in a manner to be described. The static bending moment can be written as a separate term in the expression for bending moment since it is independent of temperature. The expression used for the total stress in the i^{th} element at any time in summation form is:

$$\sigma_i = -E_i \alpha_i \Delta T_i + \frac{E_i \sum_{i=1}^{54} E_i \alpha_i \Delta T_i A_i}{\sum_{i=1}^{54} E_i A_i}$$

$$+ E_i Z_{ie} \frac{\left(M_{ST} + 2 \sum_{i=1}^{54} E_i \alpha_i \Delta T_i Z_{ie} A_i \right)}{2 \sum_{i=1}^{54} Z_{ie}^2 E_i A_i} \qquad (5.2)$$

where the subscript i refers to any element and

σ = the total stress at any time,

E = the modulus of elasticity,

α = the coefficient of thermal expansion,

ΔT = the change in temperature from a uniform reference temperature,

A = the cross-sectional area,

Z_{ie} = the distance from the neutral axis of the section to the centroid of the i^{th} element, and

M_{ST} = the static bending moment.

The modulus of elasticity, E, and the coefficient of thermal expansion, α, are functions of temperature and are defined by the following expressions:

$$E(\Delta T) = [\,10 + 4.6539 \times 10^{-4}\Delta T - 1.2446 \times 10^{-5}(\Delta T)^2\,]\text{psi} \tag{5.3}$$

$$\alpha(\Delta T) = [\,13 + 0.00357\Delta T\,] \times 10^{-6} \text{ in/in } ^{\circ}F \tag{5.4}$$

The pertinent equations for obtaining the neutral axis location are as follows:

$$Z_{ie} = Z_i - \overline{Z}$$

$$\overline{Z} = \sum_{i=1}^{54} Z_i E_i A_i \Big/ \sum_{i=1}^{54} E_i A_i$$

where z_i is the distance from the centroid of the model to the centroid of the i^{th} element, and

z is the distance from the centroid to the neutral axis.

This stress analysis was also carried out on the M. I. T. Whirlwind I Computer. Tabulation of the Whirlwind stresses at points corresponding to the analytical temperatures are presented in Tables 5.15 and 5.16, for 5-second intervals for the duration of heating times.

5.4 Correlation

The maximum deviation in experimental temperatures from the average temperatures shown in Figs. 5.1 and 5.2 at any model location in either series was less than 10 percent. This indicates that the radiant flux input was very nearly the same for each model in each series. Comparisons between the experimental and analytical temperature distributions at various heating times for each series of models taken from Tables 5.1, 5.2, 5.13, and 5.14 are shown in Figs. 5.6 and 5.7. It can be readily seen that for temperatures below 500°F the correlation is fairly good; however, above 500°F, particularly in the series-2 case, the correlation is poor. The discrepancies result primarily because of too high an absorptivity value and also the neglect of convective cooling and reradiation in the analytical solution.

Comparison of the experimental stress distributions at various times with the analytical solutions for each model is included in Tables 5.15 and 5.16. The tables indicate that at low temperature levels and/or early times, correlation of stresses is generally good. At late times and/or high temperature levels the correlation worsens because of the discrepancy in temperatures noted above and also because of the limitations in the recording equipment in measuring low stress levels and the coupled effects of high temperatures in the models and stresses beyond the elastic limit.

In the analytical solutions, the stresses are obtained from the calculated temperatures; hence, the errors due to too large a value of absorptivity and the neglect of convection and reradiation effects are inherent in the stress solutions as well. Furthermore, the variation in the modulus of elasticity employed in the analysis is only valid for the elastic range. As the temperature increases, the elastic range of the material is decreased as shown in Figs. 4.9 and 4.10. The approximation expressed by Eq. 5.3 does not take this into account. As can be seen from an examination of the stress-strain curves, Figs. 4.9 and 4.10, and the temperature time history curves, Figs. 5.1 and 5.2, the temperature rises will carry portions of the box-beam beyond the yield point at different times depending on the initial stress distributions. When this happens, this calculation procedure is no longer valid. Therefore, analytical stresses are predicted which correspond to strains which exceed ultimate at the high temperatures; these are included only for illustrative purposes in Tables 5.15 and 5.16.

In general, the agreement between the experimental results and the analytical calculations is good. Probable sources of error which led to the differences between experimental and analytical data are indicated below:

Sources of Error in Experimental Temperature Measurements

1. Inaccurate positioning of thermocouples.
2. Small variations in experimental testing procedures.
3. Inherent small errors in data reduction procedures.

Sources of Error in Experimental Stress Measurements

1. Inaccurate positioning of strain gages.
2. Use of strain gages on 63ST aluminum which were designed primarily for 24ST aluminum.
3. Inaccuracies in the apparent-strain correction curves.
4. Inaccurate definition of elevated temperature stress-strain data because of the limited number of elevated-temperature stress-strain tests.
5. The employment of elevated-temperature stress-strain data derived from tension tests in the compressive stress data reduction.
6. The employment of a modulus of elasticity versus temperature approximation curve in the analytical work where the strain levels were actually beyond the elastic limit.
7. Inherent small errors in data reduction procedures.
8. Small variations in experimental testing procedures.

5.5 Calculation of Buckling Stress at Room Temperature

The buckling stress of the compression cover can be calculated by the formula

$$\frac{\sigma_{cr}}{\eta} = K_s \frac{\pi^2 E}{12(1-\nu^2)} \left(\frac{t_s}{b_s}\right)^2 \qquad (5.5)$$

where Ks is the edge fixity factor. For a structure such as a box-beam, the fixity factor is a function of the configuration and the state of stress in the four sides of the box-beam. The methods of moment distribution have been applied to such problems in Refs. 5.3 and 5.4, and in Ref. 5.3, the method has been extended to the case of a box-beam under pure bending. A factor Ks = 5.5 can be obtained from charts in Ref. 5.3 for the beams tested in these investigations.

The factor η is a plasticity correction factor and will be taken as

$$\eta = \sqrt{E_t/E} \tag{5.6}$$

where E_t is the tangent modulus of elasticity corresponding to σ_{cr} and E is the initial modulus.

Compressive stress-strain data is not available for the materials used. However, if the tensile stress-strain data is used, a value of $\eta = 0.56$ (series-2 material) is obtained for a buckling stress of 18,400 psi. This value is above the yield stress of the material and hence the buckling stress is also the failing stress.

SECTION VI

RESULTS AND CONCLUSIONS

The objectives of the present study were

1. To examine structural behavior under combined loadings,
2. To define failure criteria, and
3. To establish methods for predicting failure.

Structural behavior of the box-beams under the combined loadings of the present series depends primarily on the initial static loading. The initial static loading establishes the heat energy required for failure; for low static loads a large quantity of heat energy is required, whereas for a highly-loaded specimen only a small amount of thermal energy will precipitate failure. Doubling the heat rate input enabled the box-beams to absorb a slightly higher total heat input before failure. The structural behavior of each box-beam for the various combinations of loadings are included in detail in the Tables and Figures following the text.

Two arbitrary failure criteria were employed during the test series to define failure of the box-beams under combined loading; these are

1. The inability of the box-beam to maintain its load carrying capacity under combined loading as evidenced by plastic buckling, or
2. A temperature of 1100°F measured in the exposed cover of the box-beam.

In the case of the two models which were exposed to only the thermal step input, the mode of failure was not actually a buckling failure but rather a material failure of the exposed cover due to the high temperature levels inposed. The criterion of a maximum 1100°F temperature rise in the exposed cover represents the condition at which the exposed cover was observed to sag and had the test been allowed to proceed the heated covers of the box-beams would have collapsed under their own weight.

For the models carrying an initial static load, the addition of thermal stresses and the reduction in strength associated with the elevated temperatures caused buckling of the box-beams. The heavy face plates of the box-beams which gave a small ratio of width to thickness, b/t, meant that plastic buckling would be likely to occur and also that failure would occur at the same time. Visual observation of the box-beams and the hydraulic pressure gages gave a good indication of when buckling occurred. A maximum reading and/or sudden reduction in the pressure gages made evident the inability of the box-beams to sustain any further load because of buckling.

Table 6.1 lists the percentages of static failing bending moment applied to each of the beams in each of the series along with the corresponding failure time due to combined loading. Also included in the table are the quantities measured and comments on each of the models. The failure static bending-moment for each of the series of models is included at the bottom of Table 6.1.

The deflection time-histories obtained using the motion picture camera, dial gage, and stop-watch served as a check on the failure times of the box-beams. A sudden change in the rate of deflection was used as the criterion and these measurements corroborated the failure times established visually. Along these lines, it should be noted that the strain-gage readings gave little or no indication of the failure and thus could not be employed for this purpose.

The failure data presented in Table 6.1 was used to develop a non-dimensional interaction curve which describes the relationship between the external static loading and the thermal loading of the combined loading failure problem. These interaction curves are based on the method of "stress ratios" proposed by Shanley and Ryder, (Ref. 6.1), whereby, the combination of any two types of loading can be written as

$$R_s^x + R_T^y = 1 \qquad (6.1)$$

where

x and y are arbitrary exponents; R_s and R_T are ratios of the applied load to the failure load for each of the loading modes.

In the present case, R_s represents the ratio of static bending moment to static failure bending-moment of the box-beam and R_T represents the ratio of total thermal energy applied to the total thermal energy required for failure with no external static load applied. The interaction curves for the two series of tests are shown in Fig. 6.1. It should be noted that since step thermal inputs were used, the ratio, R_T, also represents the ratio of failure time for each combined loading model to the failure time of the thermal model.

The exponents of Eq. 6.1 were determined for the "best fit" curves of both series of tests represented in Fig. 6.1 and resulted in the following expressions:

for Series-1 (q = 4.0 cal/sq. cm. sec.)

$$R_s^{1.4} + R_T^{1.0} = 1 \tag{6.2}$$

for Series-2 (q = 8.0 cal/sq. cm. sec.)

$$R_s^{1.6} + R_T^{2.1} = 1 \tag{6.3}$$

The straight line shown in Fig. 6.1 represents values of combined loading which could be added algebraically. Beyond this line, direct superposition is not valid in defining failure; instead, failure must be defined by such conditions as expressed by Eqs. 6.2 and 6.3. However, the straight line of Fig. 6.1 could be termed a conservative failure criterion.

The curve for Series-2 in Fig. 6.1 has a greater curvature than that for Series-1 which indicates that the box-beams were able to absorb more thermal energy for the same static loading before failure occurred when the rate of heat input was doubled. This is also indicated by the larger exponents of Eq. 6.3 for the Series-2 case.

In all cases, failure was caused either by plastic buckling of the compression covers or material deterioration of the tension covers. The thermal loadings acted to relieve the loadings in the heated or tension covers, and thereby caused a redistribution of the static loading to the web and the compression cover. In addition, the strength properties of the heated cover were depreciated with increasing

temperature and this acted to accelerate this redistribution of loading and fail the model. It is important to note that although the thermal stresses were higher for the higher rate of thermal input, these thermal stresses are not in proportion to the rate of thermal input. The higher rate of thermal input ($q = 8.0$ cal/sq. cm. sec.), meant that the redistribution of loading, reduction in strength properties, and consequent failure would occur in a shorter time; however, because the rate of thermal input was higher, the model was able to absorb a greater total thermal energy before both the effects of conduction and the higher exposed cover plate temperatures could act to cause failure.

An examination of the stresses (see Fig. 5.5) in the top (compression) cover of the box-beam at the instant of failure discloses that there is a considerable variation in magnitude from the lightly-loaded specimens to the heavily loaded specimens. It can be seen from Fig. 5.4 that the temperatures in the compression cover are relatively low; sufficiently low, in fact, so that failure of the compression cover cannot be attributed to material degradation. The decrease in failure stress can be attributed to the change in edge conditions of the compression cover, which depend upon the other three sides of the box-beam. These changes are brought on by the combination of elevated temperatures and stresses. For the heavily-loaded specimens, the edge condition is essentially that given by a fixity factor of 5.5 (see Eq. 5.5) for the light-loaded specimens. The fixity factor corresponding to a buckling stress of 8500 psi (see Fig. 5.5) is less than 4 which is the value for a simply supported edge condition. This means that the compression cover is not failing in the manner of classical plate buckling but rather that the mode of failure must be changing. If the extreme case in which the other three sides have completely melted away is considered, then it is seen that the mode of failure must be as an Euler column and that the cover will buckle in one long wave rather than in the classical square wave pattern associated with plate buckling. Photographs of the specimens after failure tend to support this reasoning. The heavily-loaded beam which failed after a short period of time is shown in Fig. 6.2 with the characteristic plate buckle in the center of the specimen. The lightly-loaded beam which endured a long heating period is shown in Fig. 6.3. In this case there is a slight buckle

with a long wave length in the top cover which is not discernable in the figure. These beams were cut at mid-span through the center of the buckles and the cross-sections of the two beams are shown in Fig. 6.4 and 6.5 for the heavily-loaded and lightly-loaded beam, respectively. The heavily-loaded beam cross-section shows that the buckling of the top cover has caused the other three sides of the box to follow its buckles in the chordwise direction. This buckling failure is characteristic of box-beams under pure bending at room temperature. The lightly-loaded beam cross-section of Fig. 6.5 indicates that the other three sides participate only to a very slight degree in the long wave buckling failure mode of the cover.

Thus, the interaction curves cover three different modes of failure: classical plate buckling, a mode intermediate between plate and column buckling, and near-melting of the tension cover. The use of the third mode of failure to normalize one axis of the interaction diagram is questionable but no alternative scheme has suggested itself.

The experimental program presented in this report was conducted during a period of more than two years. During that time much work related to the combined loading problem, but not actually pertaining to it, was necessary. Improved techniques, new methods, and refinements to existing procedures were continually being sought and examined during the period of investigation.

For example, the radiometers and calorimeters used to obtain the radiant flux intensity of the Mark I heater had to be developed, built, and calibrated before they could be used. The small-oven-heater used to heat the tension test specimens also had to be developed and built. Methods of applying thermocouples to withstand and accurately measure high temperatures in a specimen that is continually deforming were also investigated; likewise for the strain-gages, since their recommended maximum operating temperature was 300°F.

Throughout the experimental program, many ideas were investigated and evaluated. All this work yielded improved methods and added assurance to experimental techniques. It is hoped that the methods and procedures described throughout this report will prove useful to others planning or currently performing experiments dealing with the influence of high temperatures on structures.

REFERENCES

1.1 Loria, J. C., Blackstock, W. J., and Mar, J. W., The Effects of Thermal Radiation on Aircraft Structures, Part I — The M. I. T. Mark I Radiant Heating Structural Test Facility, WADC TR 54-384, Part I, October 15, 1954, Unclassified.

2.1 Alcoa Structural Handbook, Aluminum Company of America, Pittsburgh, Pennsylvania, 1955.

3.1 Williams, F. L., The Combined Effects of High Intensity Heating and Dynamic Loading on a One Cell Box Beam, M. S. Thesis, M. I. T., January 1955.

3.2 Gardon, R., An Instrument for the Direct Measurement of Intense Thermal Radiation, Review of Scientific Instruments, Vol. 24, May 1953.

3.3 Carter, J. A., Research and Development Report on Calibration of Circular Foil Radiometers and Silver Disc Calorimeters, Material Laboratory, New York Naval Shipyard, Brooklyn, N. Y., Laboratory Project 5046-2, Part 11, Final Report, November 1954.

5.1 Timoshenko, S., and Goodier, Theory of Elasticity, McGraw-Hill Book Company, Inc., New York, 1934.

5.2 Schmit, L. A., and Williams, F. L., The Effects of Thermal Radiation on Aircraft Structures, Part II — The Response of A Simple Structure to Radiant Heating, WADC TR 54-384, Part II, February 1, 1955.

5.3 Eggwertz, S. F., Buckling Stresses of Box-Beams Under Pure Bending, The Aeronautical Research Institute of Sweden, Report No. 33, 1950.

5.4 Lundquist, E. E., Stowell, E. Z., and Schuette, E. H., Principles of Moment Distribution Applied to Stability of Structures Composed of Bars or Plates, NACA, ARR No. 3K06, 1943.

6.1 Shanley, F. R., and Ryder, E. I., Stress Ratios, Aviation Magazine June, 1937.

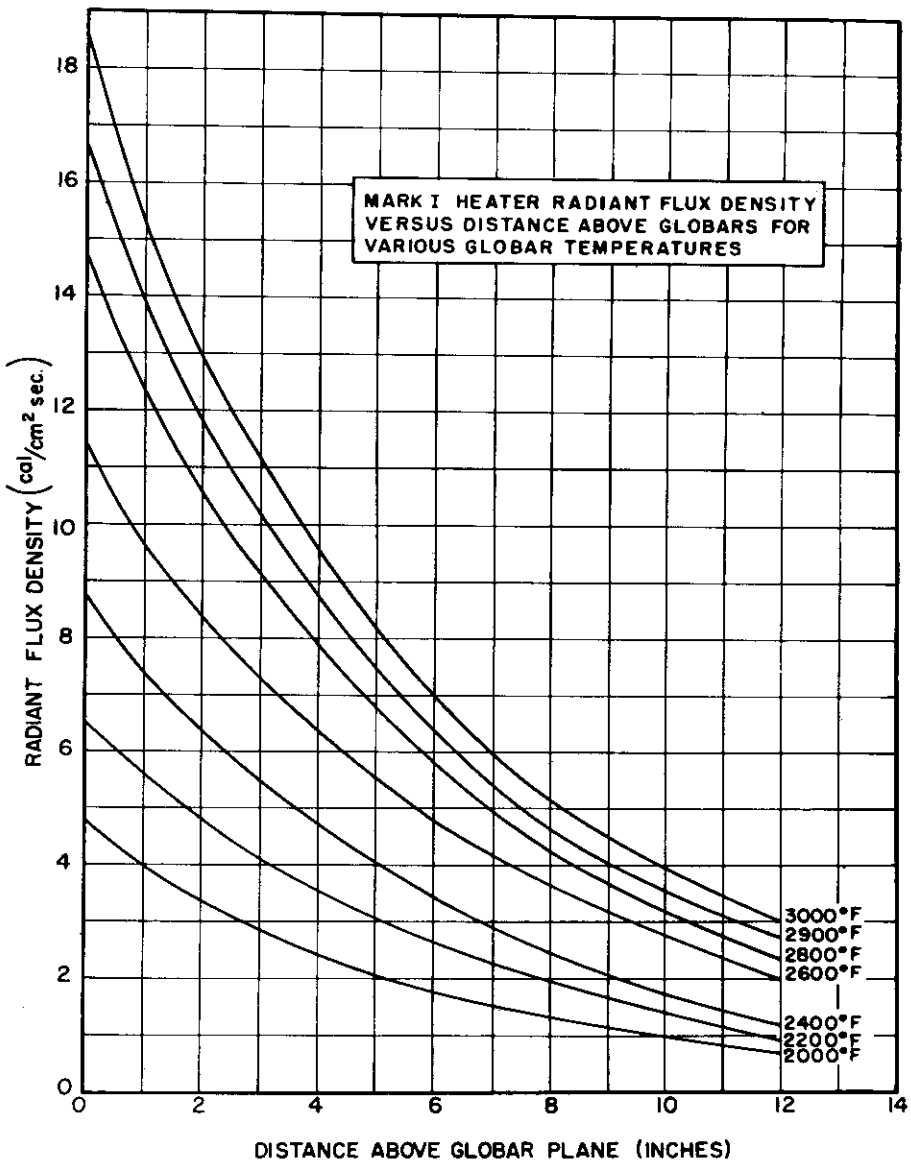

FIG. 1.1 RADIANT FLUX INTENSITY OF MARK I HEATER AT VARIOUS DISTANCES FROM THE GLOBARS FOR VARIOUS GLOBAR TEMPERATURES

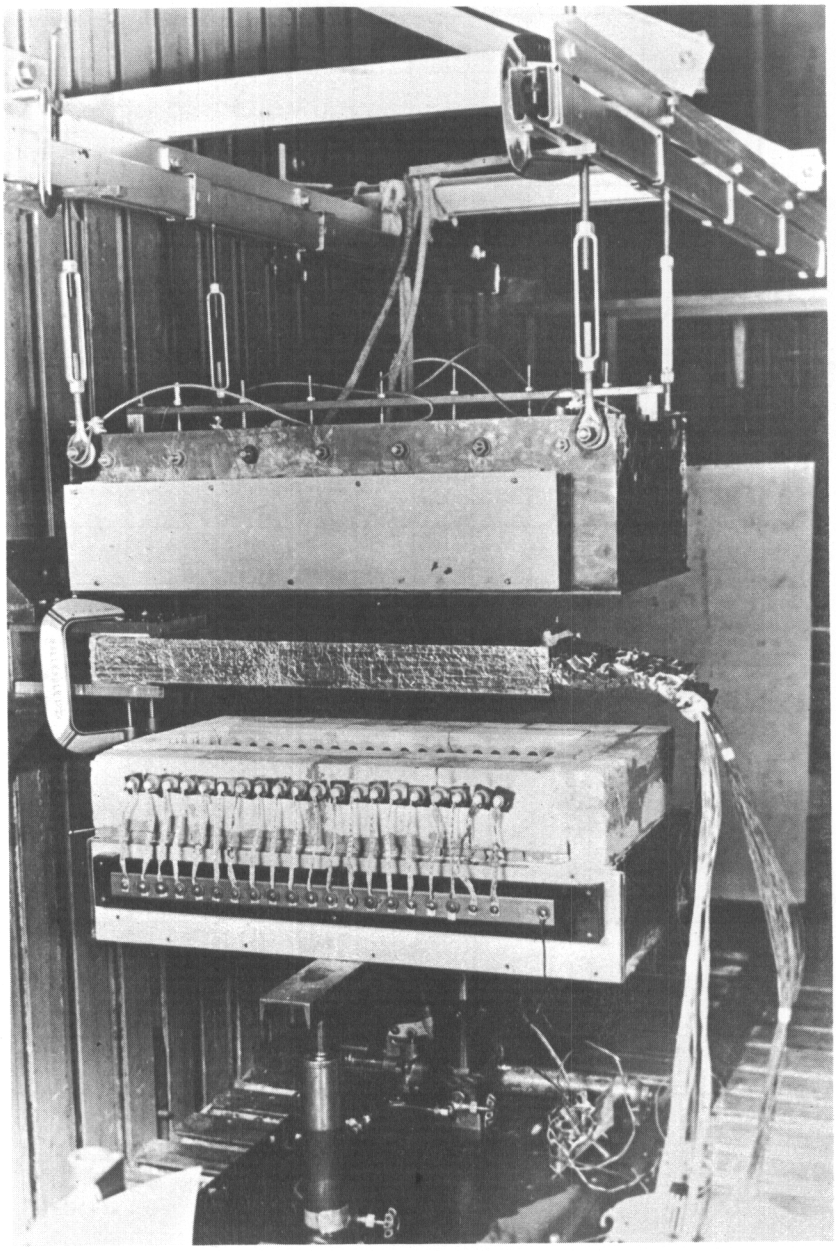

FIG. 1.2 MARK I RADIANT HEATER TEST FACILITY

MODEL SECTION

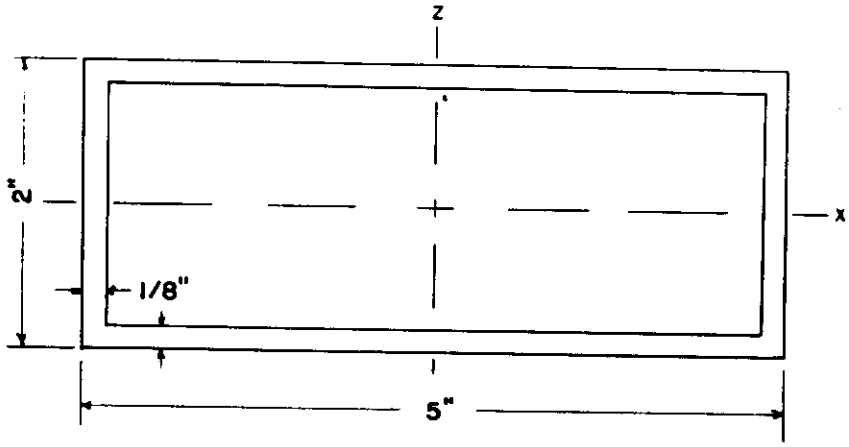

MATERIAL 63S-T5 EXTRUSION

I_x = 1.215 $IN.^4$

C_p = 0.22 BTU/LBS. °F

γ (DENSITY) = 0.098 $LBS./IN^3$

k = 0.00269 BTU/SEC.-IN.-°F

α = 0.125 $IN^2/SEC.$

WEIGHT OF MODEL = 0.1653 LBS./IN.

MODULUS OF ELASTICITY = 10^7 $LBS./IN^2$

FIG. 2.1 CROSS-SECTION OF BOX-BEAM MODEL AND SOME OF ITS ROOM TEMPERATURE MATERIAL PROPERTIES

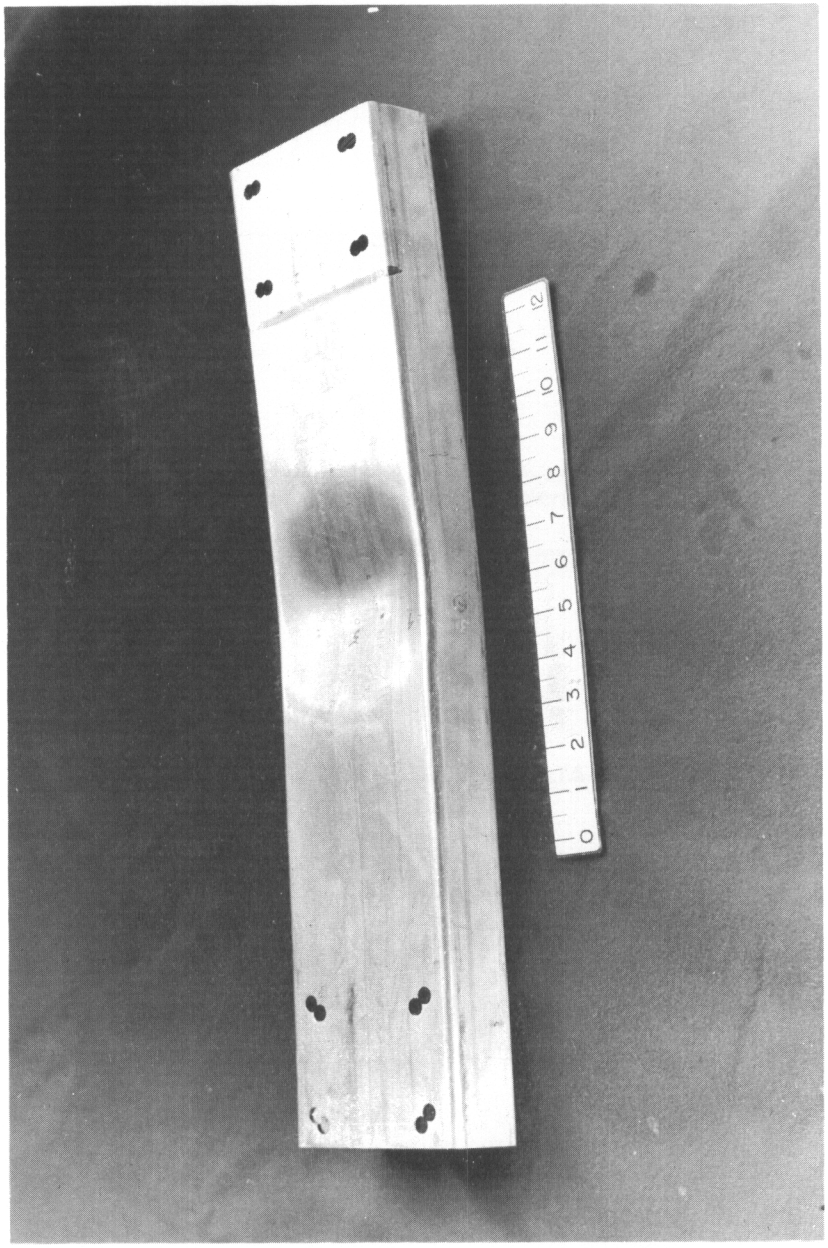

FIG. 2.2 TYPICAL BOX-BEAM MODEL AFTER TESTING

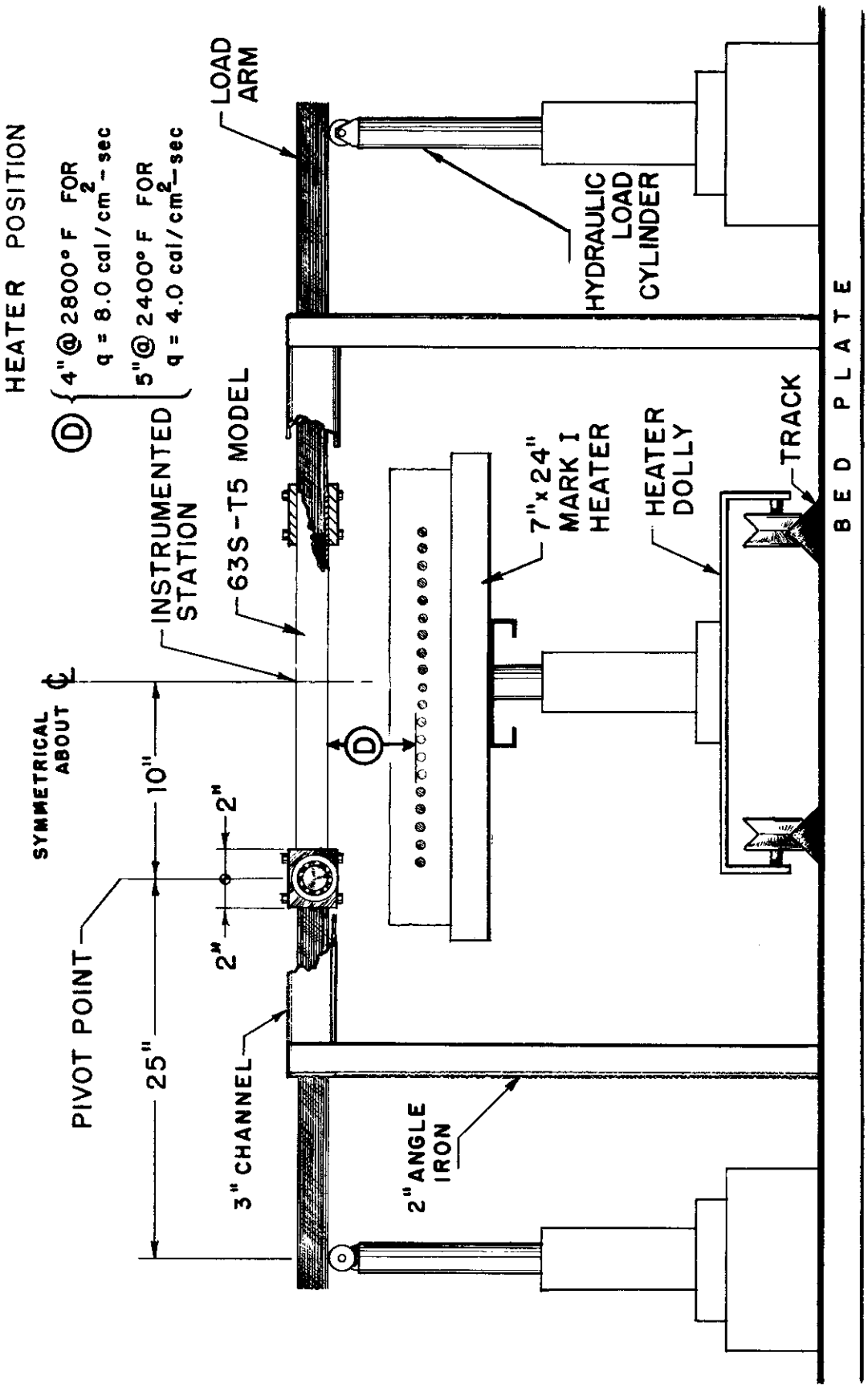

FIG. 2.3 DIMENSIONAL SKETCH OF LOAD SYSTEM, POSITIONING FRAME AND MARK I HEATER

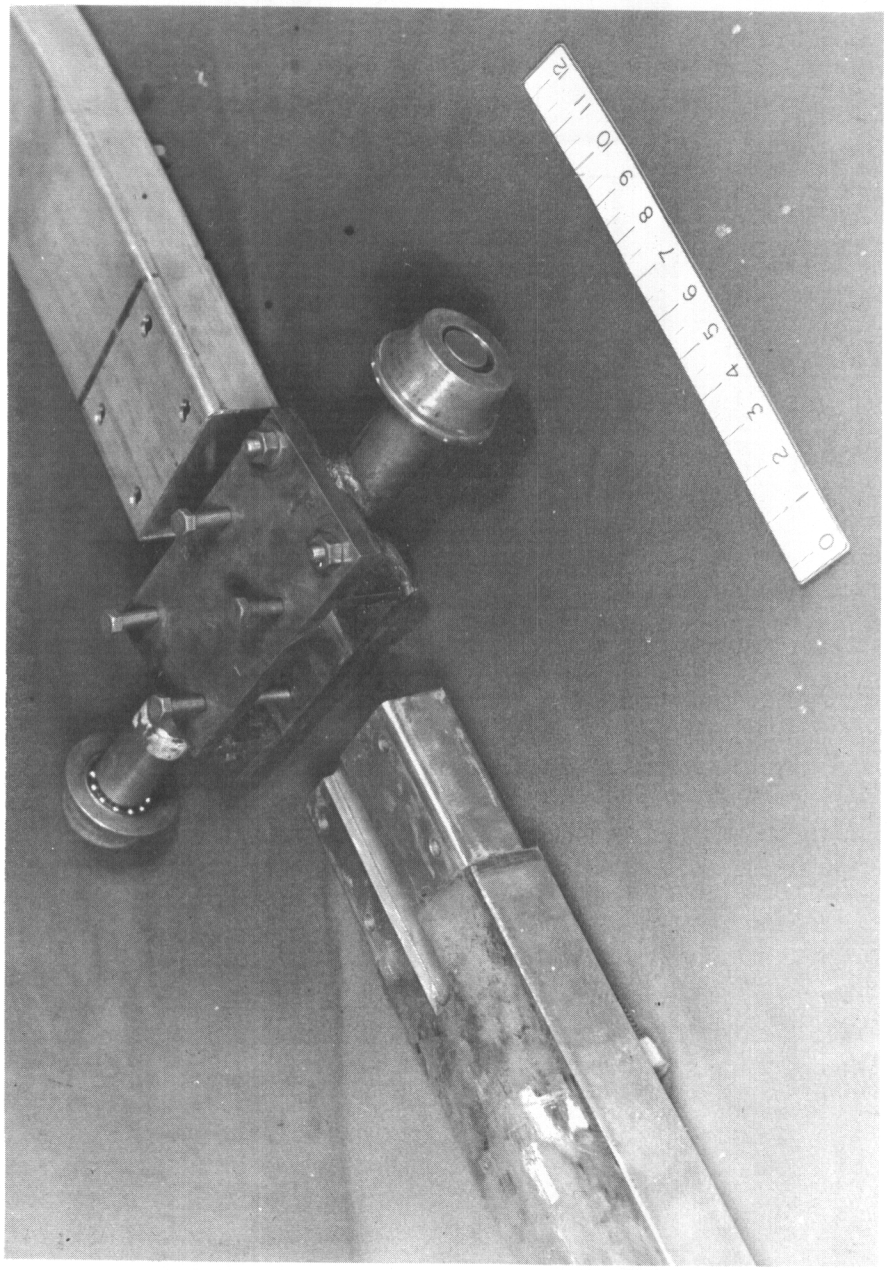

FIG. 2.4 EXPLODED VIEW OF LOAD ARM AND PIVOT POINT ASSEMBLY

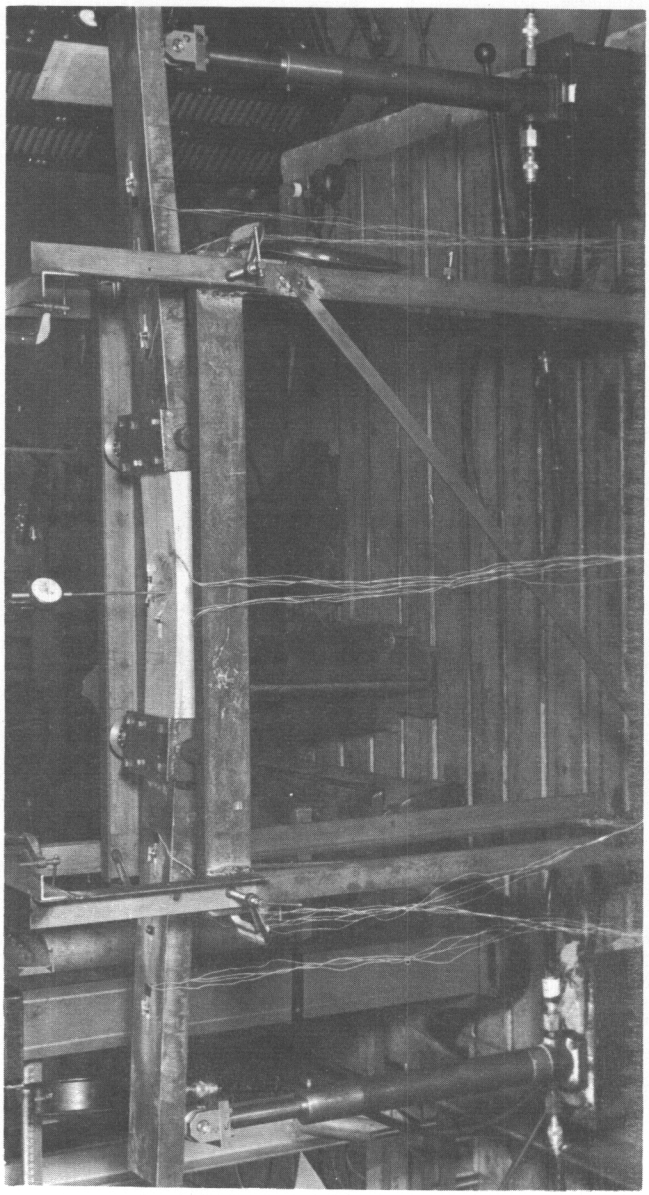

FIG. 2.5 COMBINED LOADING TEST ARRANGEMENT

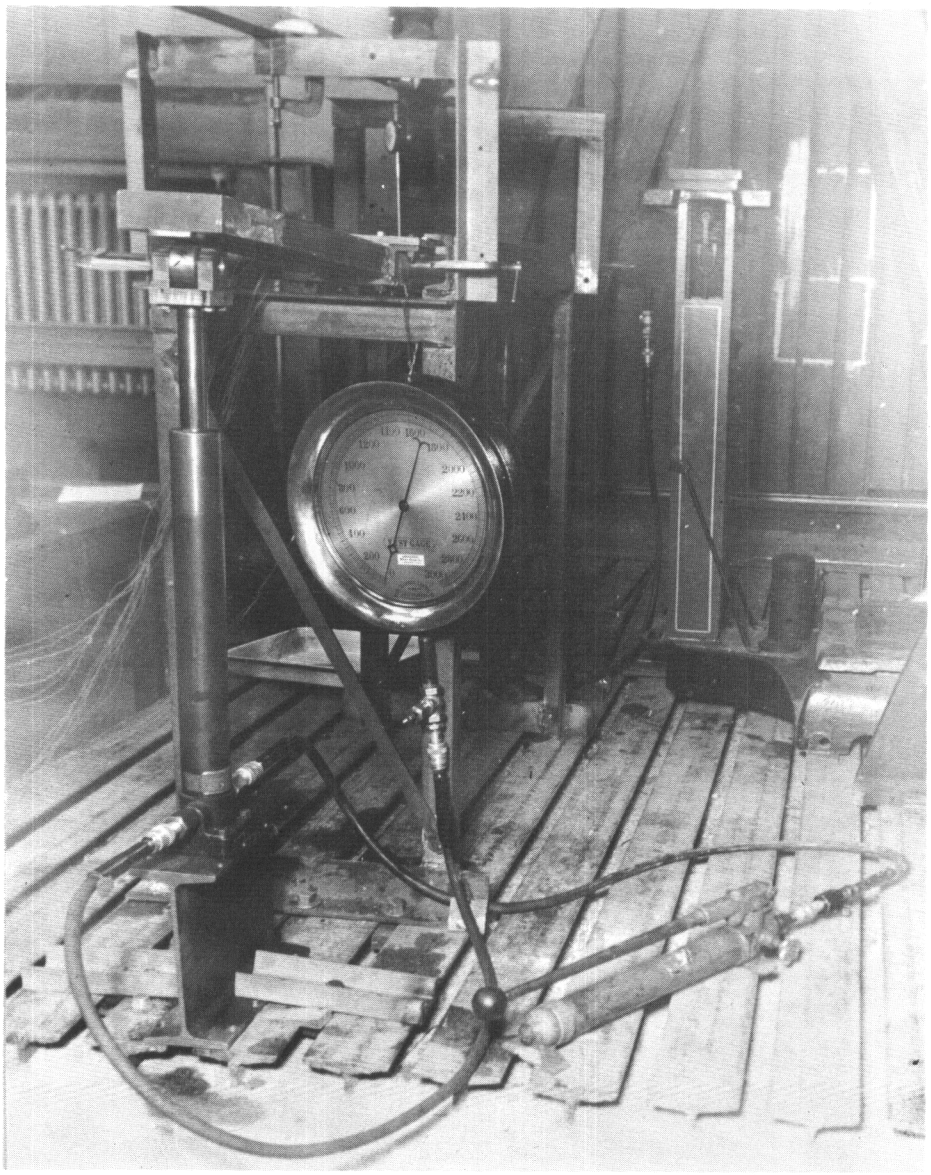

FIG. 2.6 HYDRAULIC LOADING SYSTEM

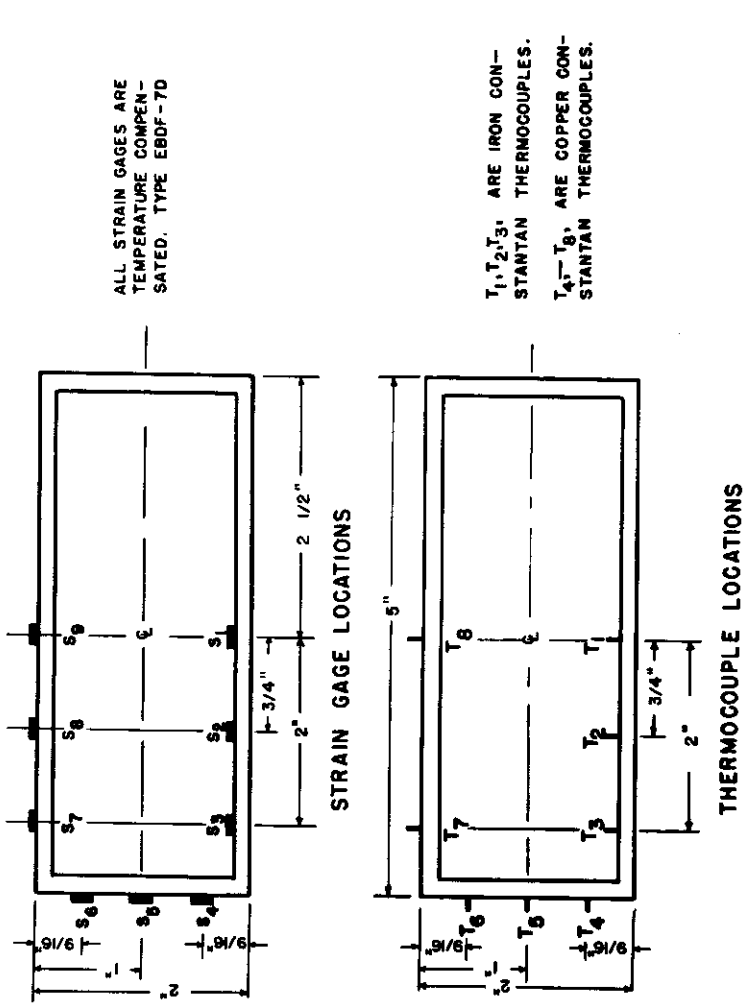

FIG. 3.1 STRAIN GAGE AND THERMOCOUPLE LOCATIONS ABOUT THE PERIPHERY OF THE BOX-BEAM MODELS

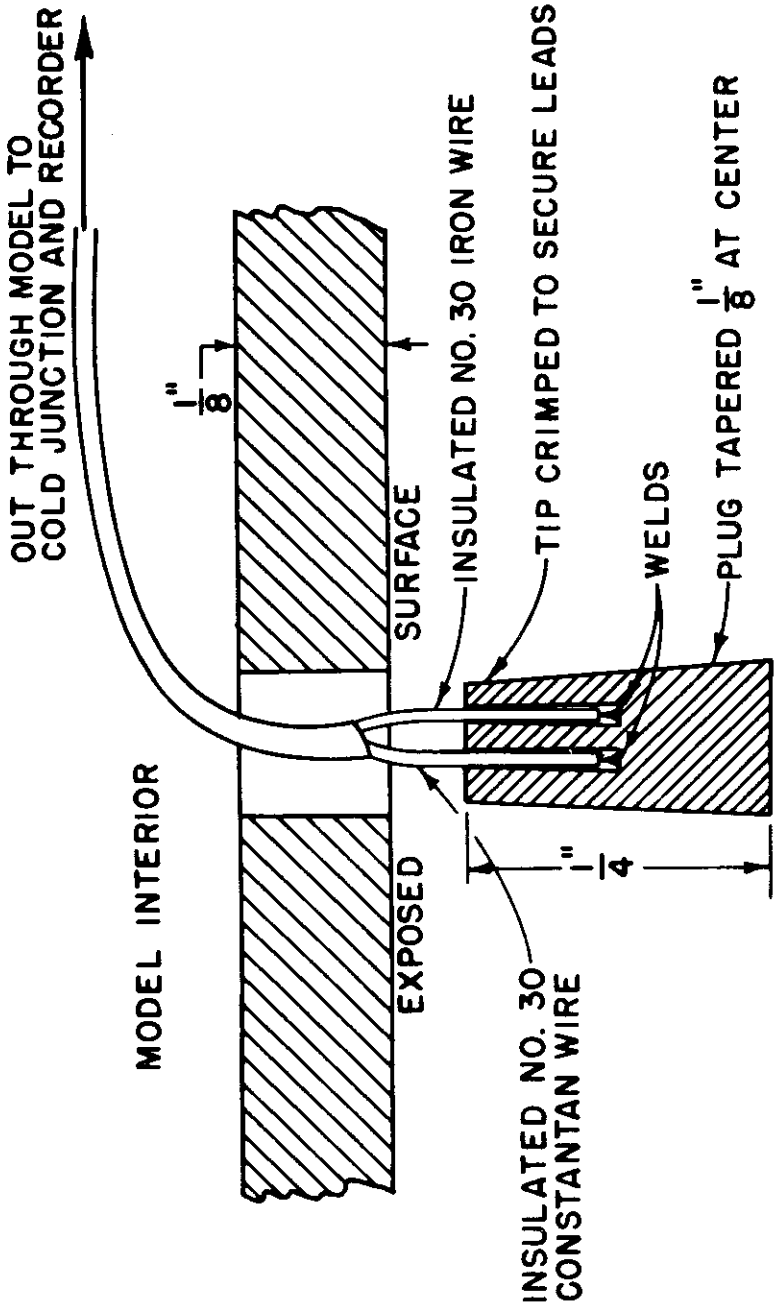

FIG. 3.2 TYPICAL THERMOCOUPLE PLUG

FIG. 3.3 TYPICALLY MOUNTED THERMOCOUPLES

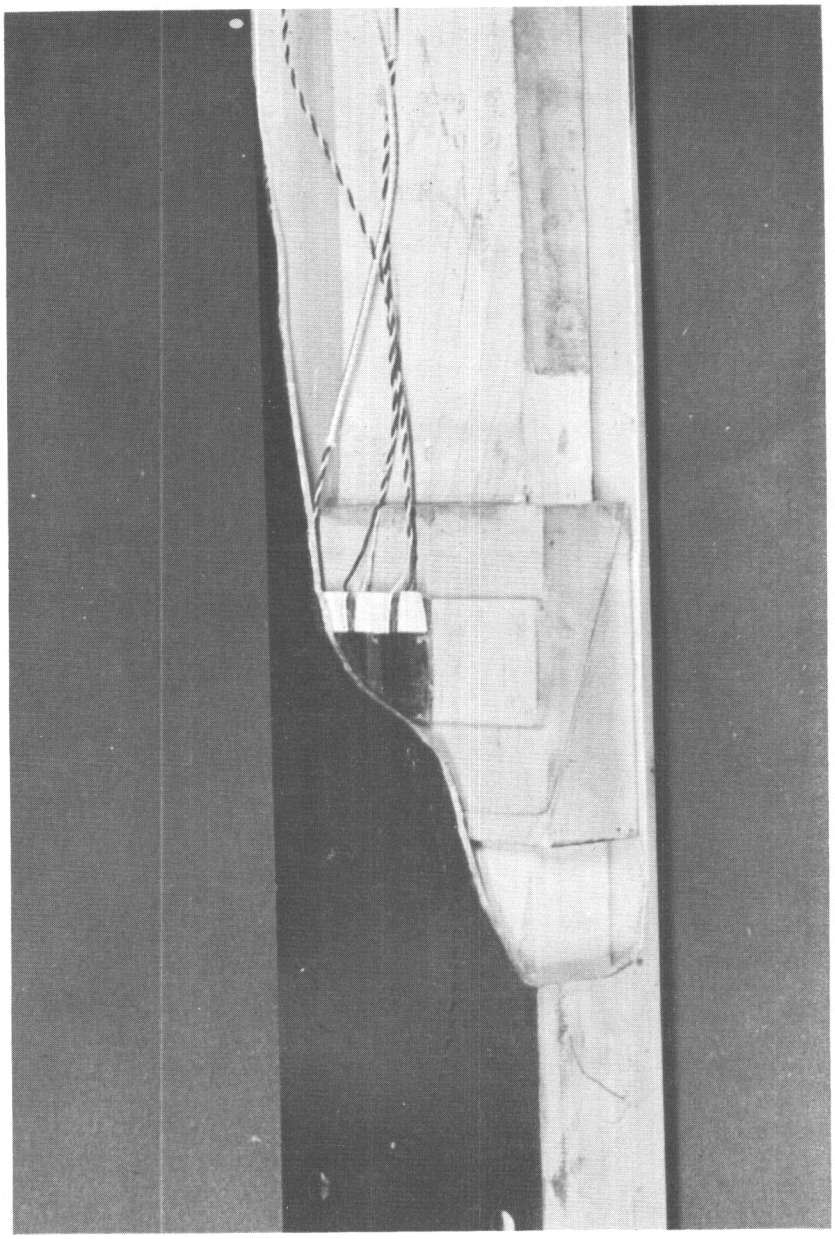

FIG. 3.4 METHOD OF MOUNTING STRAIN GAGES TO INNER SURFACE OF HEATED COVER

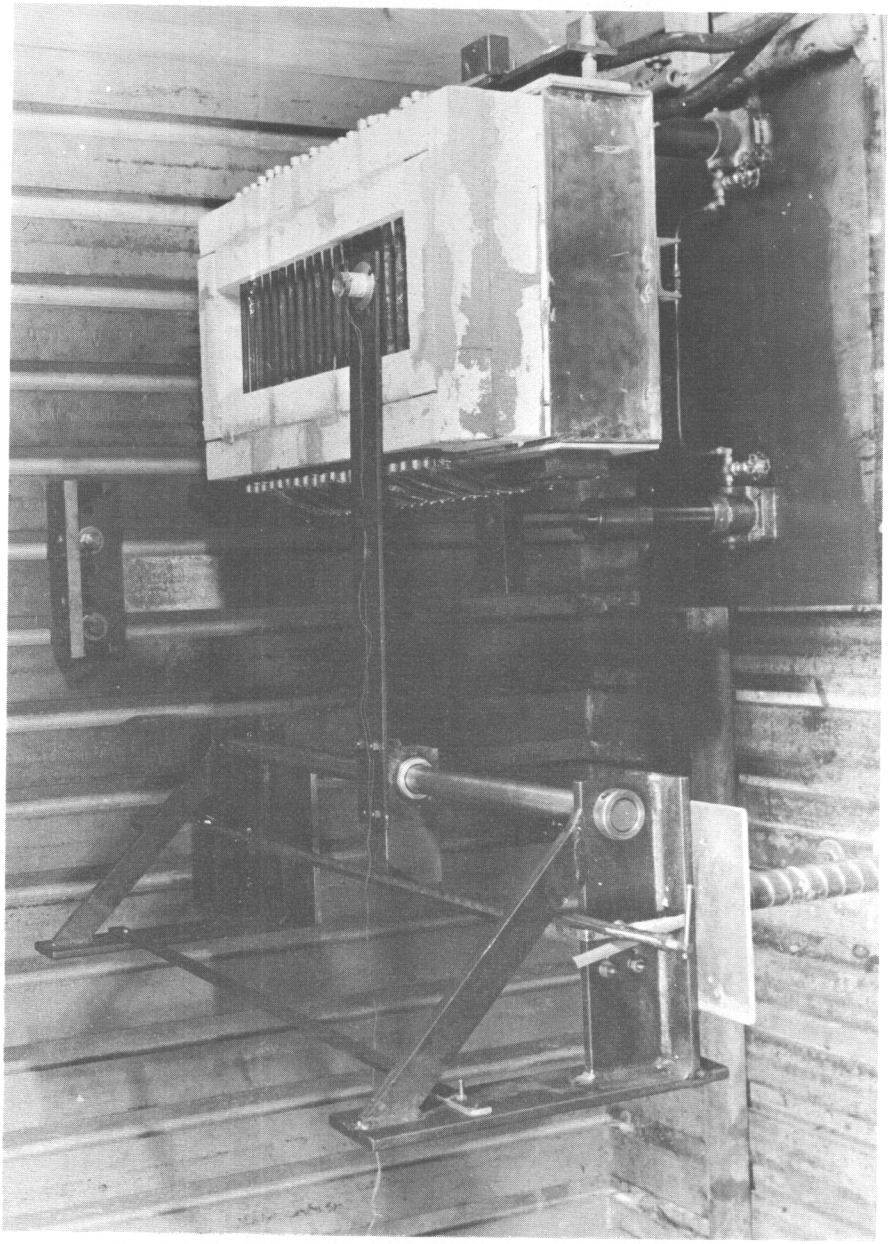

FIG. 3.5 RADIOMETER SURVEY OF MARK I HEATER

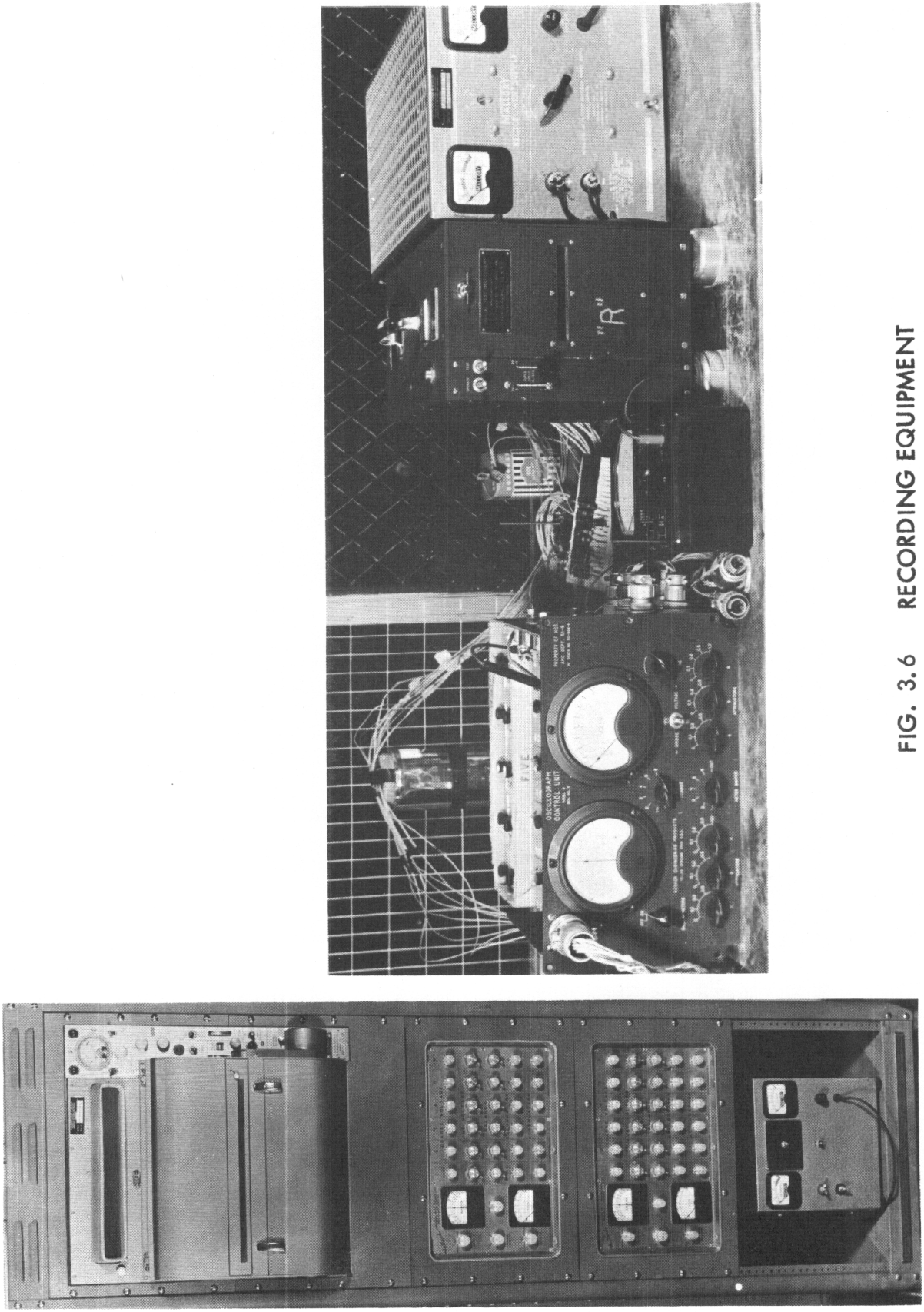

FIG. 3.6 RECORDING EQUIPMENT

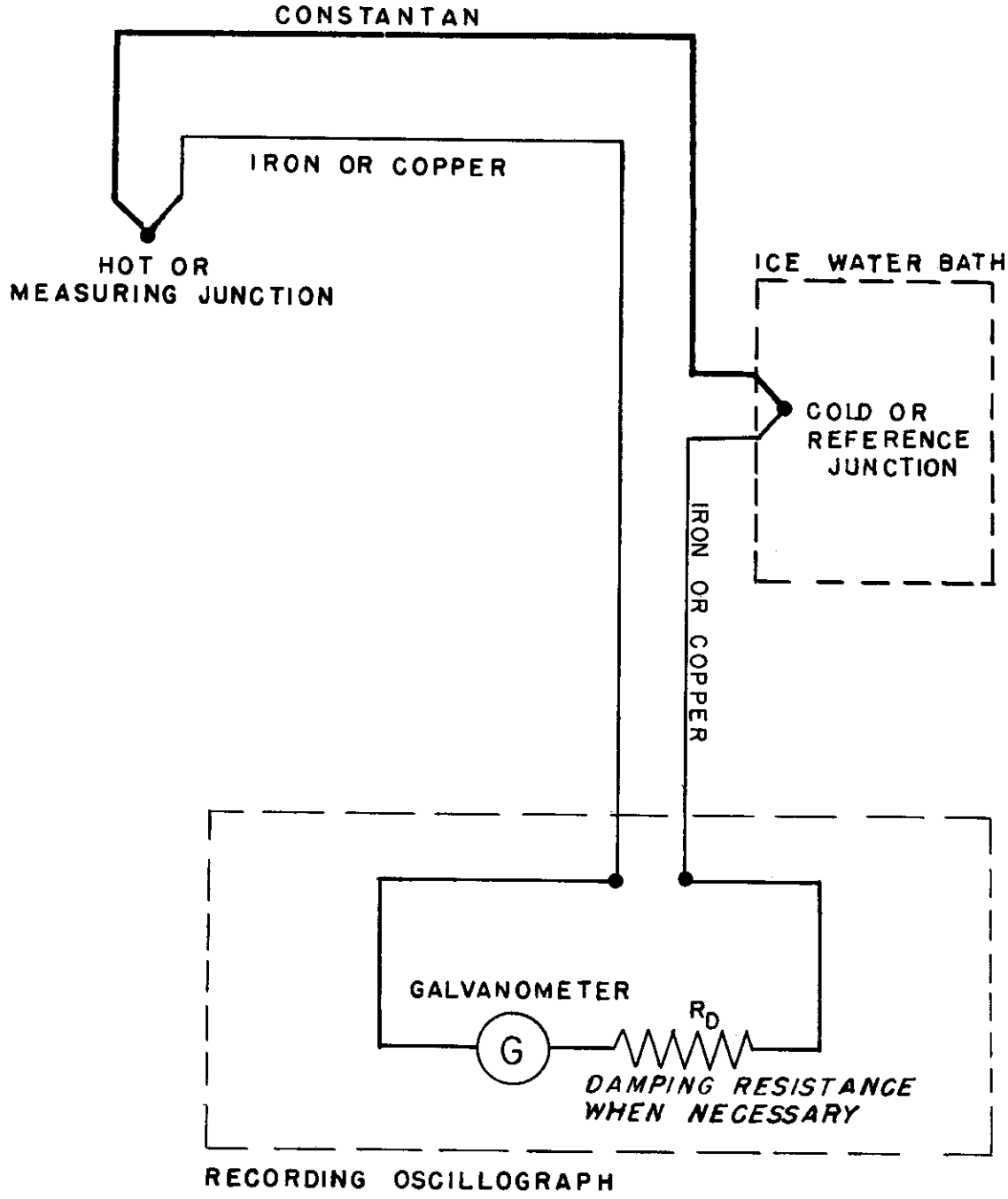

FIG. 3.7 TYPICAL THERMOCOUPLE MEASURING CIRCUIT

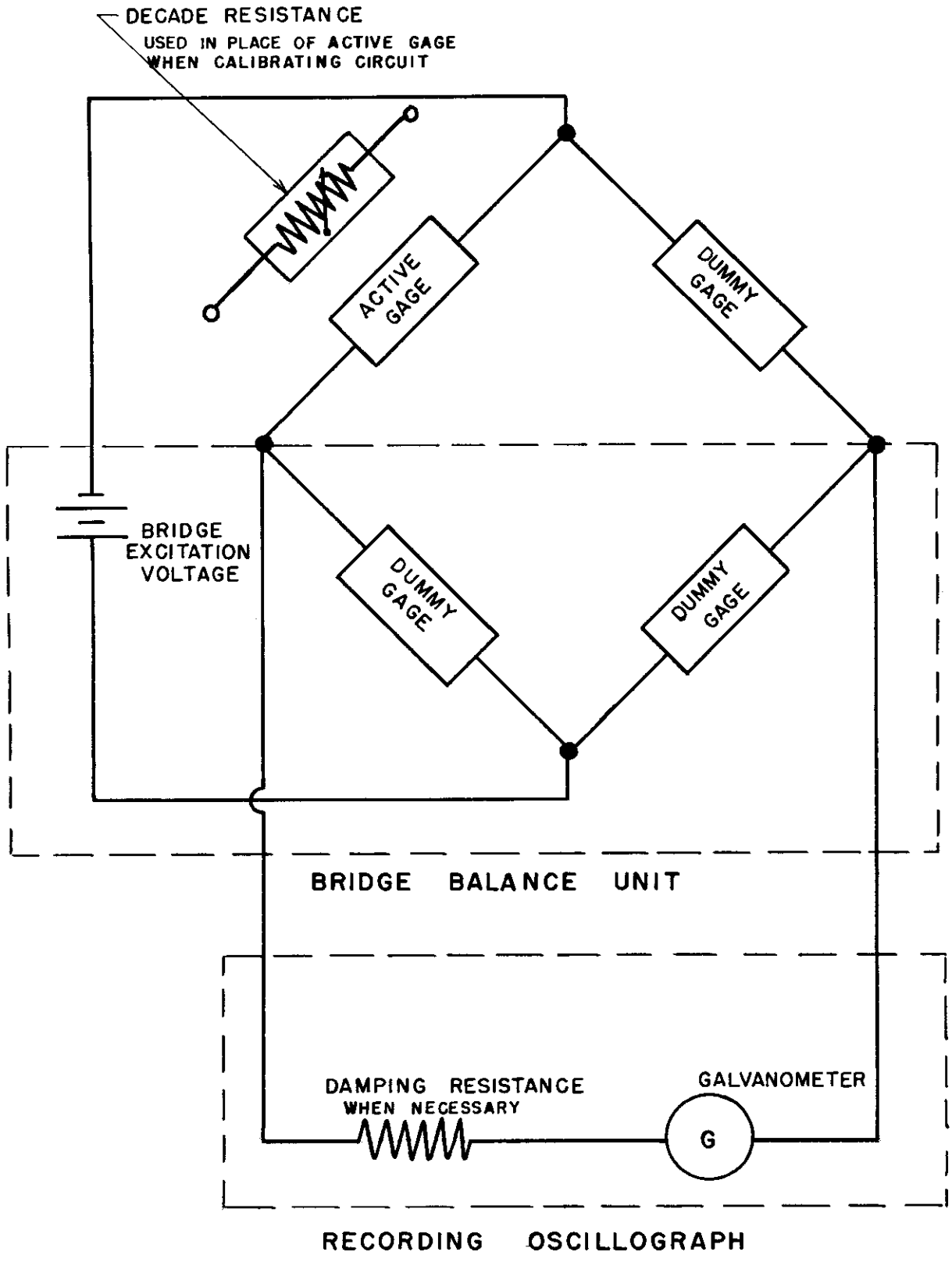

FIG. 3.8 TYPICAL STRAIN-GAGE CIRCUIT

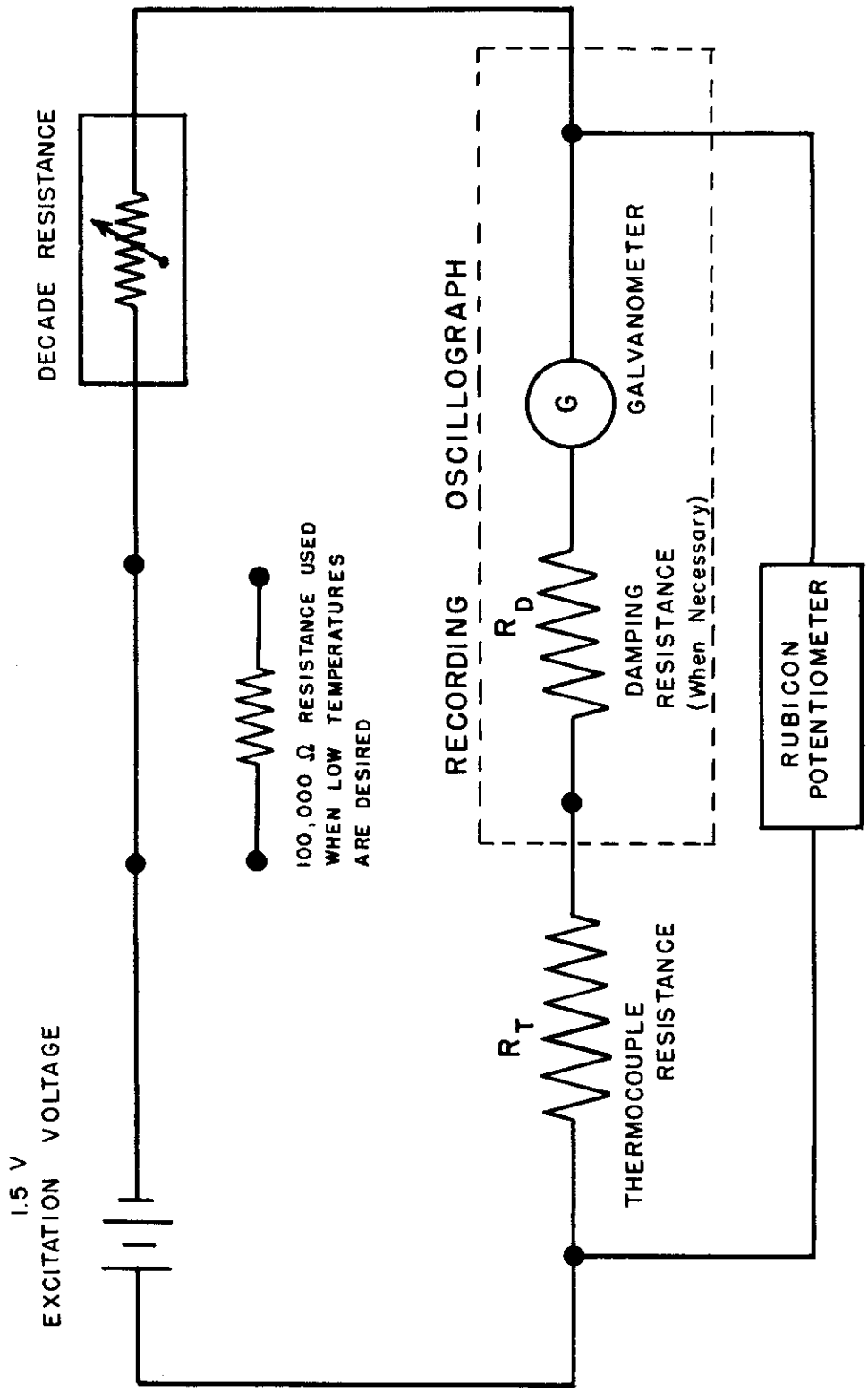

FIG. 4.1 TYPICAL THERMOCOUPLE CALIBRATION CIRCUIT

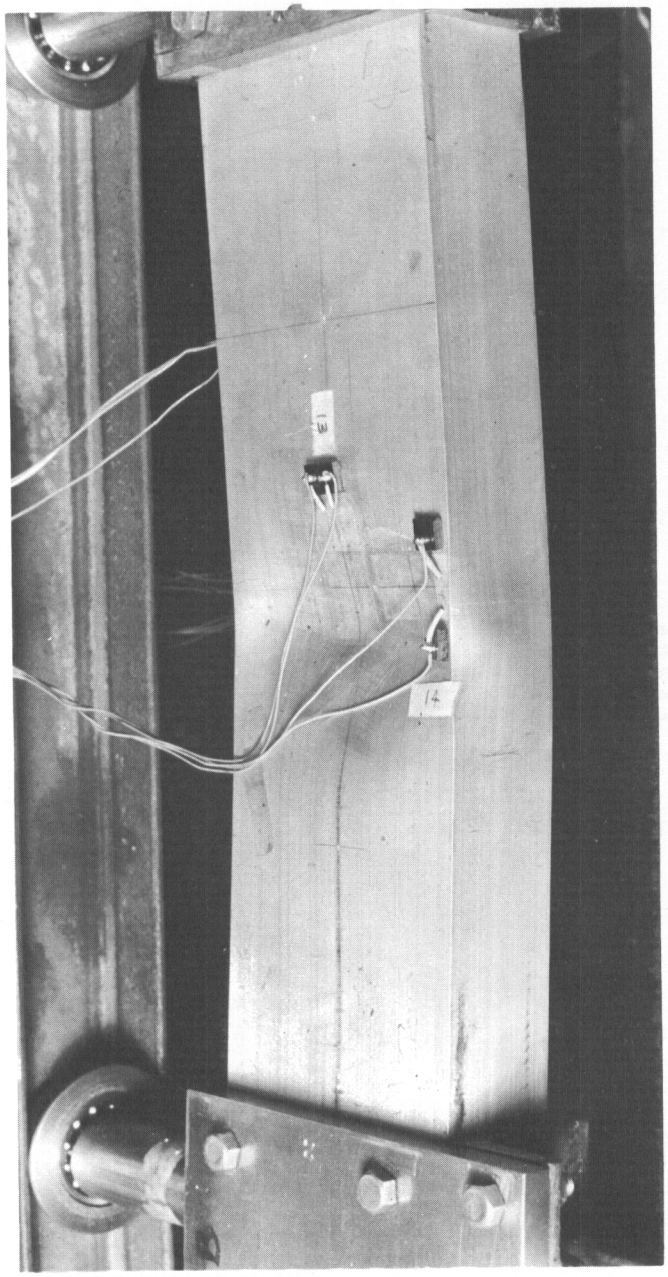

FIG. 4.2 TYPICAL COMBINED LOADING BUCKLE PATTERN

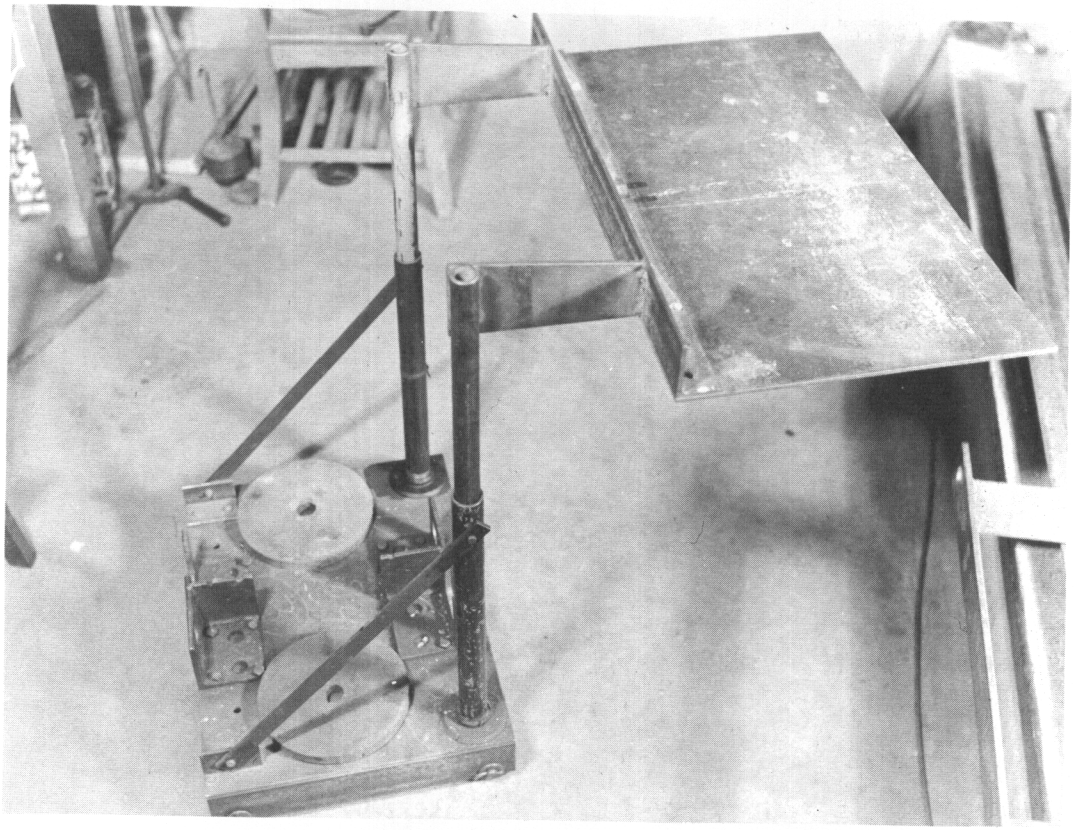

FIG. 4.3 THERMAL SHIELD AND SUPPORTING DOLLY

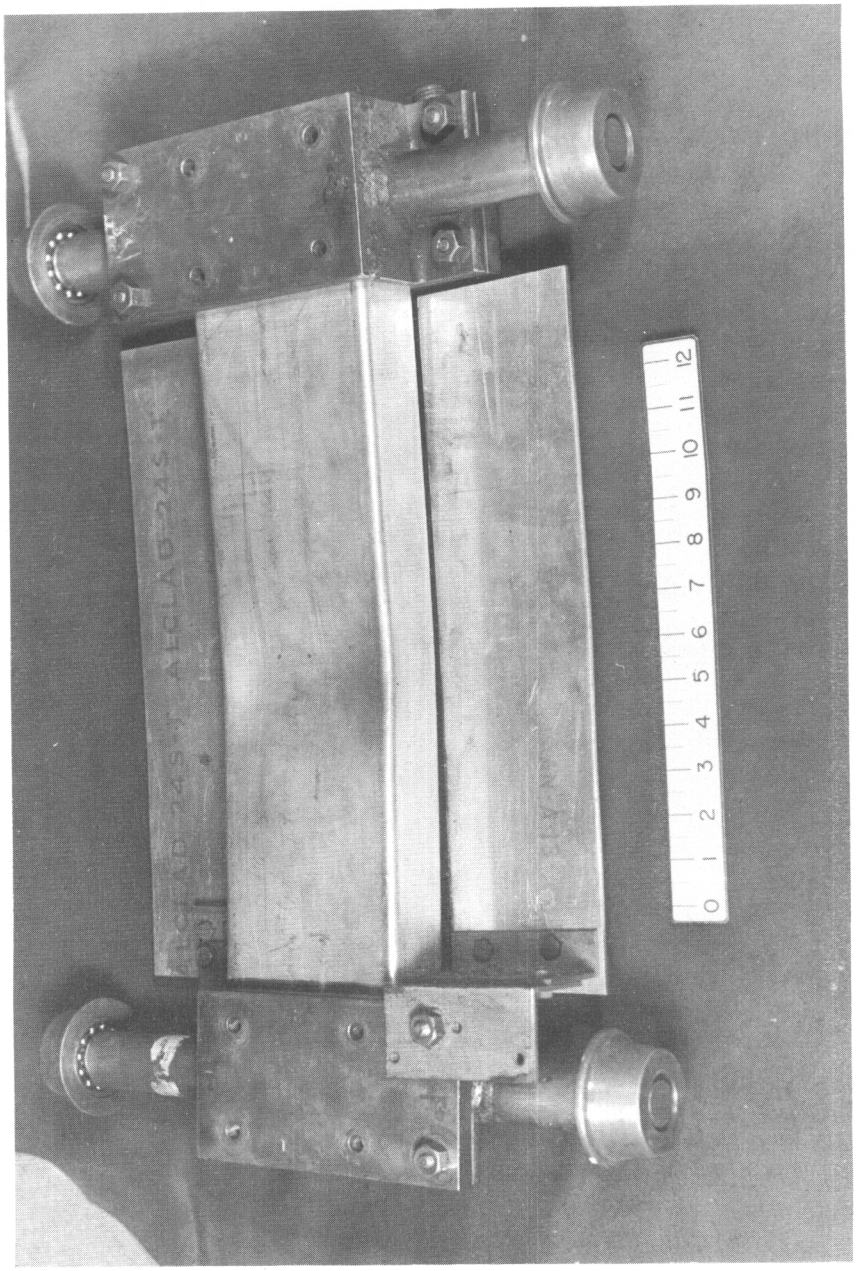

FIG. 4.4 SIDE THERMAL SHIELDS ATTACHED TO PIVOT POINTS

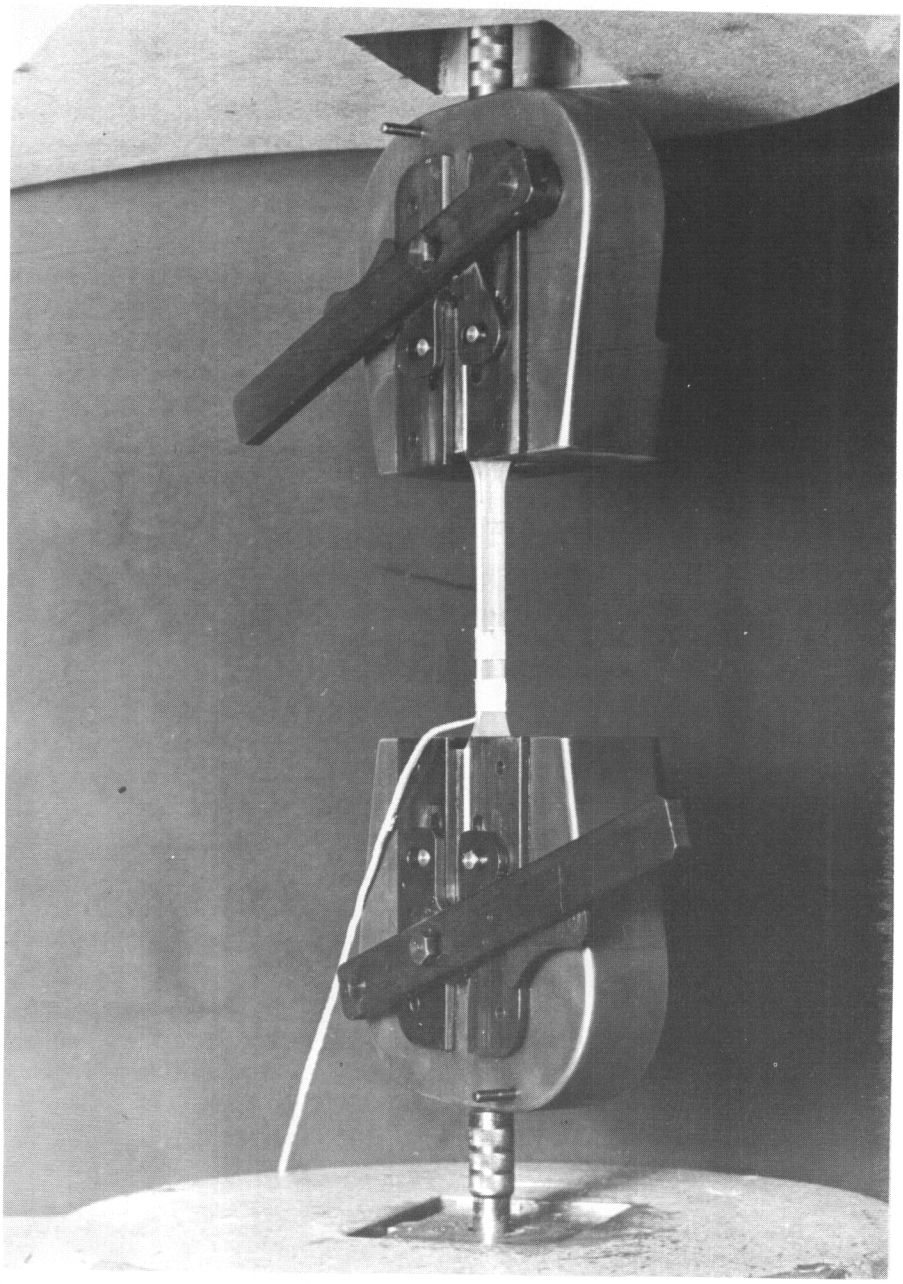

FIG. 4.5 TENSILE TEST ARRANGEMENT WITHOUT CALROD HEATER

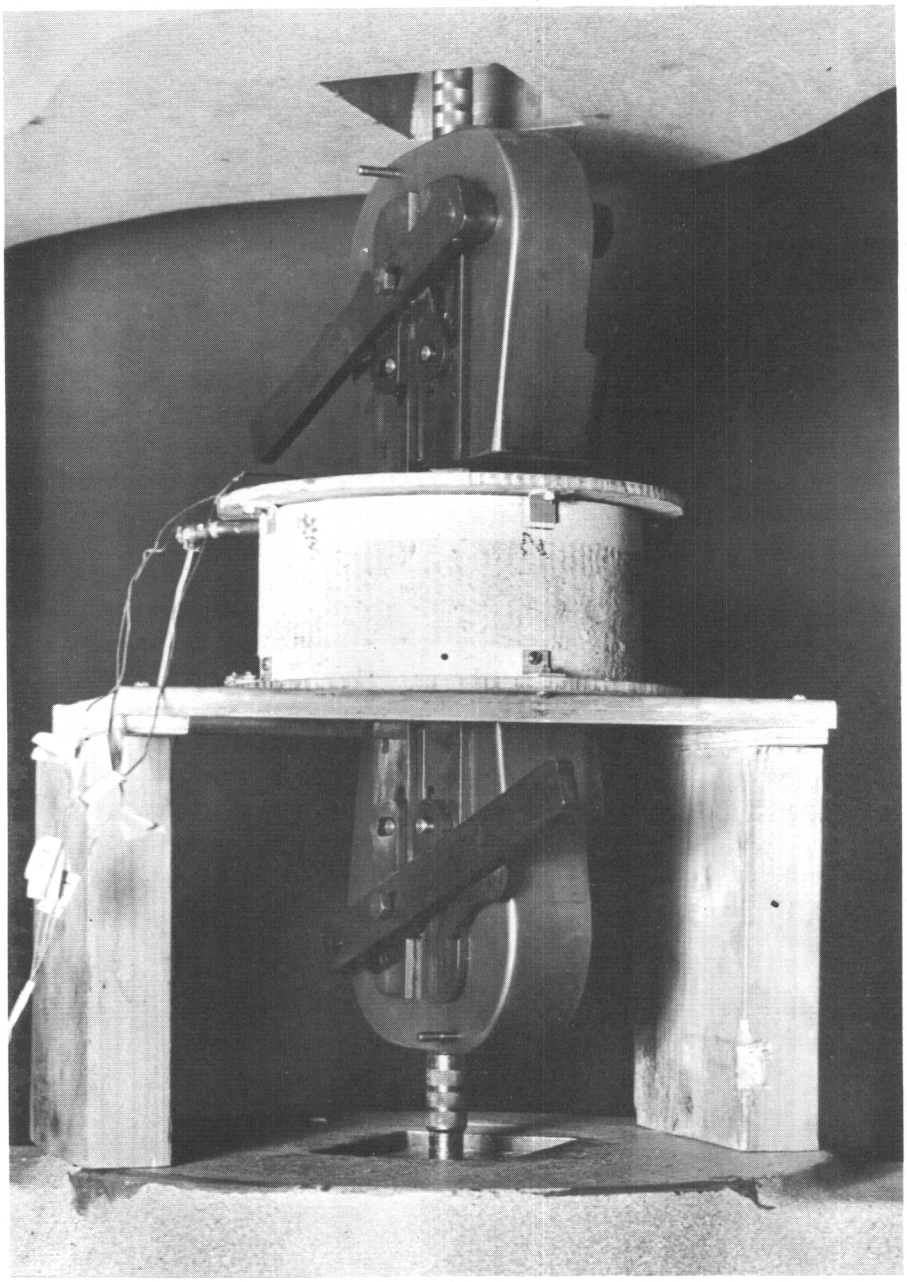

FIG. 4.6 TENSILE TEST ARRANGEMENT WITH CALROD HEATER IN POSITION

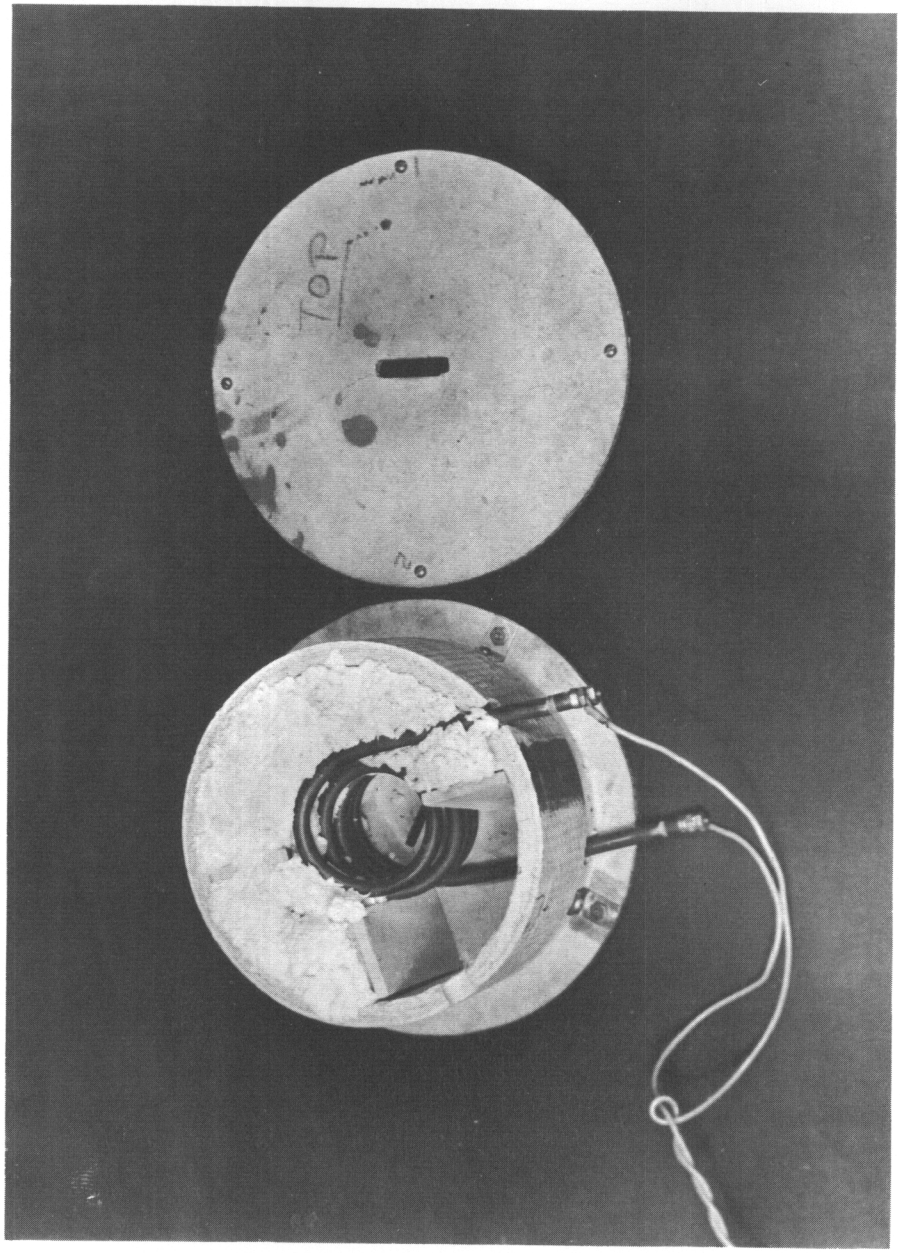

FIG. 4.7 OPEN VIEW OF CALROD OVEN HEATER

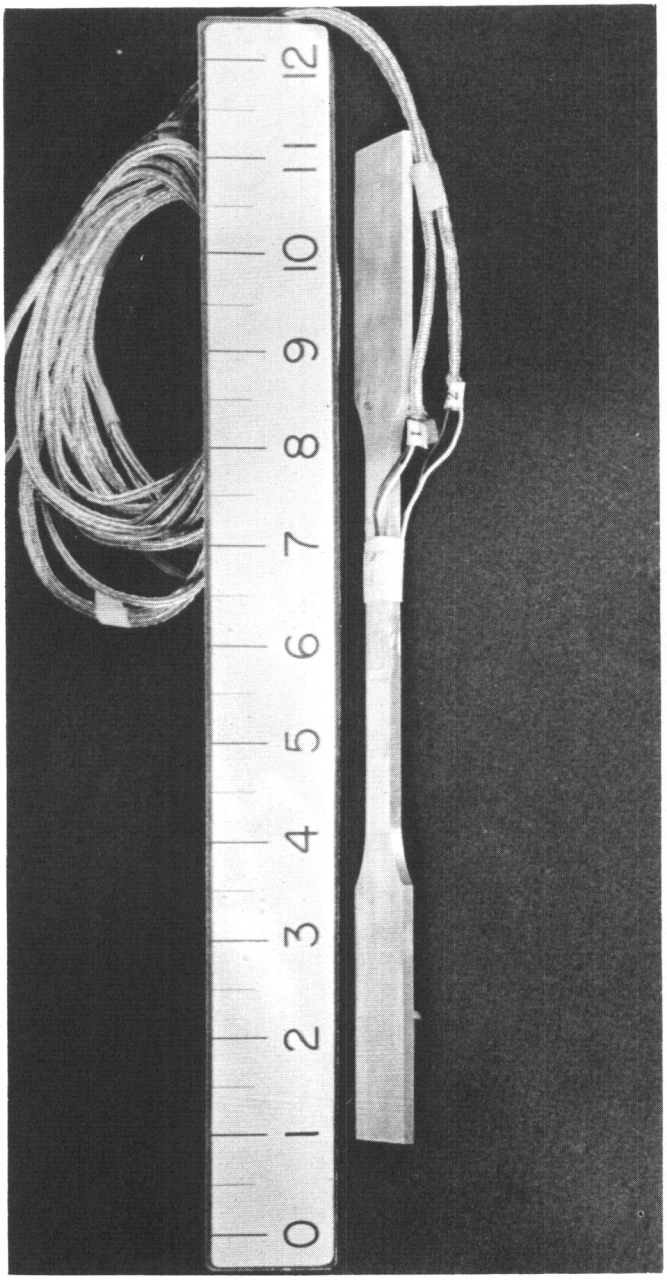

FIG. 4.8 INSTRUMENTED TENSILE TEST COUPON

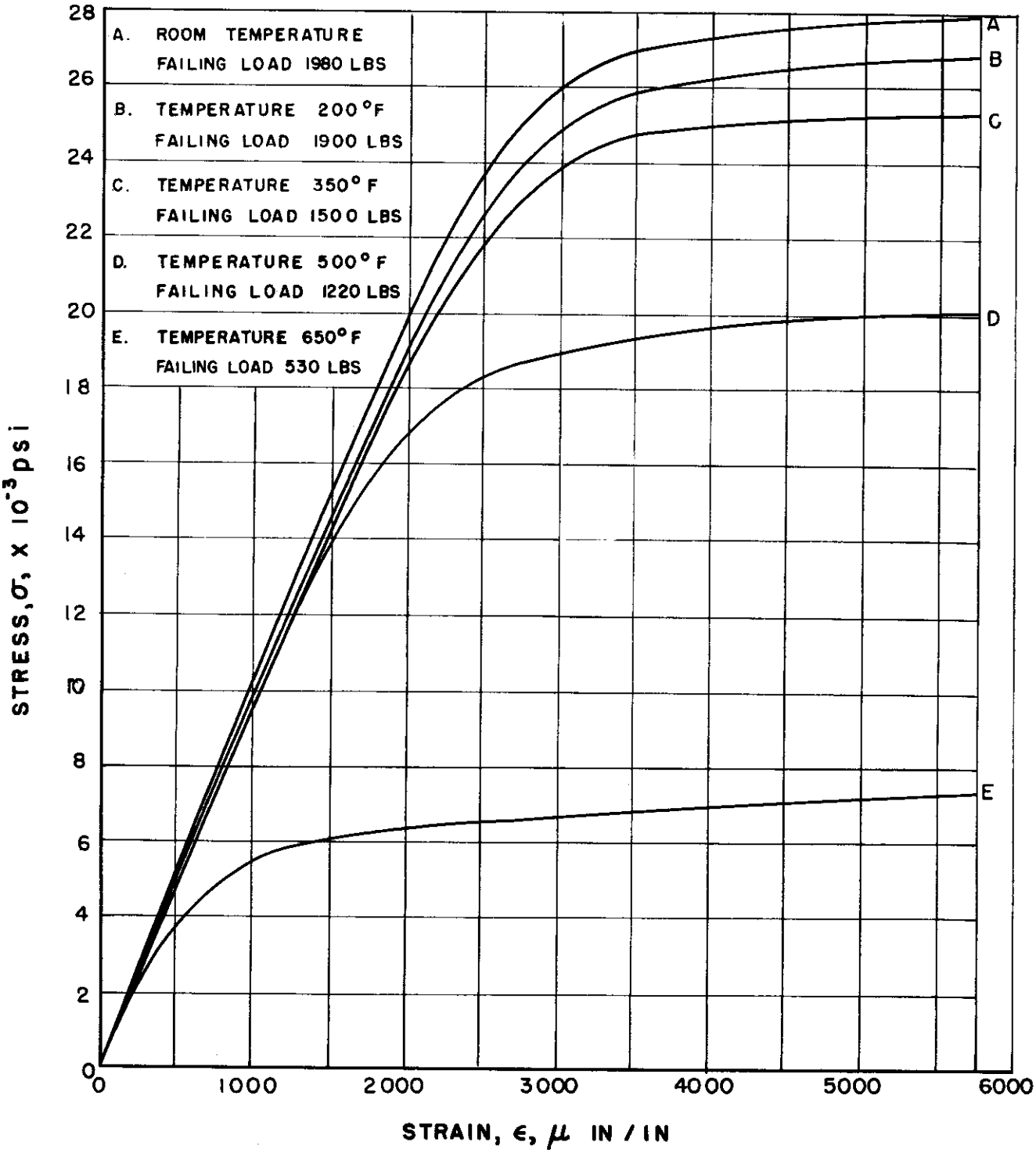

FIG. 4.9 ELEVATED TEMPERATURE STRESS-STRAIN CURVES FOR SERIES I

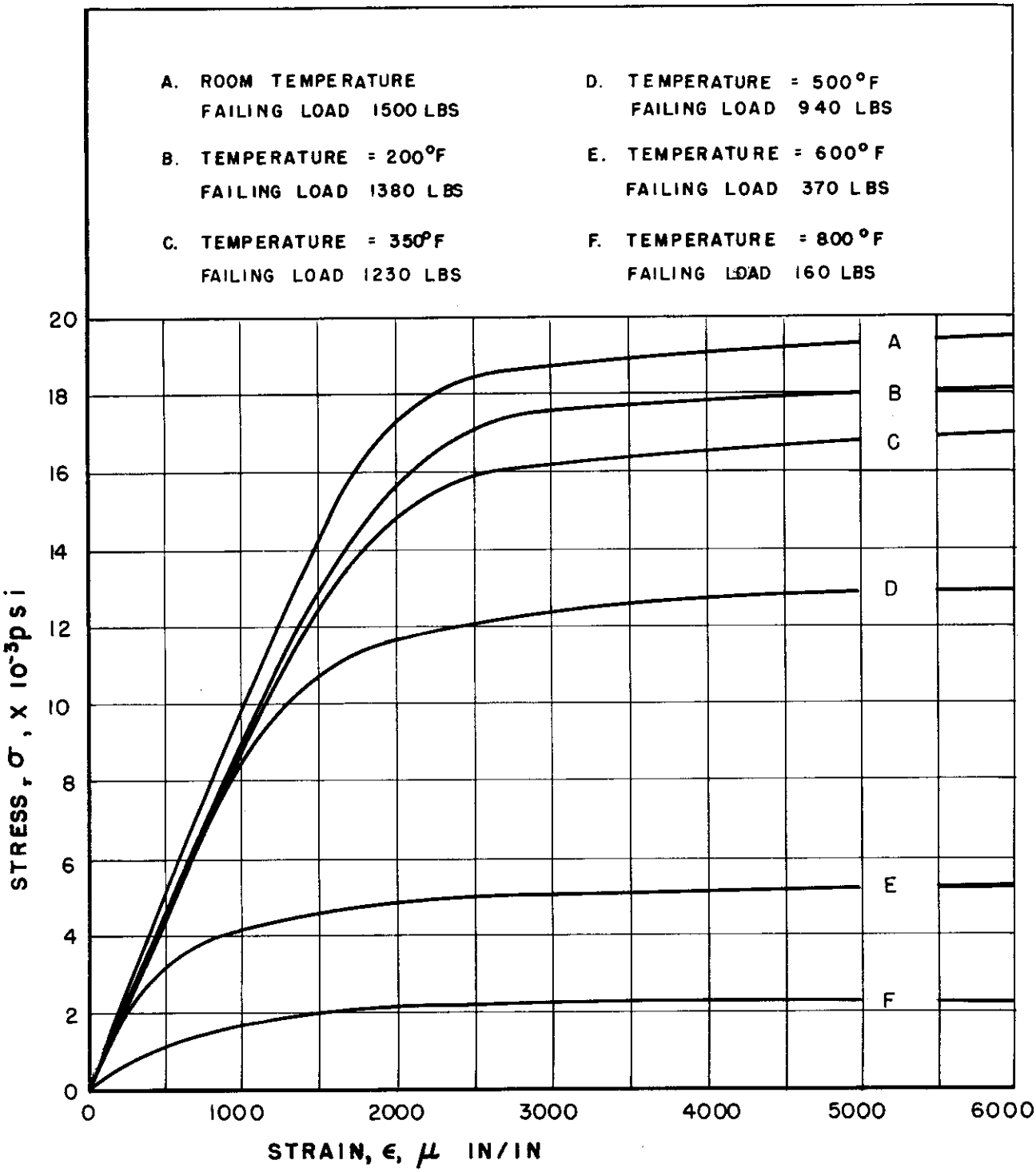

FIG. 4.10 ELEVATED TEMPERATURE STRESS-STRAIN CURVES FOR SERIES 2

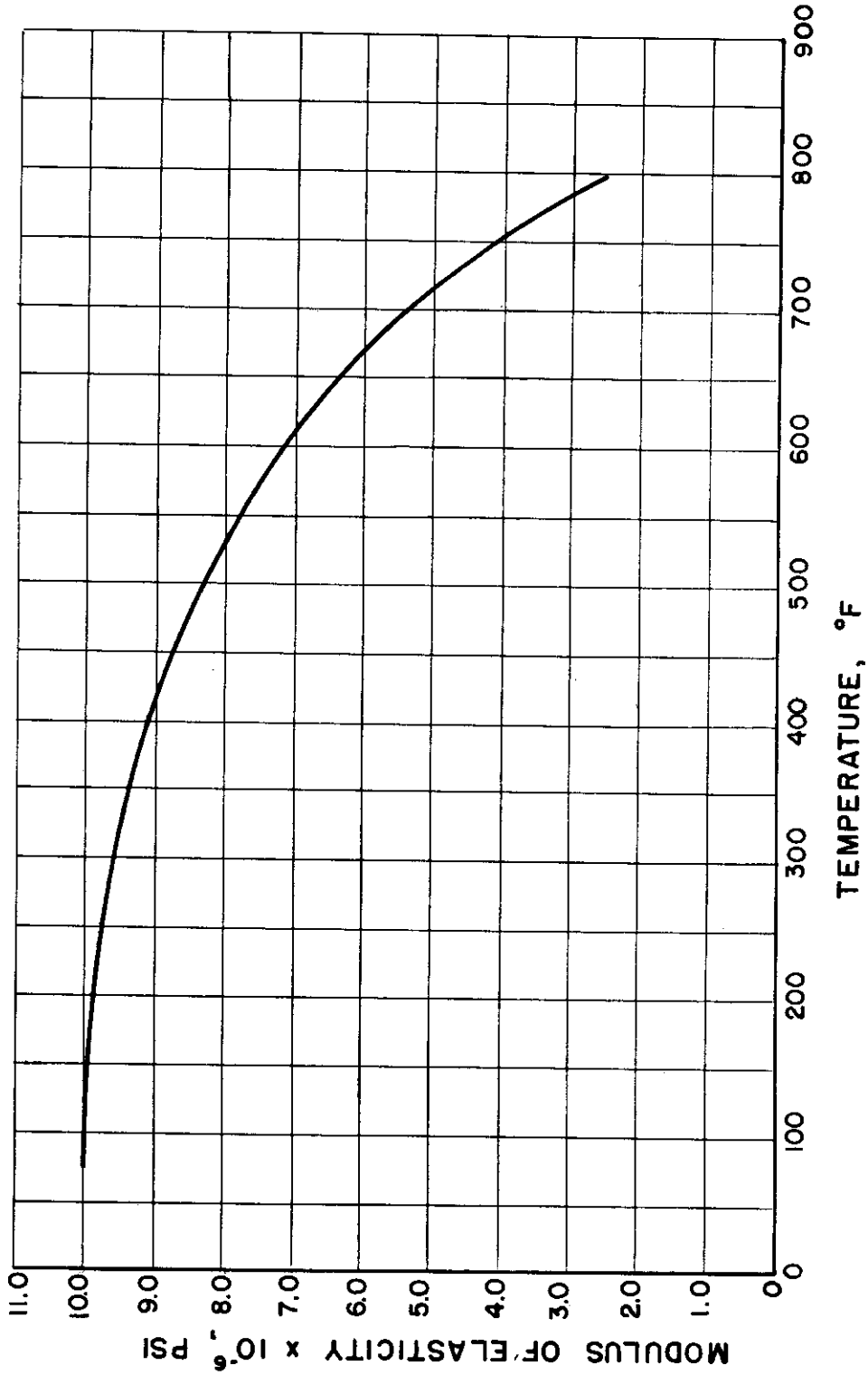

FIG. 4.11 EXPERIMENTAL VARIATION OF MODULUS OF ELASTICITY OF 63S-T5 WITH TEMPERATURE

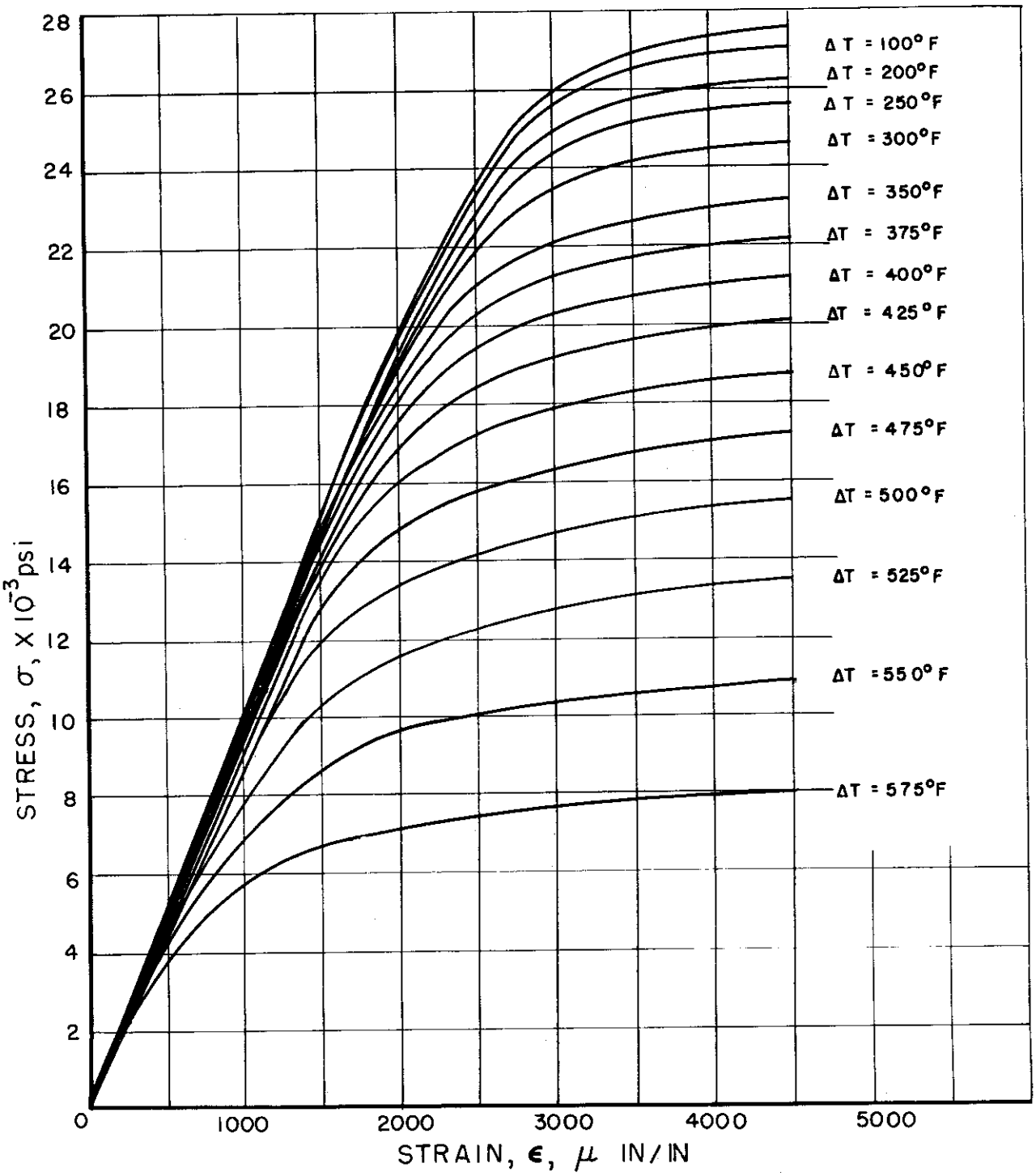

FIG. 4.12 STRESS – STRAIN INTERPOLATION CHART FOR VARIOUS TEMPERATURE RISES, SERIES – I

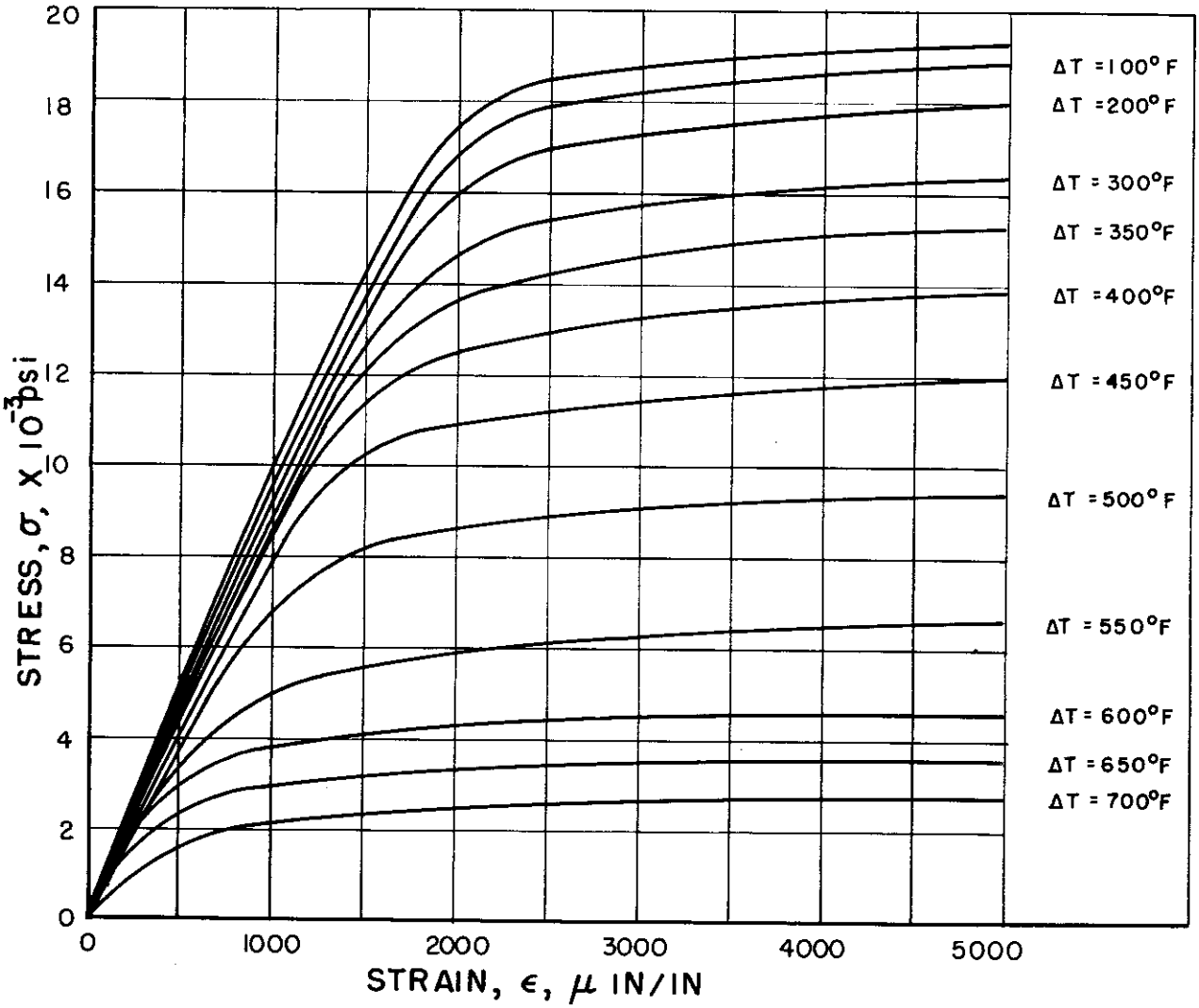

FIG. 4.13 STRESS – STRAIN INTERPOLATION CHART FOR VARIOUS TEMPERATURE RISES, SERIES 2

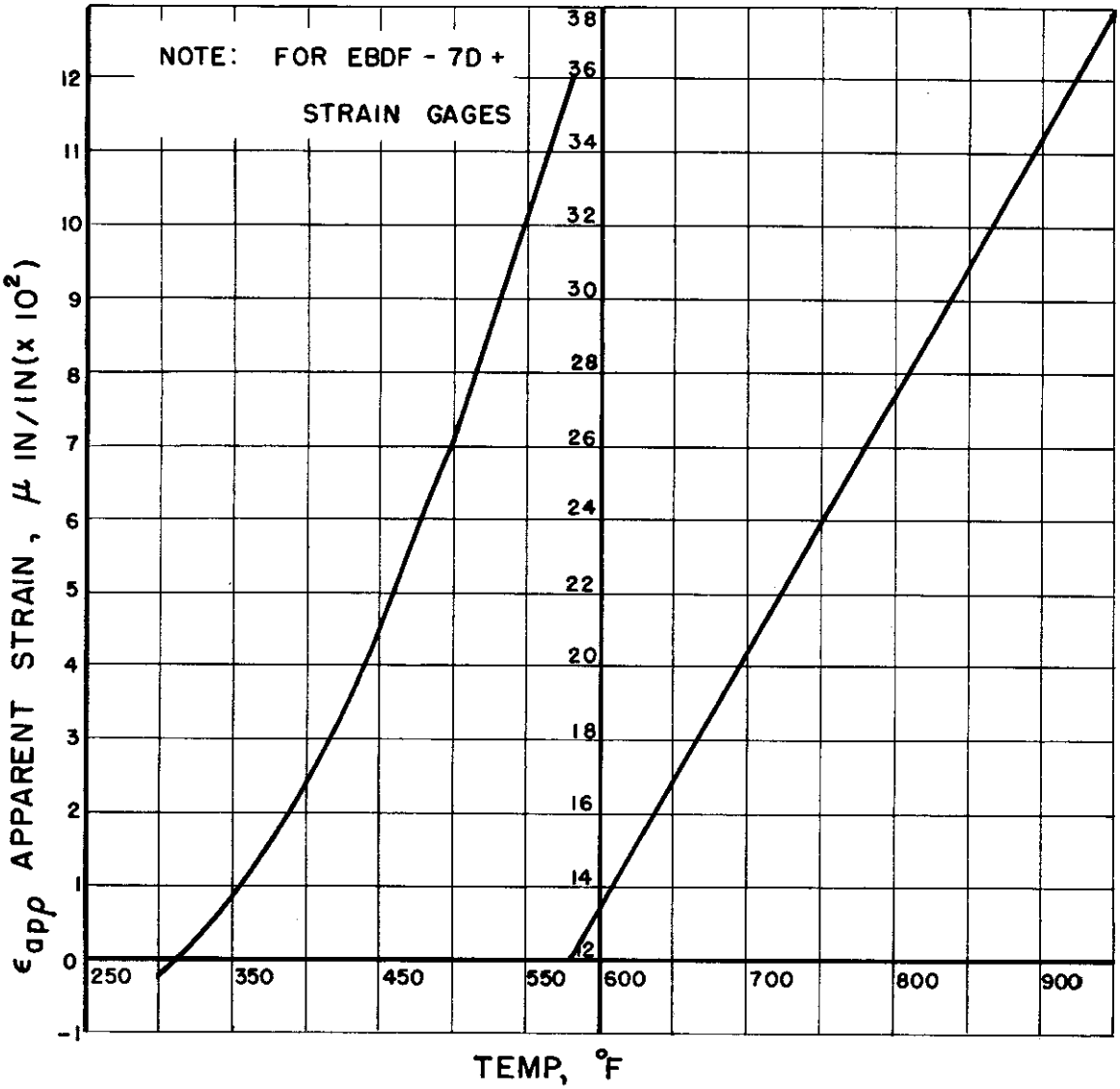

FIG. 4.14 APPARENT STRAIN CORRECTION FOR HIGH TEMPERATURES

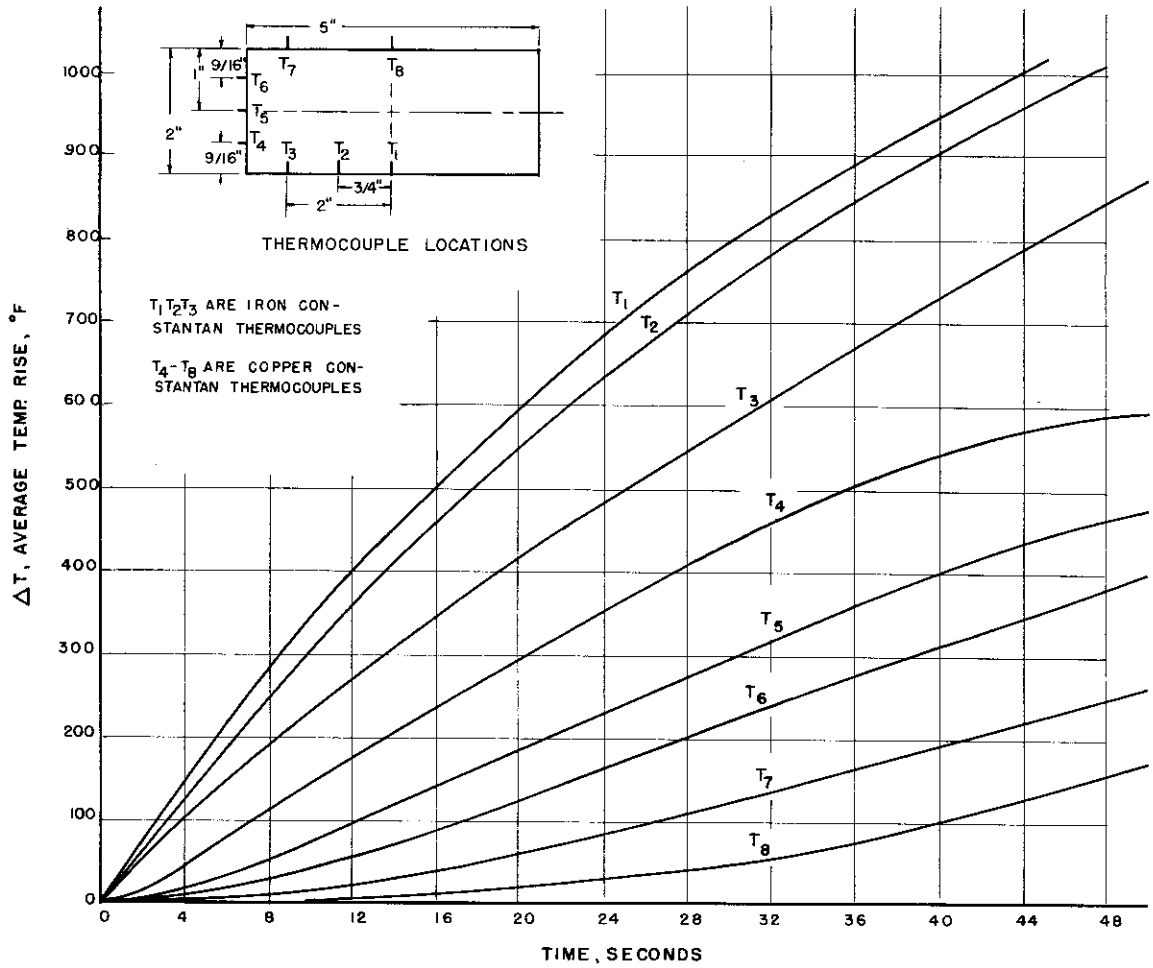

FIG. 5.1 AVERAGE EXPERIMENTAL TEMPERATURE RISE IN BOX-BEAM MODELS OF SERIES-I ($q = 4.0$ cal/cm²sec)

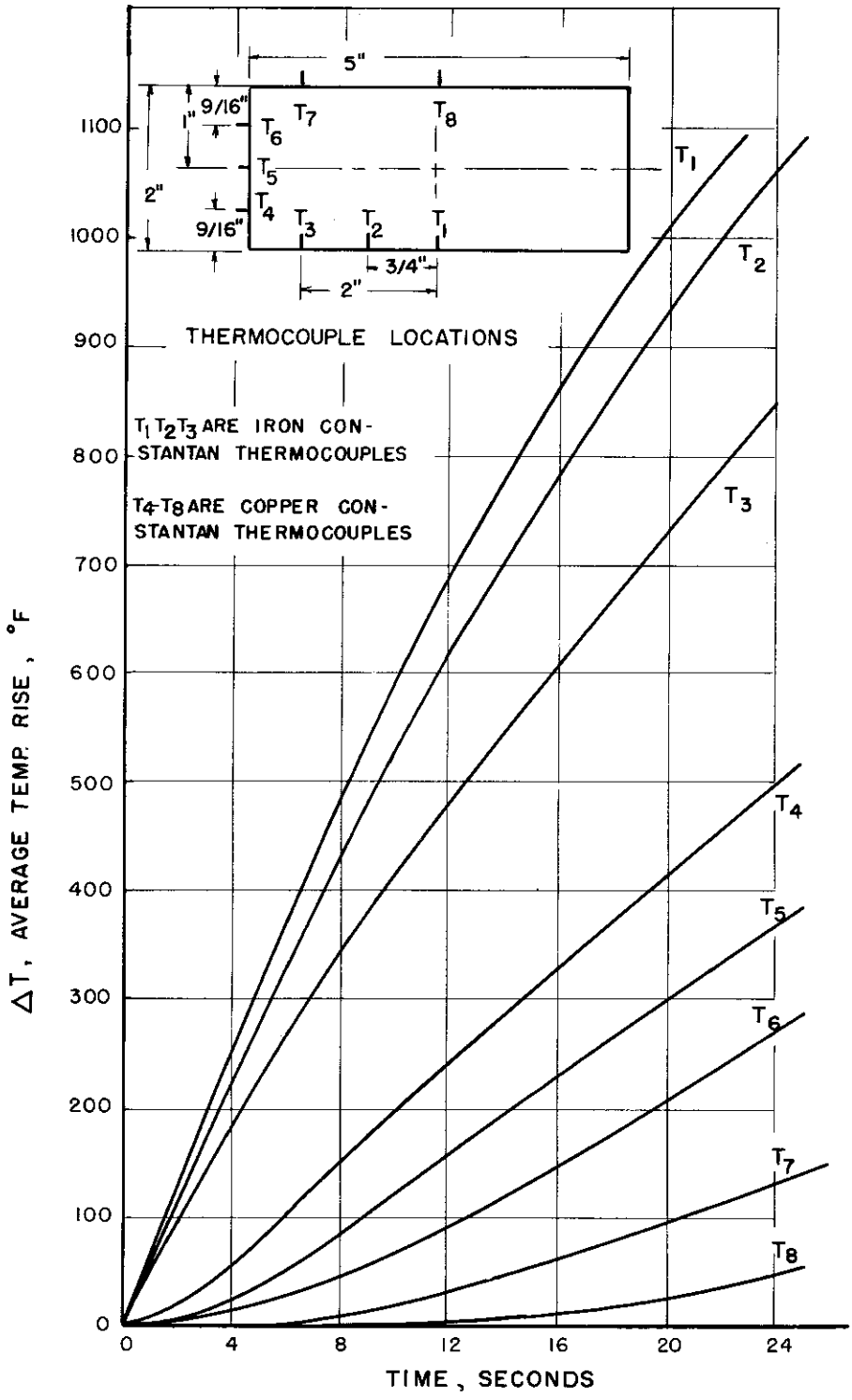

FIG. 5.2 AVERAGE EXPERIMENTAL TEMPERATURE RISE IN BOX-BEAM MODELS OF SERIES - 2 ($q = 8.0$ cal/cm² sec)

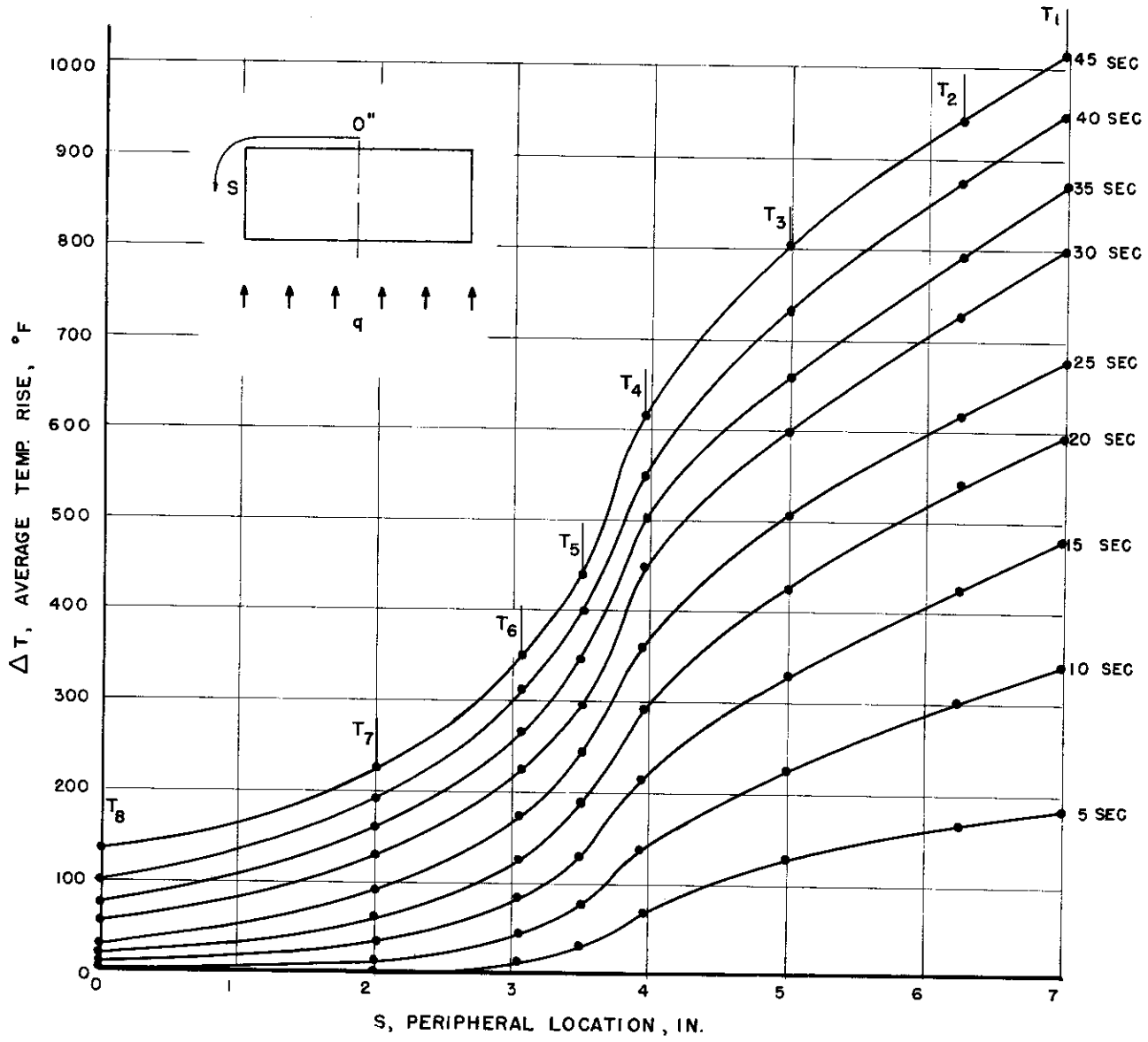

FIG. 5-3 AVERAGE EXPERIMENTAL TEMPERATURE DISTRIBUTION IN BOX-BEAM MODELS OF SERIES-I FOR VARIOUS HEATING TIMES

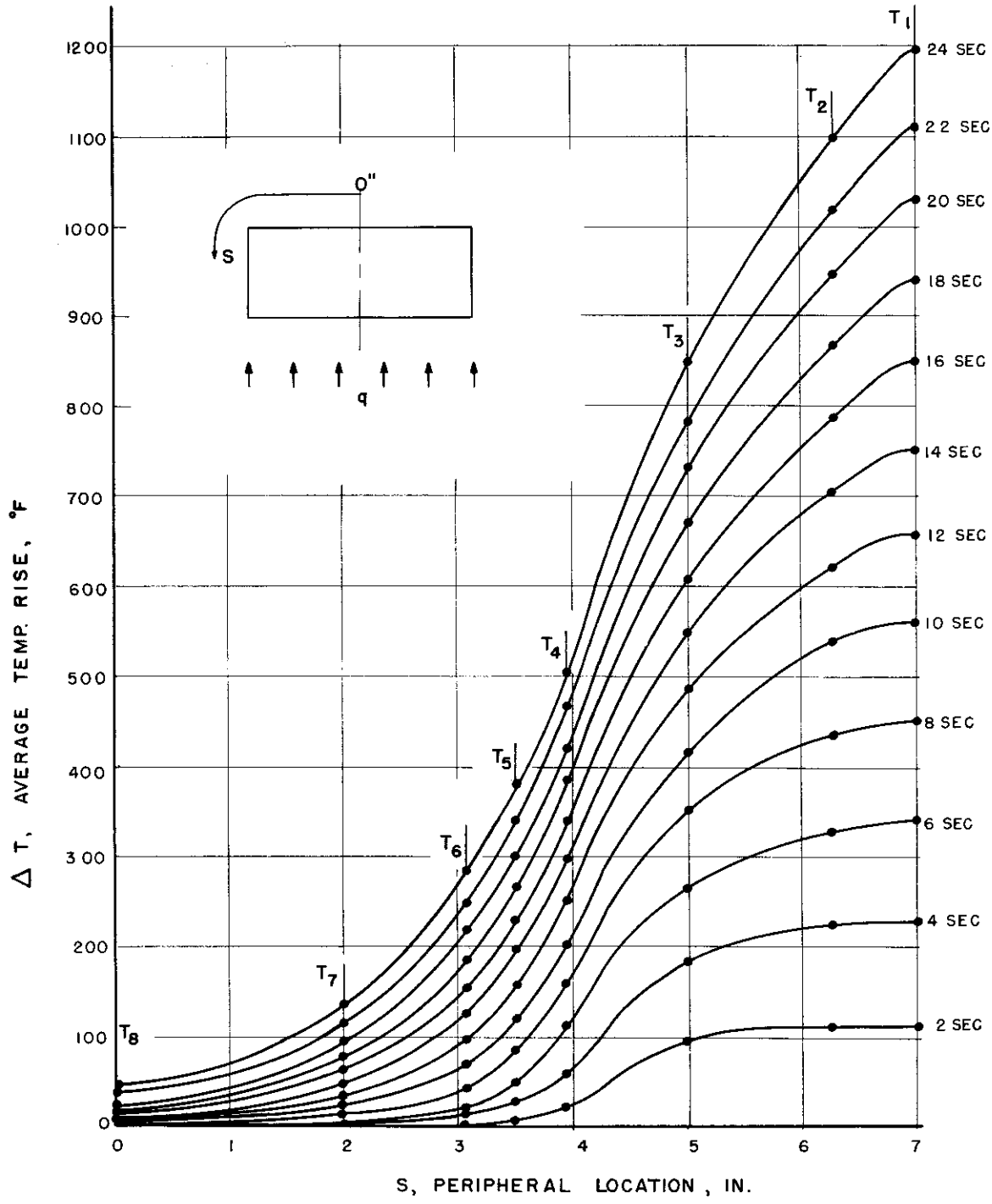

FIG. 5.4 AVERAGE EXPERIMENTAL TEMPERATURE DISTRIBUTION IN BOX-BEAM MODELS OF SERIES-2 FOR VARIOUS HEATING TIMES

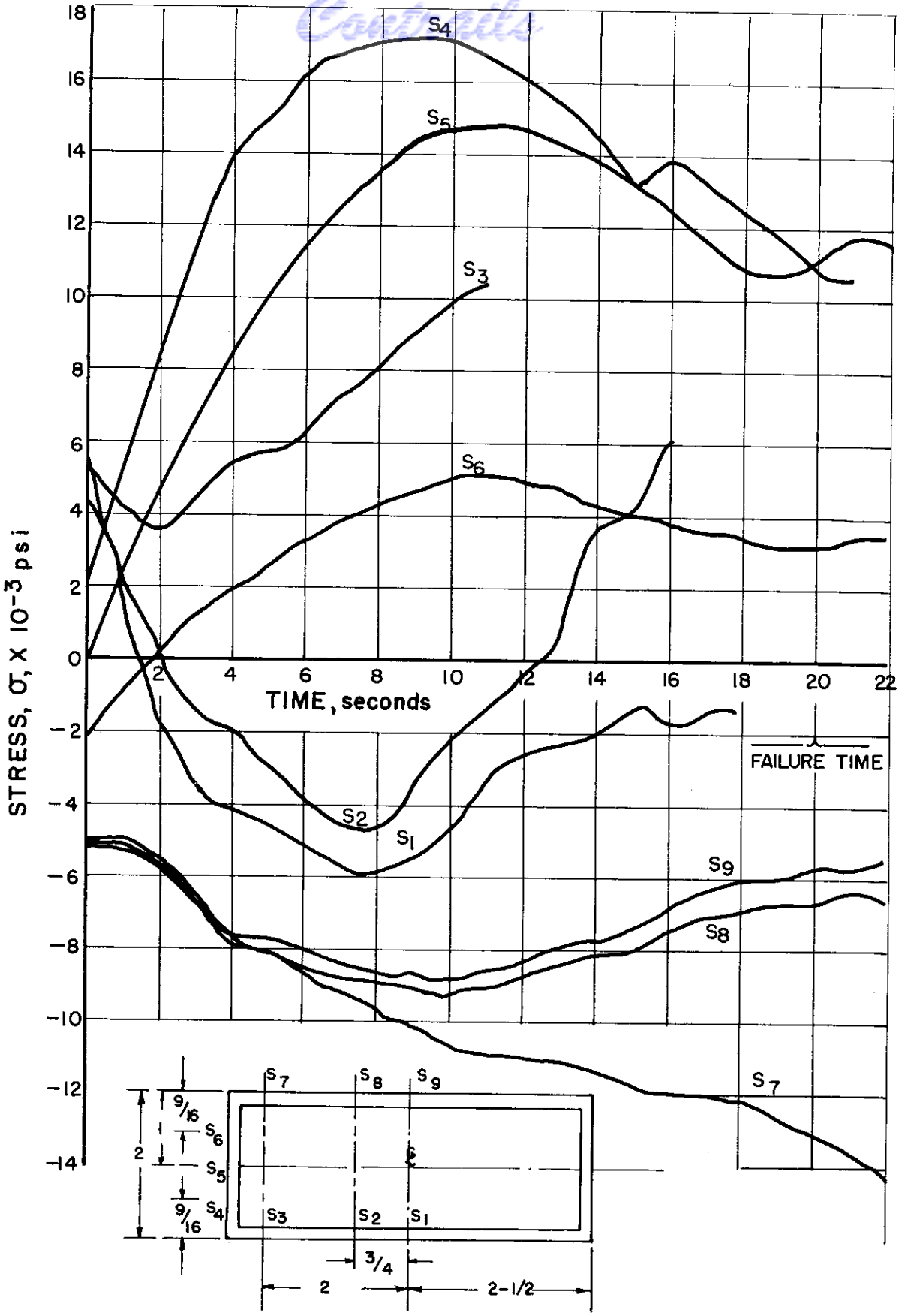

FIG. 55 STRESS TIME—HISTORY FOR MODEL 10 SERIES—2 LOADED TO 28 PER CENT OF BM_{MAX}

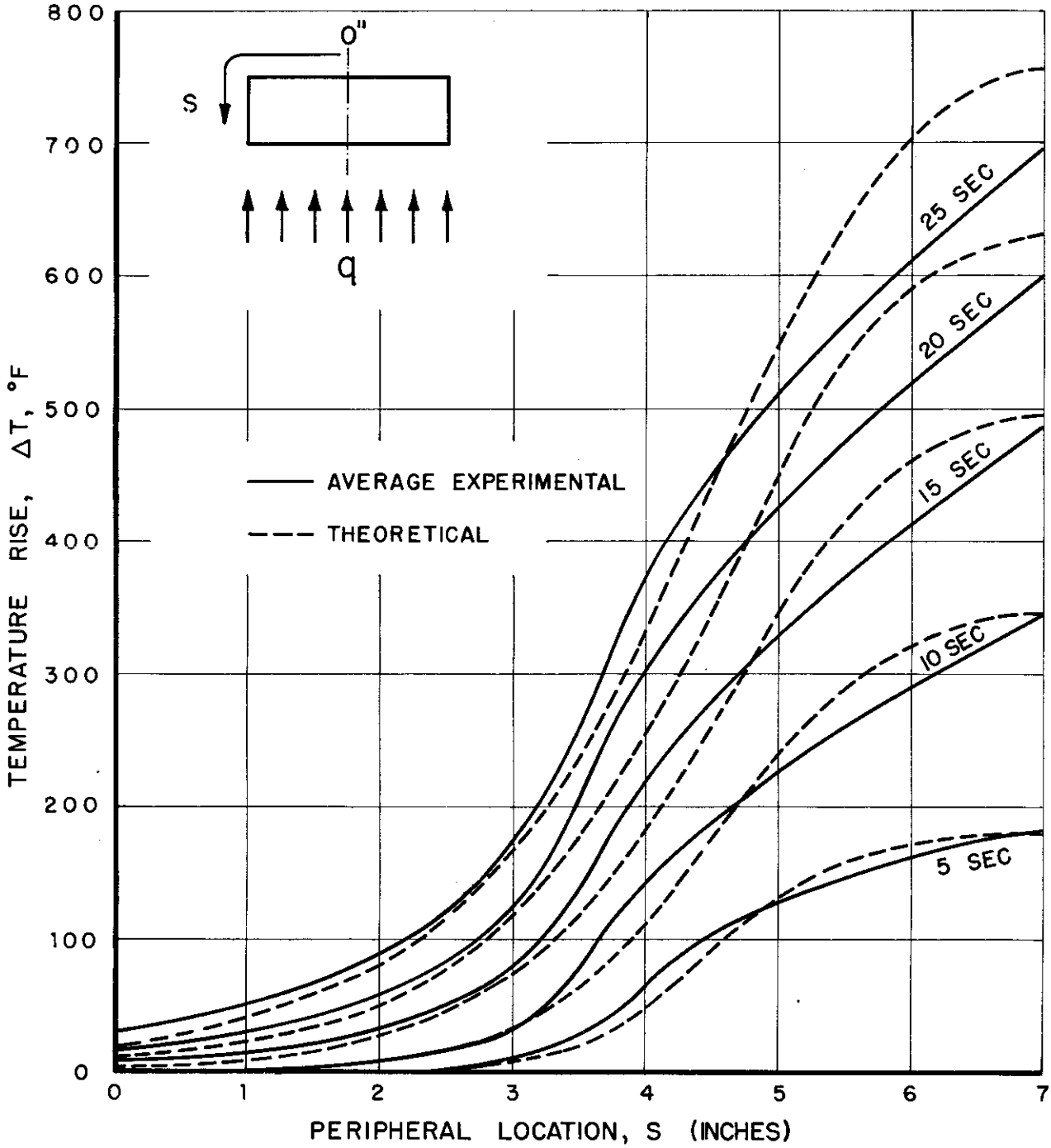

FIG. 5.6 THEORETICAL AND EXPERIMENTAL COMPARISON OF TEMPERATURE DISTRIBUTIONS IN BOX-BEAM MODELS OF SERIES-1 FOR VARIOUS TIMES

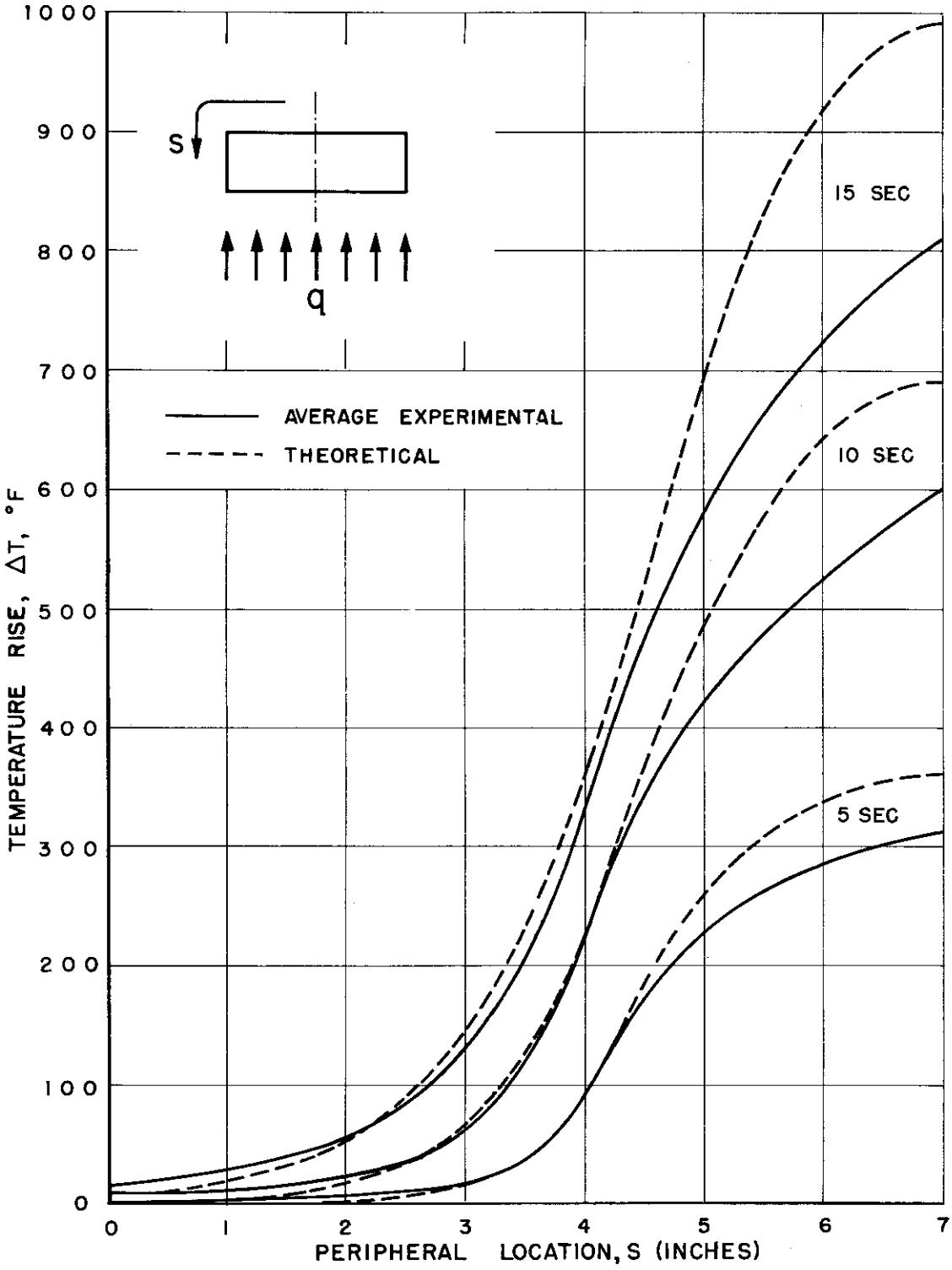

FIG. 5.7 THEORETICAL AND EXPERIMENTAL COMPARISON OF TEMPERATURE DISTRIBUTIONS IN BOX-BEAM MODELS OF SERIES-2 FOR VARIOUS TIMES

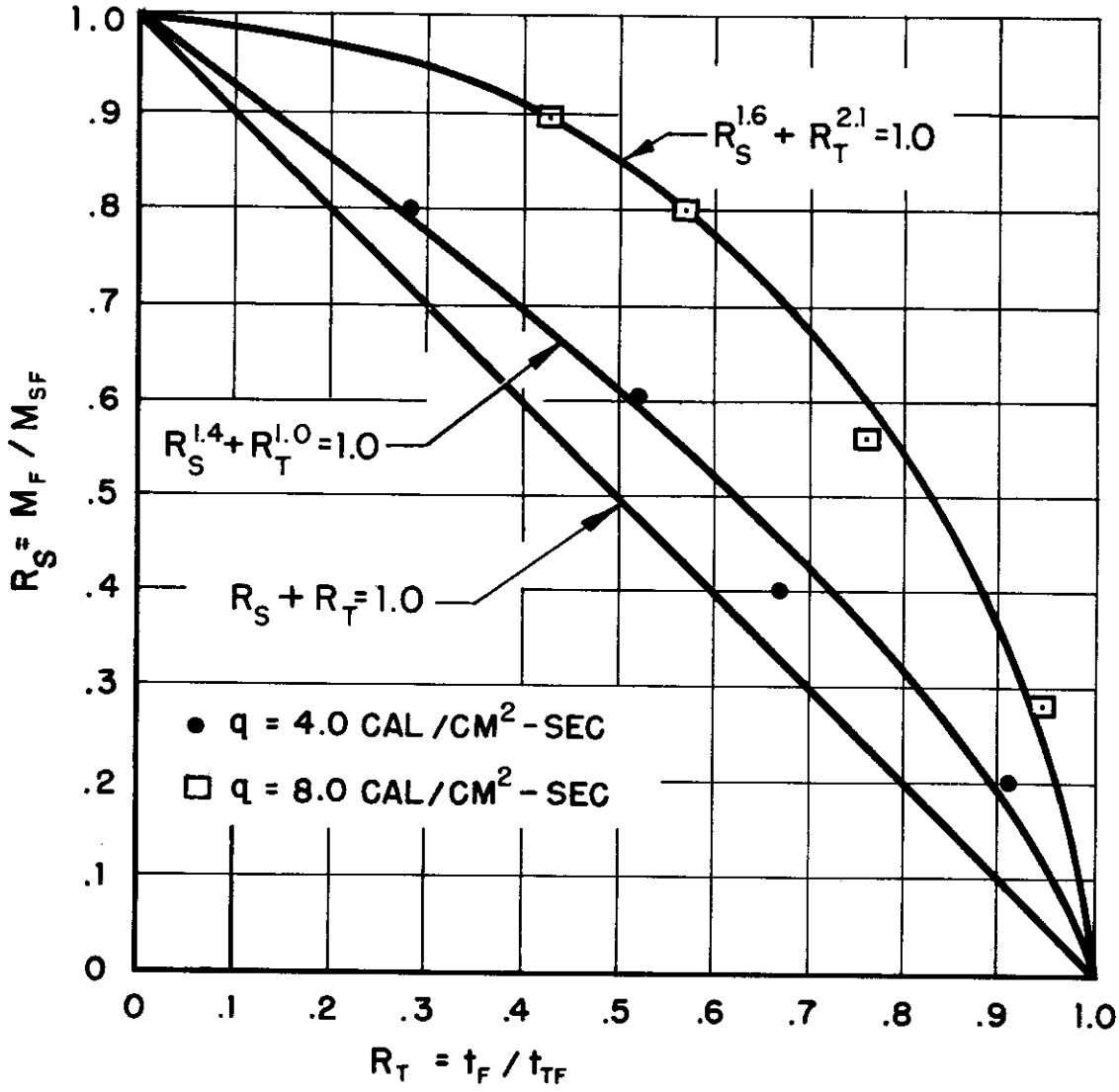

FIG. 6.1 INTERACTION CURVES OF COMBINED LOADING FAILURE

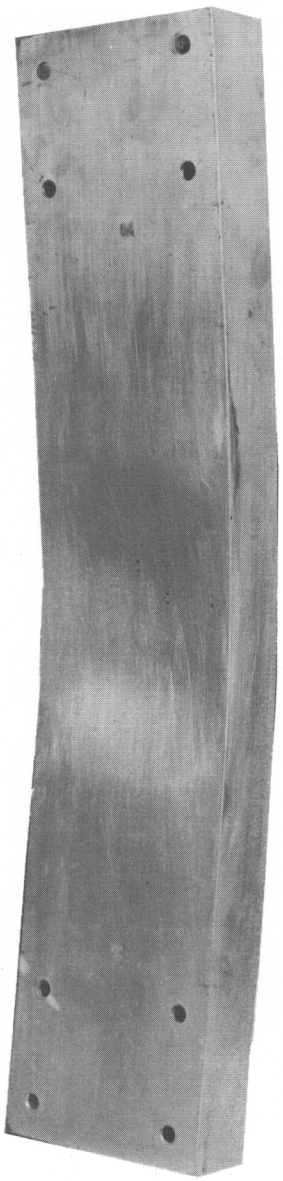

FIG. 6.2 HEAVILY-LOADED BOX-BEAM AFTER FAILURE UNDER COMBINED LOADS

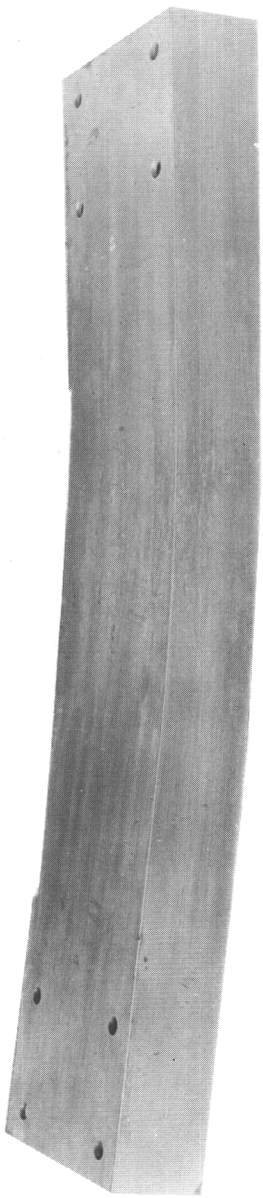

FIG. 6.3 LIGHTLY-LOADED BOX-BEAM AFTER FAILURE UNDER COMBINED LOADS

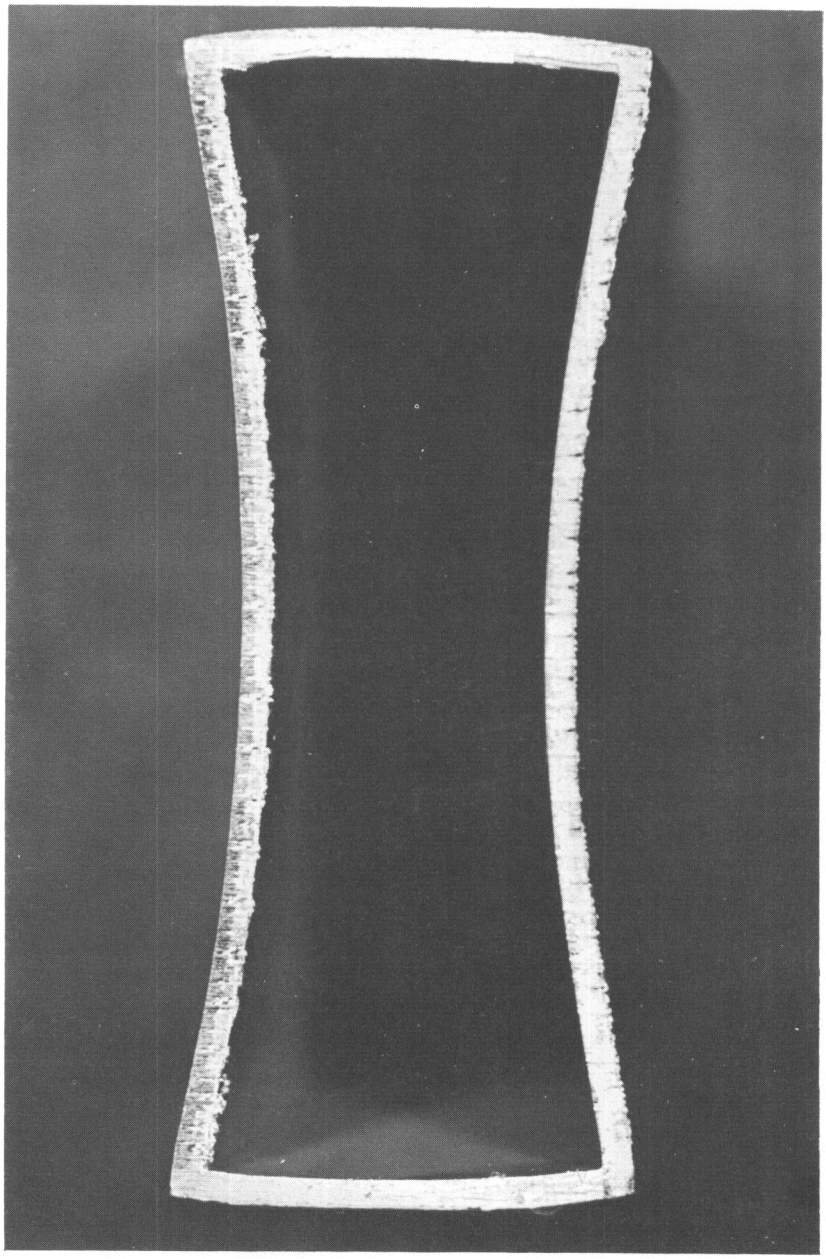

FIG. 6.4 CROSS-SECTION OF HEAVILY-LOADED BOX-BEAM AT CENTER SPAN

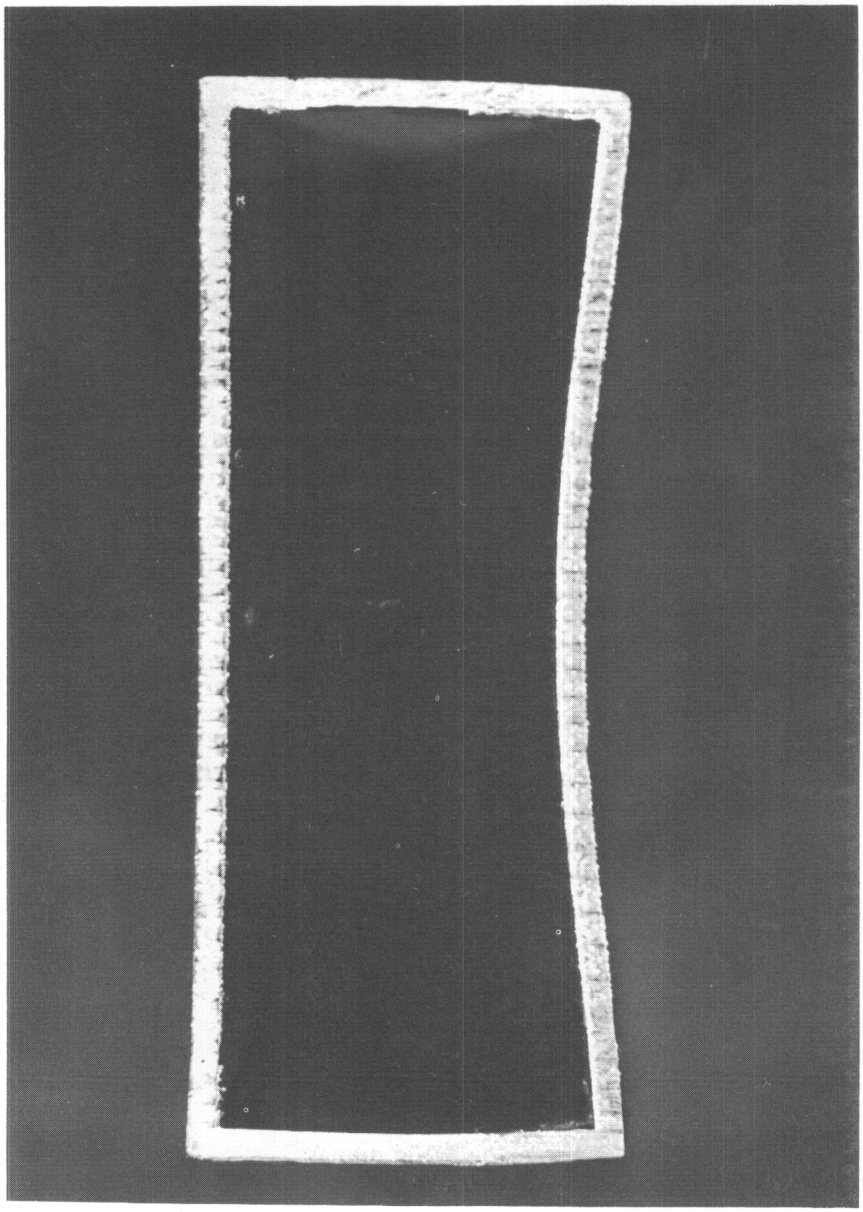

FIG. 6.5 CROSS-SECTION OF LIGHTLY-LOADED BOX-BEAM AT CENTER SPAN

TABLE 5.1

AVERAGE TEMPERATURE ABOUT THE BOX-BEAM CENTER LINE PERIPHERY FOR A RADIANT FLUX OF 4.0 CAL/SQ. CM. SEC.

Time	ΔT_1	ΔT_2	ΔT_3	ΔT_4	ΔT_5	ΔT_6	ΔT_7	ΔT_8
1	39	29	30	4	0	0	0	0
2	77	61	51	11	6	4	0	0
3	112	93	78	22	9	5	0	0
4	148	122	102	34	17	7	0	0
5	180	154	124	45	27	10	0	0
6	216	189	145	56	31	14	5	0
7	248	215	166	70	39	21	7	0
8	280	243	185	84	54	28	8	0
9	311	272	205	98	61	36	9	0
10	339	298	222	108	71	42	12	0
11	370	322	245	121	85	46	15	0
12	401	348	268	135	96	52	18	2
13	423	375	287	148	104	62	22	4
14	451	396	305	161	117	72	29	6
15	477	421	326	177	125	82	34	9
16	502	440	344	190	138	89	38	11
17	526	459	363	203	152	95	44	13
18	547	501	383	212	161	105	49	15
19	570	526	395	225	171	115	51	17
20	593	543	413	240	185	124	57	19
21	616	564	433	252	195	134	62	21
22	636	583	447	264	206	140	67	23
23	648	602	463	276	215	150	73	25
24	677	619	478	289	225	162	80	27
25	698	639	496	300	237	171	85	28
26	720	658	511	315	249	180	91	32
27	738	689	524	327	261	189	99	37
28	758	708	540	344	269	198	106	42
29	776	722	563	350	281	207	118	48
30	798	745	576	364	293	219	126	55
31	815	762	590	375	301	228	131	59
32	828	783	606	381	314	233	139	63
33	846	792	622	395	324	242	144	66
34	861	804	639	404	335	253	151	69
35	874	821	655	420	344	262	158	72

TABLE 5.1 (CONT'D.)

AVERAGE TEMPERATURE ABOUT THE BOX-BEAM CENTER LINE PERIPHERY FOR A RADIANT FLUX OF 4.0 CAL/SQ. CM. SEC.

Time	AT_1	ΔT_2	ΔT_3	ΔT_4	ΔT_5	ΔT_6	ΔT_7	ΔT_8
36	889	837	668	431	348	271	160	76
37	893	852	681	439	355	279	166	81
38	917	865	697	453	366	288	174	85
39	936	878	713	464	379	299	181	90
40	945	891	729	475	390	307	186	98
41	960	908	745	486	398	312	194	102
42	973	923	758	494	406	324	200	106
43	986		771	531	417	332	205	115
44	998		784	523	427	343	212	123
45	1015		800	534	438	348	220	132
46	1028		817	544	448	359	228	136
47	1040		829	550	458	367	235	140
48	1056		842	565	469	375	241	148
49	1071		855	575	476	383	248	156
50	1090		871	588	489	396	255	164

$\Delta T = T - 78^{\circ}F$

TABLE 5.2

AVERAGE TEMPERATURE ABOUT THE BOX-BEAM CENTER LINE PERIPHERY FOR A RADIANT FLUX OF 8.0 CAL./SQ. CM. SEC.

Time	ΔT_1	ΔT_2	ΔT_3	ΔT_4	ΔT_5	ΔT_6	ΔT_7	ΔT_8
0	0	0	0	0	0	0	0	0
1	54	51	50	7	2	2	0	0
2	121	114	99	20	5	3	1	0
3	184	171	140	41	15	6	2	1
4	249	229	184	59	26	10	3	2
5	312	285	228	85	37	19	5	3
6	373	324	268	104	51	25	7	4
7	435	343	312	130	66	35	9	5
8	491	401	349	149	84	46	12	6
9	548	493	388	176	102	57	17	7
10	601	535	424	201	124	66	22	8
11	653	583	459	225	140	81	28	9
12	702	623	490	248	158	94	34	10
13	737	651	517	271	177	106	42	11
14	786	708	547	290	190	122	47	12
15	814	748	582	314	209	134	54	13
16	864	780	617	337	228	151	63	14
17	905	828	649	358	245	167	72	17
18	938	866	674	381	264	183	81	20
19	975	904	704	402	282	198	90	23
20	1010	930	737	425	300	212	100	27
21	1040	955	750	447	308	228	104	31
22	1075	1000	790	465	327	240	115	36
23	1100	1030	825	480	350	255	123	41
24	1120	1060	850	495	375	275	130	45

$\Delta T = T - 78^{\circ}F$

TABLE 5.3

EXPERIMENTAL STRESSES AT VARIOUS LOCATIONS IN THE SERIES -1, q = 4.0 CAL/SQ. CM. SEC.
BOX-BEAM WITH NO EXTERNAL LOAD (MODEL 3)

Time	σ_1	σ_2	σ_3	σ_4	σ_5	σ_6	σ_7	σ_8	σ_9
0	0	0	0	0	0	0	0	0	0
1	- 1450	- 1100	0	0	0	0	0	0	570
2	- 2150	- 2200	0	1450	1050	0	0	0	1140
3	- 3600	- 3800	0	3250	2750	550	- 520	- 690	1140
4	- 4300	- 4900	749	5050	4150	1150	- 780	- 1040	1140
5	- 5050	- 5988	746	5750	4850	1150	- 1300	- 1380	1710
6	- 5750	- 6523	1438	7193	4850	1700	- 1560	- 1730	1710
7	- 6500	- 7589	1433	8283	6550	1700	- 1820	- 1730	1710
8	- 7200	- 8118	1425	8973	7250	2000	- 2080	- 2070	1710
9	- 5050	- 8003	2149	10050	7942	2000	- 2600	- 2070	2280
10	- 5640	- 7979	2134	10714	8633	2000	- 2600	- 2070	1710
11	- 6331	- 9009	1396	11385	8923	2300	- 2860	- 2070	1710
12	- 5560	-10008	1386	12079	9263	2300	- 3120	- 2070	1710
13	- 5514	- 9398	1375	12386	9582	2000	- 3640	- 2070	1140
14	- 4802	- 9874	2081	12678	9910	2000	- 3640	- 2070	1140
15	- 4072	- 9290	1697	12954	10236	1700	- 4160	- 2070	1140
16	- 3760	- 9544	1222	13262	10203	1698	- 4420	- 2070	1140
17	- 3514	- 9703	1546	13544	10862	1696	- 4680	- 1730	1140
18	- 3308	- 9672	561	13460	10829	1694	- 4940	- 1730	1140
19	- 3162	-10072	- 47	12648	10796	1444	- 5200	- 1730	570
20	- 2320	-10379	139	12277	10741	1443	- 5460	- 1380	570
21	- 736	-10276	965	11564	10696	1143	- 5460	- 1380	570
22	- 822	-10221	1093	10562	11267	1141	- 5720	- 1040	0
23	- 634	- 9348	634	9447	9874	842	- 5980	- 1040	0

TABLE 5.3 (CONT'D)

EXPERIMENTAL STRESSES AT VARIOUS LOCATIONS IN THE SERIES -1, q = 4.0 CAL/SQ. CM. SEC.
BOX-BEAM WITH NO EXTERNAL LOAD (MODEL 3)

Time	σ_1	σ_2	σ_3	σ_4	σ_5	σ_6	σ_7	σ_8	σ_9
24	- 849	- 9369	135	8677	9874	842	- 5980	- 690	- 570
25	- 396	- 8062	- 620	7956	9500	543	- 5980	- 350	- 1140
26	0	- 7384	- 1395	7379	9148	296	- 6240	0	- 1140
27	812	- 7453	- 1896	6603	8467	0	- 6240	0	- 1140
28	1172	- 7118	- 2465	5515	7788	- 294	- 6240	350	- 1710
29	1548	- 6113	- 3237	4324	7253	- 538	- 6240	690	- 1710
30	1936	- 5374	- 3236	3488	6627	- 536	- 5980	1040	- 2280
31	2003	- 5288	- 3120	2414	5909	- 826	- 6190	1380	- 2280
32	1470	- 5062	- 3558	1539	5382	- 1115	- 6184	1380	- 2850
33	1386	- 5040	- 3571	357	4717	- 1112	- 6178	1730	- 2850
34	1166	- 4908	- 3480	- 577	4469	- 1107	- 6165	2070	- 3420
35	461	- 5460	- 3872	- 1661	4403	- 1392	- 6159	2070	- 3420
36	- 157	- 5751	- 3308	- 2430	4116	- 1627	- 6146	2420	- 3420
37	- 778	- 6000	- 3201	- 3361	3408	- 1618	- 6133	2420	- 3420
38	- 1302	- 6859	- 3104	- 4042	3660	- 1376	- 6121	2760	- 3420
39	- 1541	- 7487	- 2542	- 4737	3182	- 1090	- 6108	2760	- 3990
40	- 1810	- 7348	- 2673	- 3591	3119	- 804	- 6090	3110	- 3990
41	- 569	- 7092	- 2494	- 3684	2601	- 802	- 6084	3450	- 4560
42		- 7105	- 2443	- 3736	1998	- 1223	- 5812	3450	- 4560
43		- 5667	- 2459	- 2926	1982	- 1082	- 5889	3450	- 4560
44		- 4761	- 2269	- 3003	1529	- 705	- 5526	3800	- 4560
45		- 2805	- 2356	- 2886	1253	- 657	- 5508	3800	- 4560

TABLE 5.3 (CONT'D)

EXPERIMENTAL STRESSES AT VARIOUS LOCATIONS IN THE SERIES -1, q = 4.0 CAL/SQ. CM. SEC.
BOX-BEAM WITH NO EXTERNAL LOAD (MODEL 3)

Time	σ_1	σ_2	σ_3	σ_4	σ_5	σ_6	σ_7	σ_8	σ_9
46		- 1050	- 2175	- 2736	981	- 608	- 5241	4100	- 4560
47			- 2130	- 2706	549	- 889	- 5225	4103	- 5083
48			- 714		167	- 1075	- 5214	4445	- 4514
49					- 1020	- 1819	- 5187	4441	- 4510
50					- 961	- 1769	- 4929	4436	- 3942

TABLE 5.4

EXPERIMENTAL STRESSES AT VARIOUS LOCATIONS IN THE SERIES-1 q=4.0 CAL/SQ. CM. SEC. BOX-BEAM LOADED TO 20% OF THE FAILING BENDING MOMENT (MODEL 4)

Time (Seconds)	σ_1	σ_2	σ_3	σ_4	σ_5	σ_6	σ_7	σ_8	σ_9
0	4300	4900	4350	2250	0	- 2640	- 5000	- 4940	- 6270
1	3600	3800	4400	4500	1820	- 1540	- 5200	- 5200	- 6270
2	2150	3250	4450	6500	3640	- 880	- 6200	- 5980	- 5270
3	700	2200	4600	7750	4680	0	- 6600	- 6240	- 5130
4	- 688	1089	4800	9000	5720	440	- 7000	- 6760	- 4840
5	- 1411	0	5039	10000	6760	660	- 7400	- 7020	- 4560
6	- 2058	- 532	5008	11000	7280	1100	- 8000	- 7540	- 4560
7	- 2746	- 1054	5661	12000	8060	1320	- 8600	- 7800	- 3990
8	- 3952	1041	5614	12750	8580	1760	- 8800	- 7800	- 3700
9	- 4165	846	5562	13500	9360	1760	- 8800	- 7540	- 3990
10	- 6224	- 141	4840	14000	9880	1980	- 9000	- 7280	- 4560
11	- 7886	- 47	4106	14820	10400	1980	- 9800	- 7540	- 4840
12	- 8181	- 322	3384	15270	10920	2020	- 9800	- 7280	- 3990
13	- 9273	- 453	3514	15450	11180	2020	-10000	- 7280	- 4560
14	- 7752	- 1242	2936	15860	11580	2020	-10600	- 7540	- 4560
15	- 7258	- 2193	3062	16000	11820	2420	-10800	- 7280	- 4560
16	- 6450	- 1946	2155	16150	12040	2420	-11200	- 7280	- 4560
17	- 5904	- 3835	816	16300	12260	2200	-11600	- 7280	- 4560
18	- 5544	- 5614	582	16240	12220	2200	-11800	- 7020	- 5130
19	- 5024	- 6905	441	15910	12180	2400	-12200	- 7020	- 5130
20	- 4760	- 3745	173	15610	12380	2170	-12600	- 7020	- 5130
21	- 4425	- 3720	- 720	14310	12080	2380	-12800	- 7020	- 5130
22	- 4224	- 3584	- 1530	13706	12070	2160	-13200	- 6760	- 5700

TABLE 5.4 (Contd.)

EXPERIMENTAL STRESSES AT VARIOUS LOCATIONS IN THE SERIES-1 q = 4.0 CAL/SQ. CM. SEC. BOX-BEAM LOADED TO 20% OF THE FAILING BENDING MOMENT (MODEL 4)

Time (Seconds)	σ_1	σ_2	σ_3	σ_4	σ_5	σ_6	σ_7	σ_8	σ_9
23	- 3980	- 3663	- 2323	13290	11740	2150	-12400	- 6500	- 5700
24	- 3618	- 3762	- 2393	12140	11450	2150	-13200	- 6240	- 5700
25	- 3312	- 3640	- 3042	17800	10890	1920	-13400	- 5980	- 6270
26	- 2786	- 3798	- 2142	16380	10580	1700	-13800	- 5980	- 6270
27	- 2561	- 3094	- 2830	15690	10290	1700	-13800	- 5720	- 6270
28	- 2187	- 2912	- 2948	14340	9560	1480	-14000	- 5720	- 6560
29	- 2010	- 2712	- 3364	14560	9450	1470	-14010	- 5460	- 6840
30	- 1899	- 2569	- 1898	13750	9620	1360	-14000	- 5200	- 7410
31	- 1899	- 2340	- 1788	13090	9370	1250	-13800	- 4940	- 7410
32	- 1728	- 2133	- 1690	13380	9240	1250	-14180	- 4940	- 7700
33	- 1547	- 2169	- 1630	12560	9170	1240	-14350	- 4940	- 7700
34	- 1575	- 1968	- 1606	12670	9280	1230	-14530	- 4940	- 7700
35	- 1596	- 1992	- 1584	12320	9280	1180	-14290	- 4680	- 7980
36	- 1350	- 2028	- 1440	11860	9420	1360	-14640	- 4680	- 7980
37	- 1320	- 1799	- 1493	11830	10250	1310	-14630	- 4680	- 8550
38	- 1212	- 1796	- 1442	10980	10450	1450	-14970	- 4940	- 8550
39	- 1122	- 1750	- 1391	10580	9550	2200	-15100	- 4940	- 8550
40	- 906	- 1659	- 1212	9690	9750	2380	-15260	- 5200	- 7980
41	- 565	- 1290	- 1106	9680	10880	3260	-15600	- 5460	- 7980
42	- 360	- 1098	- 1095	9940	11880	4180	-15740	- 5720	- 7980
43	- 8	- 744	- 941	8970	12880	4820	-16090	- 6180	- 7920
44	348	- 355	- 891	9070	15030		-16430	- 6680	- 7880

TABLE 5.4 (Contd.)

EXPERIMENTAL STRESSES AT VARIOUS LOCATIONS IN THE SERIES-1 q = 4.0 CAL/SQ. CM. SEC.
BOX-BEAM LOADED TO 20% OF THE FAILING BENDING MOMENT (MODEL 4)

Time (Seconds)	σ_1	σ_2	σ_3	σ_4	σ_5	σ_6	σ_7	σ_8	σ_9
45	700	30	- 704	8360	16100		-16550	- 7170	- 6740
46	932	448	- 512		16240		-16510	- 7410	- 6730
47	789	640	- 151						- 6160
48	548	964	- 11						- 5590
49	276	840	497						- 5020
50	281	554	1026						- 3900
51			1560						- 2770
52									- 2240

TABLE 5.5

EXPERIMENTAL STRESSES AT VARIOUS LOCATIONS IN THE SERIES-1
q = 4.0 CAL/Sq. CM. SEC. BOX-BEAM LOADED TO 40% OF
THE FAILING BENDING MOMENT (MODEL 5)

Time (Second)	σ_1	σ_2	σ_3	σ_4	σ_5	σ_7
0	9500	10100	10200	5700	0	-11100
1	8900	9000	9200	8250	1900	-11700
2	8300	8400	9200	10200	3750	-12300
3	6428	6633	8300	11400	5000	-12300
4	4601	5499	7722	12700	6250	-12900
5	4061	3791	7691	14000	7500	-13600
6	2278	2680	7652	14000	8150	-13600
7	1272	2086	7582	15200	8750	-14200
8	- 750	1130	7535	16335	9400	-14200
9	- 2092	- 843	7464	17569	10000	-14800
10	- 4479	- 2558	7410	17480	10000	-15400
11	- 5529	- 3998	6993	18013	10600	-16000
12	- 8879	- 5475	6305	18236	11300	-16000
13	- 7943	- 7954	5669	18600	11804	-16000
14	- 5645	- 8299	5178	19158	11757	-17300
15	- 5468	- 6497	4774	19569	11733	-17300
16	- 4977	- 5454	4641	19929	12275	-17900
17	- 4432	- 4784	6621	19669	12812	-18500
18	- 4088	- 4380	9423	19052	12786	-18500
19	- 3875	- 3910	7426	19053	13386	-19100
20	- 3663	- 3510	6235	18533	13330	-19100
21	- 3363	- 3429	5775	17640	13234	-20300
22	- 3137	- 3372	5194	16892	13179	-20300
23	- 2745	- 2940	3645	16686	13110	-21000
24	- 2646	- 3020	3552	15800	13559	-22200
25	- 2304	- 2547	3203	15862	13905	-22000
26	- 2233	- 2528	2793	15300	14062	-22800
27	- 2110	- 2226	2736	16571	15596	-22800
28	- 1863	- 2015	2921	17850	14432	-22213
29	- 1634	- 1782	3001	17782	16095	-22989
30	- 1588	- 1573	3486	16695	17630	-24288
31	- 1274	- 1330	3562	15892	20570	-24192
32	- 957	- 1067	3634	14548	22260	-24192
33	- 726	- 675	3465	13524	22300	-24864
34	- 438			12232	22275	-25080
35				12040	22160	-25365

TABLE 5.6

EXPERIMENTAL STRESSES AT VARIOUS LOCATIONS IN THE SERIES-1
q = 4.0 CAL/SQ. CM. SEC. BOX-BEAM LOADED TO 60% OF
THE FAILING BENDING MOMENT (MODEL 6)

Time (Second)	σ_1	σ_2	σ_3	σ_4	σ_5	σ_7
0	14500	14900	14500	7900	0	-16700
1	13200	13800	13500	10000	1300	-16700
2	11200	12700	13000	11600	3100	-17300
3	10536	11600	12600	13200	3800	-17900
4	9089	9821	12499	13700	5600	-18600
5	8419	9250	12449	15300	6300	-19200
6	7074	8545	12753	16400	6900	-19200
7	6296	7207	12688	16900	7500	-19900
8	5019	6270	12197	16856	7500	-19900
9	3203	4909	12441	17654	8800	-20200
10	1124	2723	12376	17952	9400	-20200
11	- 232	1075	12298	18336	10000	-20200
12	- 1658	371	11728	19488	10000	-20800
13	- 2633	- 1146	11221	20140	11300	-21200
14	- 2369	- 1771	10717	20962	11900	-22000
15	- 3488	- 2685	10986	21111	11805	-22800
16	- 2723	- 4807	12330	21804	12387	-22800
17	- 4290	- 5725	9170	21840	12969	-23100
18	- 4537	- 6278	8889	21780	13634	-23100
19	- 4356	- 6873	8522	21449	13593	-23600
20	- 3647	- 5011	9472	21472	14730	-24200
21	- 2063	- 4558	7910	20984	14784	-24300
22	- 2535	- 4180	7425	20825	15295	-24600
23	- 1580	- 2432	7778	20584	16435	-24600
24	- 2778	- 2070	7756	20295	16826	-25100
25	- 2245	- 1194	7497	20240	18518	-25100
26	- 1290	- 265	7546	20461	20553	-25600
27	- 723	1043	- 9040	20328	23800	-26000
28	- 1134	- 2505	-10046	20400	23828	-26000

TABLE 5.7

EXPERIMENTAL STRESSES AT VARIOUS LOCATIONS IN THE SERIES-1
q = 4.0 CAL/SQ. CM. SEC. BOX-BEAM LOADED TO 80% OF
THE FAILING BENDING MOMENT (MODEL 7)

Time (Second)	σ_1	σ_2	σ_3	σ_4	σ_5	σ_7
0	21600	19100	18700	9800	0	-21600
1	19500	18700	16600	11700	1860	-21900
2	18400	17500	17300	13300	3100	-22400
3	17127	16600	17200	14200	4000	-22700
4	14896	15610	17028	15800	5300	-23700
5	13635	14655	17963	17000	6200	-24000
6	12415	13592	18835	18000	6800	-24400
7	7938	12662	18214	18900	7800	-24500
8	7136	10974	18547	19980	8400	-24600
9	6145	9672	18374	20384	9000	-24800
10	5411	6965	18240	21340	9610	-25000
11	3846	5574	17010	22464	10500	-25500
12	2472	4406	16016	22800	11200	-25800
13	1122	2980	16965	23312	11979	-26000
14	3415	2213	16235	23808	13410	-26300
15	5174	3279	16268	24366	14396	-26600
16	3774	4463	15390	24564	15531	-26700
17	4750	7743	18486	24480	17664	-27000
18	6536	6063	19874	24386	20995	-27200
19	6642	7380	20128	24228	24035	-27400
20	6432	8032	19525	24186	24816	-27400
21	5733	7448	18348		25389	-27500
22	5206	6750	17640		25482	-27500

TABLE 5.8

EXPERIMENTAL STRESSES AT VARIOUS LOCATIONS IN THE SERIES-2, q = 8.0 CAL/SQ. CM. SEC. BOX-BEAM WITH NO EXTERNAL LOAD (MODEL 9)

Time (Seconds)	σ_1	σ_2	σ_3	σ_4	σ_5	σ_6	σ_7	σ_8	σ_9
1	- 1478	- 1862	72	3560	2330	- 724	- 877	- 776	1110
2	- 3869	- 2769	- 277	6775	4846	- 1946	- 1608	- 1552	2306
3	- 5988	- 4549	- 402	9494	6990	- 2127	- 2339	- 2206	3501
4	- 7587	- 5590	- 410	11798	8854	- 2625	- 2924	- 2737	4526
5	-10320	- 6893	- 752	13970	10438	- 3077	- 3508	- 3105	5380
6	-10030	- 7140	- 1523	14900	11828	- 3122	- 3874	- 3431	6149
7	-10810	- 8090	- 2362	15710	12911	- 3620	- 4605	- 3799	6747
8	- 8130	- 8430	- 1951	16300	13910	- 3706	- 4971	- 3840	7174
9	- 5950	- 7420	- 2842	16340	14424	- 3706	- 5336	- 3922	7430
10	- 4600	- 5770	- 2015	16070	14642	- 3523	- 5629	- 3799	7515
11	- 3400	- 5160	- 4595	14040	14180	- 3244	- 5775	- 3472	7259
12	- 2800	- 4030	- 2685	12700	13487	- 2790	- 5775	- 3064	6917
13	- 2070	- 3290	- 3080	10308	12215	- 2148	- 5738	- 2532	6234
14			- 3080	6561	10766	- 1430	- 5554	- 1920	5508
15			- 3105	3890	9349	- 668	- 5475	- 1144	4782
16			- 2900	4083	8219	0	- 5469	- 490	4270
17				3104	7220	526	- 5434	82	3672
18				2254	5580	1142	- 5717	531	3160
19				2528	4183	1739	- 5775	1103	2861
20				1958	2880	2158	- 5942	1552	2562
21				2202	1704	2667	- 6079	1961	2306
22				2015	720	2952	- 6129	2165	1964
23				654	- 2508	3244	- 6170	2368	1319
24				- 138	- 3218	2905	— 6488	2817	- 90
25				- 1156	- 5970	2768	- 6644	3187	- 2258

TABLE 5.9

EXPERIMENTAL STRESSES AT VARIOUS LOCATIONS IN THE SERIES-2, q = 8.0 CAL/SQ. CM. SEC.
BOX-BEAM LOADED TO 28 % OF THE FAILING BENDING MOMENT
(MODEL 10)

Time (Seconds)	σ_1	σ_2	σ_3	σ_4	σ_5	σ_6	σ_7	σ_8	σ_9
0	5320	4520	4470	2180	0	- 2130	- 4970	- 5150	- 5040
1	1790	2370	4110	5430	2330	- 850	- 4970	- 5150	- 4870
2	- 1390	0	3800	8510	4660	490	- 5330	- 5560	- 5380
3	- 3530	- 1400	4580	11590	6990	1310	- 6730	- 6940	- 6490
4	- 4350	- 1890	5630	14160	8480	1950	- 7820	- 7920	- 7600
5	- 4550	- 2870	5780	15010	9970	2890	- 7820	- 7920	- 7600
6	- 4970	- 3740	6390	16390	11390	3390	- 8770	- 8660	- 7940
7	- 5650	- 4470	7560	16700	12590	4030	- 9030	- 8660	- 8330
8	- 5730	- 4460	8050	17100	13650	4480	- 9650	- 8990	- 8630
9	- 5230	- 3720	9170	17110	14510	4900	- 9950	- 9070	- 8540
10	- 4570	- 2380	10120	17110	14700	5090	-10600	- 9230	- 8800
11	- 2810	- 1320	10420	16740	14800	5180	-10750	- 8950	- 8540
12	- 2620	- 560		16290	14750	4980	-10970	- 8740	- 8280
13	- 2255	730		15490	14630	4770	-11040	- 8330	- 7770
14	- 1995	3750		14280	13830	4360	-11390	- 8170	- 7690
15	- 1190	4160		13100	13070	4050	-11690	- 7920	- 7340
16	- 1780	6410		14090	12400	3840	-11680	- 7350	- 6700
17	- 1370			13190	11660	3630	-11860	- 7030	- 6320
18	- 1290			12380	10960	3510	-12150	- 6780	- 6020
19				11880	10770	3300	-12640	- 6740	- 5890
20				10680	11080	3280	-13110	- 6620	- 5640
21				10740	11830	3450	-13380	- 6290	- 5720
22					11480	3520	-14140	- 6540	- 5420

TABLE 5.10

EXPERIMENTAL STRESSES AT VARIOUS LOCATIONS IN THE SERIES-2, q = 8.0 CAL/SQ. CM. SEC. BOX-BEAM LOADED TO 56 % OF THE FAILING BENDING MOMENT

(MODEL 11)

Time (Seconds)	σ_1	σ_2	σ_3	σ_4	σ_5	σ_6	σ_7	σ_8	σ_9
0	11845	8544	9373	4500	- 373	- 4435	- 9869	-11237	-10718
1	8611	7712	8751	7615	1957	- 2896	- 9722	-10049	-10291
2	6290	6221	9156	11126	4567	- 1810	-10928	-11315	-11572
3	3464	2580	9289	13876	6804	- 724	-11736	-11193	-12298
4	0	957	9496	15440	8621	317	-12390	-12623	-12767
5	- 3136	- 3014	9044	16660	10289	950	-13487	-13603	-13707
6	- 6265	- 5059	7323	17350	11728	1810	-13743	-13644	-13707
7	- 7823	- 7180	7052	17650	13204	2353	-14803	-14338	-14390
8	- 4450	- 8352	5854	17480	14542	3077	-15168	-14379	-14390
9	- 3420	- 7667	4448	17480	14900	4065	-15300	-14676	-14646
10	- 2710	- 5990	5356	17480	15460	4152	-15500	-14869	-14646
11	- 2215	- 4860	3486	17110	16130	4498	-16040	-14900	-14902
12	- 1760	- 3720	2594	16830	16340	4935	-15970	-14800	-14433
13	- 1070	- 3090	3421	16460	16450	5409	-16270	-14700	-14433
14	- 955	- 2620	3410	16170	16650	5975	-16860	-15400	-14646
15	- 735	- 1905		15690	16740	7000	-17250	-14900	-14600
16					16830	9691	-17640	-15300	-14600
17						13060	-17840	-15250	-14650
18						14880	-18130	-16100	-15200
19						17020	-18230	-16700	-15700
20							-18420	-16800	-15800

TABLE 5.11a

EXPERIMENTAL STRESSES AT VARIOUS LOCATIONS IN THE SERIES-2, q = 8.0 CAL/SQ. CM. SEC. BOX-BEAM LOADED TO 80% OF THE FAILING BENDING MOMENT, STATION 12 (MODEL 12)

Time (Seconds)	σ_1	σ_2	σ_3	σ_4	σ_5	σ_6	σ_7	σ_8	σ_9
0	13500	13200	14600	6680	0	- 6350	-14530	-13430	-15000
1	10740	11000	13600	9930	2490	- 4640	-14320	-13170	-14770
2	9490	10000	14600	13220	4760	- 4730	-16250	-14920	-15300
3	7410	8400	14700	15640	6010	- 3290	-16750	-15300	-16200
4	6130	6960	14880	16430	6810	- 2390	-16800	-15400	-16600
5	4200	4990	14510	17250	8590	- 1670	-16900	-15400	-16800
6	2600	3790	15470	17930	10190	- 230	-17200	-15900	-17100
7	140	13840	14960	18140	12240	130	-17600	-15800	-17100
8	- 20	12140	14540	18140	15440	1200	-17700	-16000	-17200
9	- 150	9020	14840	17860	16460	1930	-18100	-16600	-17600
10	- 90	6950	13960	17760	17170	3270	-18200	-16600	-17100
11	220	5370	13540	17660		4340	-18500	-16800	-17600
12	800	4110	12780			8160	-18600	-17100	-17600
13	820						-18700	-17100	-17900
14	930						-18800	-17100	-18000
15	800						-18900	-17150	-18100
16	580						-18500	-17150	-17840
17							-18600	-16980	-17740
18							-18600	-16980	-17740
19							-18600	-16980	-17560
19.4							-18600	-16610	-17500

TABLE 5.11b

EXPERIMENTAL STRESSES AT VARIOUS LOCATIONS IN THE SERIES-2, q = 8.0 CAL/SQ. CM. SEC. BOX-BEAM LOADED TO 80 % OF THE FAILING BENDING MOMENT= STATION 9 1/2

(MODEL 12)

Time (Seconds)	σ_2	σ_3	σ_4	σ_5	σ_6	σ_7	σ_8	σ_9
0	10700	13470	6410	0	- 6190	-14510	-14360	-15200
1	9200	13160	9700	3140	- 4360	-14300	-14160	-15200
2	8630	15220	12990	5950	- 3300	-15700	-15400	-16200
3	7000	14600	15600	8640	- 2050	-15600	-15500	-16250
4	6740	16060	16730	11220	- 1560	-16800	-16200	-17000
5	4100	16120	17420	13720	- 270	-16800	-16200	-17000
6	2560	16290	17840	15090	400	-17400	-16900	-17600
7	1350	15650	18040	16460	1330	-17800	-17300	-17700
8	320	15360	18050	17350	2310	-18000	-17350	-17800
9	700	14880	17960		2930	-18300	-17500	-17900
10	450	14740	17770		4350	-18400	-17500	-17900
11	990	12850	17480		5320	-18600	-17800	-18100
12	1580	10940			9410	-18700	-17850	-18300
13	1910					-18800	-17800	-18100
14	1140					-18800	-17500	-17900
15	620					-18800	-17500	-17600
16	360					-18800	-17500	-17440
17						-18900	-17300	-17350
18						-18900	-17250	-17070
19						-18900	-16990	-16490
19.4						-18800	-16800	-16400

TABLE 5.11c

EXPERIMENTAL STRESSES AT VARIOUS LOCATIONS IN THE SERIES-2, q = 8.0 CAL/SQ. CM. SEC. BOX-BEAM LOADED TO 80 % OF THE FAILING BENDING MOMENT, STATION 7 1/2

(MODEL 12)

Time (Seconds)	σ_1	σ_2	σ_3	σ_4	σ_5	σ_6	σ_7	σ_8	σ_9
0	11420	12700	12400	6830	0	- 7690	-15500	-14250	-13950
1	11390	12590	14350	10320	2940	- 5990	-14500	-14180	-13880
2	12680	12400	15520	13960	5460	- 5570	-16400	-15200	-15200
3	11820	10330	15260	15980	7430	- 4080	-16400	-15200	-15250
4	10820	9110	16170	16930	9950	- 3550	-16800	-16300	-16500
5	7310	5460	16190	17520	11930	- 2380	-16900	-16900	-16600
6	4340	2620	15750	18120	14410	- 1800	-17700	-17200	-17100
7	2210	590	15220	17860	15390	- 1220	-18100	-17600	-17400
8	400	- 970	14510	17950	16300	- 1380	-18500	-17800	-17600
9	- 680	- 760	14060	18140	17270	- 210	-18500	-18000	-18000
10	- 1300	- 1510	12850	18200		900	-18600	-18000	-18100
11	- 1320	- 1000	12060			1490	-18800	-18300	-18500
12	- 1000	- 780	9770			4000	-18900	-18300	-18500
13	- 1080	- 110	7920			7070	-18800	-17900	-18100
14	- 830	- 500	6020			8990	-18600	-17200	-17600
15	- 740	- 530	5050			9960	-18700	-16900	-17400
16	- 650	- 540	3950			10500	-18600	-16800	-17200
17	- 550	- 430	2510			11110	-17670	-16100	-16400
18	- 450	- 380	1530			11290	-17600	-15200	-16100
19	- 350	- 360	700			11340	-17460		-15300
19.4	- 250	- 330	560			11150	-17400		-15000

TABLE 5.12

EXPERIMENTAL STRESSES AT VARIOUS LOCATIONS IN THE SERIES-2, q = 8.0 CAL/SQ. CM. SEC BOX-BEAM LOADED TO 90 % OF THE FAILING BENDING MOMENT (MODEL 13)

Time (Seconds)	σ_1	σ_2	σ_3	σ_4	σ_5	σ_6	σ_7	σ_8	σ_9
0	19970	16120	15790	9198	- 1072	- 6880	-16200	-16100	-16100
1	16700	13000	12637	12560	- 4008	- 4710	-16000	-16000	-15700
2	15710	10628	10199	15720	- 6617	- 3122	-16600	-16200	-16150
3	15130	8511	8069	16730	- 8900	- 1900	-16700	-16600	-16400
4	14800	7658	7059	17640	-11140	- 950	-17300	-17200	-17200
5	13610	9642	8391	18230	-12950	- 770	-18000	-17800	-17700
6	12310	11250	9941	18240	-14360	- 96	-18200	-17900	-17900
7		13950	12220	18150	-16170	0	-18600	-17800	-17800
8			15400		-16760	360	-18650	-16700	-16440
9					-17460	1447	-18700	-16200	-15900
10					-17860	3960	-18750	-16150	-15700
11						7636		-16150	-15300
12						12989		-16000	-15250
13						7040		-16100	-15700

TABLE 5.13

CALCULATED TEMPERATURE DISTRIBUTIONS FOR
q=4.0 CAL/SQ.CM. SEC. AT 5 SECOND TIME INTERVALS

Time (Seconds)	ΔT_1	ΔT_2	ΔT_3	ΔT_4	ΔT_5	ΔT_6	ΔT_7	ΔT_8
5	181	176	131	43	20	8	1	0
10	347	335	243	106	64	36	9	0
15	496	477	349	176	117	76	27	3
20	632	608	451	248	175	121	51	10
25	758	729	549	321	237	171	81	23

TABLE 5.14

CALCULATED TEMPERATURE DISTRIBUTIONS FOR
q=8.0 CAL/SQ. CM. SEC. AT 5 SECOND TIME INTERVALS

Time (Seconds)	ΔT_1	ΔT_2	ΔT_3	ΔT_4	ΔT_5	ΔT_6	ΔT_7	ΔT_8
5	361	352	262	85	40	17	2	0
10	694	669	486	213	128	73	19	1
15	993	955	699	352	235	151	53	6

TABLE 5.15

CORRELATION OF STRESSES FOR q = 4.0 CAL/SQ. CM. SEC.

0% BM_{max} (MODEL 3)

Time (Seconds)		σ_1	σ_2	σ_3	σ_4	σ_5	σ_6	σ_7	σ_8	σ_9
5	exper.	- 5050	- 5988	746	5750	4850	1150	- 1300	- 1380	1710
	calc.	- 6967	- 6355	- 203	7498	6144	3305	- 1327	- 1212	- 1209
10	exper.	- 5640	- 7979	2134	10714	8633	2000	- 2600	- 2070	1710
	calc.	-12890	-11361	745	11837	9363	4715	- 2437	- 1362	- 1281
15	exper.	- 4072	- 9290	1697	12954	10236	1700	- 4160	- 2080	1140
	calc.	-16111	-14277	934	14532	11176	5095	- 3647	- 892	- 596
20	exper.	- 2320	-10379	139	12277	10741	1443	- 5460	- 1380	570
	calc.	-16187	-14870	129	15592	11810	4779	- 4842	- 93	506
25	exper.	- 396	- 8062	- 620	7556	9500	543	- 5980	- 350	- 1140
	calc.	-12747	-12834	- 1783	14700	11102	3788	- 5869	948	1877

TABLE 5.15 (CONTD.)

CORRELATION OF STRESSES FOR q = 4.0 CAL/SQ. CM. SEC.

20% BM_{max} (MODEL 4)

Time (Seconds)		σ_1	σ_2	σ_3	σ_4	σ_5	σ_6	σ_7	σ_8	σ_9
5	exper.	- 1411	0	5039	10000	6760	660	- 7400	- 7020	- 4560
	calc.	- 2186	- 1565	4662	9991	6191	905	- 6873	- 6757	- 6754
10	exper.	- 6224	- 141	4840	14000	9880	1980	- 9000	- 7280	- 4560
	calc.	- 8318	- 6737	5693	14555	9571	2388	- 8024	- 6947	- 6866
15	exper.	- 7258	- 2193	3062	16000	11820	2420	-10800	- 7280	- 4560
	calc.	-11897	- 9932	6018	17625	11667	2906	- 9308	- 6552	- 6254
20	exper.	- 4760	- 3745	173	15610	12380	2170	-12600	- 7020	- 5130
	calc.	-12528	-10958	5412	19265	12725	2821	-10619	- 5877	- 5279
25	exper.	- 3312	- 3640	- 3042	17800	10890	1920	-13400	- 5980	- 6270
	calc.	- 9989	- 9629	3807	19301	12779	2217	-11835	- 5045	- 4117

TABLE 5.15 (CONTD.)

CORRELATION OF STRESSES FOR q = 4.0 CAL/SQ. CM. SEC.

40% BM_{max} (MODEL 5)

Time (Seconds)		σ_1	σ_2	σ_3	σ_4	σ_5	σ_6	σ_7	σ_8	σ_9
5	exper.	4061	3791	7691	14000	7500		-13600		
	calc.	2596	3225	9526	12484	6238	- 1495	-12418	-12301	-12298
10	exper.	- 4479	- 2558	7410	17480	10000		-15400		
	calc.	- 3746	- 2112	10641	17273	9778	61	-13611	-12533	-12452
15	exper.	- 5468	- 6497	4774	19569	11733		-17300		
	calc.	- 7683	- 5586	11103	20719	12157	717	-14970	-12712	-11914
20	exper.	- 3663	- 3510	6235	18522	13330		-19100		
	calc.	- 8869	- 7046	10695	22938	13693	864	-16396	-11662	-11063
25	exper.	- 2304	- 2547	3203	15862	+3905		-22000		
	calc.	- 7231	- 6425	9396	23902	14456	646	-17800	-11039	-10111

TABLE 5.15 (CONTD.)

CORRELATION OF STRESSES FOR q = 4.0 CAL/SQ. CM. SEC.

60% BM_{max} (MODEL 6)

Time (Seconds)		σ_1	σ_2	σ_3	σ_4	σ_5	σ_6	σ_7	σ_8	σ_9
5	exper.	8419	9250	12449	15300	6300		-19200		
	calc.	7377	8015	14391	14977	6286	- 3895	-17963	-17846	-17844
10	exper.	1124	2723	12376	17952	9400		-20200		
	calc.	826	2512	15590	19991	9986	- 2265	-19199	-18119	-18037
15	exper.	- 2488	- 2685	10986	21111	11805		-22800		
	calc.	- 3469	- 1240	16187	23813	12648	- 1471	-20631	-17873	-17574
20	exper.	- 3647	- 5011	9472	21472	14730		-24200		
	calc.	- 5210	- 3134	15978	26611	14635	- 1094	-22173	-17446	-16857
25	exper.	- 2245	- 1194	7497	20240	18518		-25100		
	calc.	- 4473	- 3221	14986	28504	16134	- 926	-23765	-17023	-16106

TABLE 5.15 (CONTD.)

CORRELATION FOR STRESSES FOR q = 4.0 CAL/SQ. CM. SEC.

80% BM_{max} (MODEL 7)

Time (Seconds)		σ_1	σ_2	σ_3	σ_4	σ_5	σ_6	σ_7	σ_8	σ_9
5	exper.	13635	14655	17963	17000	6200		-24000		
	calc.	12158	12805	19255	17270	6333	- 6295	-23508	-23390	-23388
10	exper.	5411	6965	18240	21340	9610		-25000		
	calc.	5399	7137	20538	22708	10193	- 4592	-23786	-23704	-23623
15	exper.	5174	3279	16268	24366	14396		-26600		
	calc.	745	3105	21271	26906	13138	- 3659	-26292	-23533	-23233
20	exper.	6432	8032	19525	24186	24816		-27400		
	calc.	- 1551	778	21261	30284	15577	- 3051	-27951	-23231	-22631

TABLE 5.16

CORRELATION OF STRESSES FOR q = 8.0 CAL/SQ. CM. SEC.

0% BM_{max} (MODEL 9)

Time (Seconds)		σ_1	σ_2	σ_3	σ_4	σ_5	σ_6	σ_7	σ_8	σ_9
55	exper.	-10320	- 6893	- 752	13970	10438	- 3077	- 3508	- 1305	5380
	calc.	-13567	-12478	- 729	15408	12635	6757	- 2803	- 2571	- 2566
10	exper.	- 4600	- 5770	- 2015	16070	14642	- 3523	- 5629	- 3799	7515
	calc.	-16874	-16363	- 2333	21496	17744	8914	- 5177	- 3020	- 2858
15	exper.			- 3105	3890	9349	- 668	- 5475	- 1144	4782
	calc.	17485	8020	-17026	2165	4685	1711	- 4363	1189	1786

28% BM_{max} (MODEL 10)

5	exper.	- 4550	- 2870	5780	15010	9970	2890	- 7820	- 7920	- 7600
	calc.	- 9008	- 7879	4215	18180	12871	4441	- 8397	- 8164	- 8160
10	exper.	- 4570	—2380	10120	17110	14700	5090	-10600	- 9230	- 8800
	calc.	-13637	-12820	3109	25660	18981	7066	-11032	- 8873	- 8710
15	exper.	- 1190	4160		13100	13070	4050	-11690	- 7920	- 7340
	calc.	14182	6379	- 9302	12777	10703	2183	-11474	- 5931	- 5333

TABLE 5.16 (CONTD.)

CORRELATION OF STRESSES FOR q = 8.0 CAL/SQ. CM. SEC.

56% BM_{max} (MODEL 11)

Time (Seconds)		σ_1	σ_2	σ_3	σ_4	σ_5	σ_6	σ_7	σ_8	σ_9
5	exper.	- 3136	- 3014	9044	16660	10289	950	-13487	-13603	-13707
	calc.	- 4449	- 3279	9160	20952	13106	2126	-13991	-13758	-13753
10	exper.	- 2710	- 5990	5356	17480	15460	4152	-15500	-14869	-14646
	calc.	-10399	- 9277	8551	29824	20218	5218	-16887	-14776	-14564
15	exper.	- 735	- 1905		- 5690	16740	7000	-17250	-14900	-14600
	calc.	10880	4737	- 1579	23388	16720	2655	-18584	-13051	-12452

90% BM_{max} (MODEL 13)

5	exper.	13610	9642	8391	18230	-12950	- 770	-18000	-17800	-17700
	calc.	110	1320	14104	23723	13341	- 190	-19585	-19352	-19347
10	exper.					-17860	2960	-18750	-16150	-15700
	calc.	- 7162	- 5734	13993	33988	21455	3370	-22743	-20580	-20417

TABLE 6.1

SUMMATION OF COMBINED LOADING TESTS

Model	Percent of BM_{max}	Intensity Cal/Cm^2Sec	Failure Time (Sec)	Non-Dim. Failure Time	Instrumentation	Comments
SERIES - 1						
1	100	0	--	---	S_1-S_3; S_7-S_9; dial gage	static model, room temperature test
2	100	0	--	---	S_1-S_3; S_7-S_9; dial gage	static model, room temperature test
3	0	4.0	46	1.0	S_1-S_9; T_1-T_8; dial gage	failure due to melting cover plate
4	20	4.0	42	.91	S_1-S_9; T_1-T_8; dial gage	plastic buckling failure
5	40	4.0	31	.67	S_1-S_5;S_7; T_1-T_8; dial gage	plastic buckling failure
6	60	4.0	24	.52	S_1-S_5; S_7; T_1-T_8; dial gage	plastic buckling failure
7	80	4.0	13	.28	S_1-S_5; S_7; T_1-T_8; dial gage	plastic buckling failure

TABLE 6.1 (Contd.)

SUMMATION OF COMBINED LOADING TESTS

Model	Percent of BM_{max}	Intensity Cal/Cm^2Sec	Failure Time (Sec)	Non-Dim. Failure Time	Instrumentation	Comments
SERIES - 2						
8	100	-	--	---	S_1-S_3; S_7-S_9; dial gage	static model, room temperature test
9	0	8.0	21	1.0	S_1-S_9; T_1-T_8; dial gage	failure due to melting cover plate
10	28	8.0	20	.95	S_1-S_9; T_1-T_8; dial gage	plastic buckling failure
11	56	8.0	16	.76	S_1-S_9; T_1-T_8; dial gage	plastic buckling failure
12	80	8.0	12	.57	S_1-S_{27}; T_1-T_8; dial gage	plastic buckling failure; (model instrumented at 3 stations)
13	90	8.0	7	.43	S_1-S_9; T_1-T_8; dial gage	plastic buckling failure

PA-3 gages used on static models (1, 2, 8)

Static failing BM's: Series - 1 33600 inch-pounds
Series - 2 20160 inch-pounds